THE POTENTIAL FOR SPRINGFLOW AUGMENTATION AT COMAL AND SAN MARCOS SPRINGS, CENTRAL TEXAS

by

Matthew Martin Uliana, B. S.

THESIS

Presented to the Faculty of the Graduate School
of the University of Texas at Austin
in Partial Fulfillment
of the Requirements
for the Degree of

MASTER OF ARTS

The University of Texas at Austin

December, 1995

THE POTENTIAL FOR SPRINGFLOW AUGMENTATION AT COMAL AND SAN MARCOS SPRINGS, CENTRAL TEXAS

APPROVED BY

SUPERVISING COMMITTEE:

[redacted]

John M. Sharp

[redacted]

Daene C. McKinney

[redacted]

Philip C. Bennett

to Kelly

ACKNOWLEDGMENTS

First and foremost, I would like to thank my advisor, Dr. Jack Sharp, for his guidance and support (both moral and financial) throughout the research and writing of this thesis. I sincerely believe that this accomplishment would not have been possible without his support, for he maintained faith in my abilities even when I had all but given up on them.

I would also like to thank the other members of my committee, Dr. Daene McKinney and Dr. Phil Bennett, for taking the time to read and review my thesis, as well as for the countless other contributions that they have made to my development as a scientist and a person, both in the classroom and out. I would also like to thank Marshall Jennings of the Austin USGS for his assistance in obtaining data for my models. In addition, I would like to acknowledge Dennis Trombatore and the UTDOGS Library, the Austin and San Antonio USGS, the TNRIS, and the TWDB, and thank them for supplying me with information, data, and personal expertise at a nominal expense.

Finally, I would like to make the following personal acknowledgments; to Mike Harren and Steve Graham, thank you for letting me play DOOM on your computers; to the Austin music scene and all the bands that I played with, thank you for providing me with enough fun to make me extend graduate school an extra year and enough aggravation to almost give me an ulcer at the age of 26; to Joel Adrian, Jason Lundquist, Derek Reiber, Jamie White, and the Schlitz Brewing Company, thank you for helping me keep this all in perspective (or, more accurately, for helping me get everything comfortably out of perspective); and to anyone involved in the worldwide industry responsible for the production and distribution of coffee, just plain thanks.

ABSTRACT

The Potential For Springflow Augmentation At Comal And San Marcos Springs, Central Texas

by

Matthew Martin Uliana, M. A.

The University of Texas at Austin, December, 1995

SUPERVISOR: John M. Sharp

The Edwards aquifer, a regionally-extensive carbonate aquifer in Central Texas, is the sole source of water for nearly two million people, including the City of San Antonio. Pumpage from this aquifer is jeopardizing springflow from Comal Springs (in New Braunfels, Texas) and San Marcos Springs (in San Marcos, Texas), two of the largest springs in the state. These springs provide a habitat for a number of endangered species, and are an integral part of the local economies and the overall distribution of water in Central Texas. For these reasons it is important that flow from these springs be maintained, either through aquifer management plans that limit the withdrawal and usage of water from the aquifer, or through physical augmentation of the springs.

In this thesis, the feasibility of maintaining springflow by augmenting discharge from the springs is investigated. Five potential methods of springflow augmentation (enhanced recharge, subsurface flow barriers, direct addition of water to the spring lakes, injection wells, and infiltration galleries) are presented and described. Based on present knowledge of the springs, the effectiveness of each method is evaluated, and the uncertainties associated with each are discussed. Computer models of the aquifer in the vicinity of the springs are constructed and used to model the effects of two of the augmentation methods (injection wells and infiltration galleries) on aquifer levels and spring discharges. The model results are used to estimate the efficiency of each of these methods and to develop general trends related to how the aquifer responds to the introduction of water through wells and infiltration galleries. Based on model results and the hydrogeology of each spring, an assessment of the each of the augmentation methods is presented, and recommendations are made as to the appropriateness of the various technologies at each spring.

TABLE OF CONTENTS

LIST OF TABLES

LIST OF FIGURES

1. INTRODUCTION

1.1 Purpose

The purpose of this thesis is to develop a set of detailed models of the Edwards aquifer in the vicinity of Comal and San Marcos Springs. These models are used to simulate the introduction of water into the aquifer through injection wells and infiltration galleries. The results of these simulations are used to estimate the efficacy of injection wells and infiltration galleries as a means of augmenting spring flow from Comal and San Marcos Springs during low flow periods.

1.2 Background

The Edwards carbonate aquifer in Central Texas is the sole source of water for nearly two million people, including the City of San Antonio (Figure 1.1). Although pumpage from the Edwards, one of the most productive aquifers in the United States, has increased steadily over the past fifty years, reaching a maximum of 530 thousand acre feet (af) (6.5 million m^3) in 1984 (Figure 1.2), index wells in the San Antonio region have not shown a correspondingly significant decline in water levels (Figures 1.3 and 1.4) (Maclay, 1989). This would indicate that groundwater storage in the aquifer is not being depleted, but flow from springs in Central Texas has decreased in proportion to increasing withdrawal of water from the Edwards (Figure 1.5). If pumping from the Edwards continues to increase, the springs could cease flowing. It is important to the endangered species and human communities that depend on the springs that spring flow be maintained, either through aquifer management plans that will place limits on water use and pumping rates, or through physical augmentation of springflow.

The two largest spring systems in the Edwards aquifer are Comal Springs, in New Braunfels, Texas, and San Marcos Springs, in San Marcos, Texas (Figure 1.6). These springs provide important economic and recreational resources to the communities of New Braunfels and San Marcos, and contribute significant flow to local rivers. The springs also create habitat for four endangered species, including the Fountain Darter (*Etheostoma fonticola*), the San Marcos Gambusia (*Gambusia georgei*), the Texas Wild Rice (*Zinzania texana*) and the San Marcos Salamander (*Eurycea nana*).

1.3 Objectives

In order to assess the feasibility of augmenting springflow in the Edwards Aquifer, the regional hydrogeology of the Edwards and the local hydrogeology around the springs are described in detail. This includes stratigraphic and structural controls on groundwater flow and a description of the flow systems carrying water to the spring orifices. A number of methods of springflow augmentation are proposed and discussed. The hydrogeologic description of the study area is then used to create a numerical finite-difference computer model and an analytical computer model that simulate the effects of injection wells and infiltration galleries, respectively, on spring flow. The hydrogeologic descriptions and the computer simulations are used to evaluate the efficiency of these two technologies. Based on this evaluation, recommendations are made as to the appropriateness of the various technologies at each spring site.

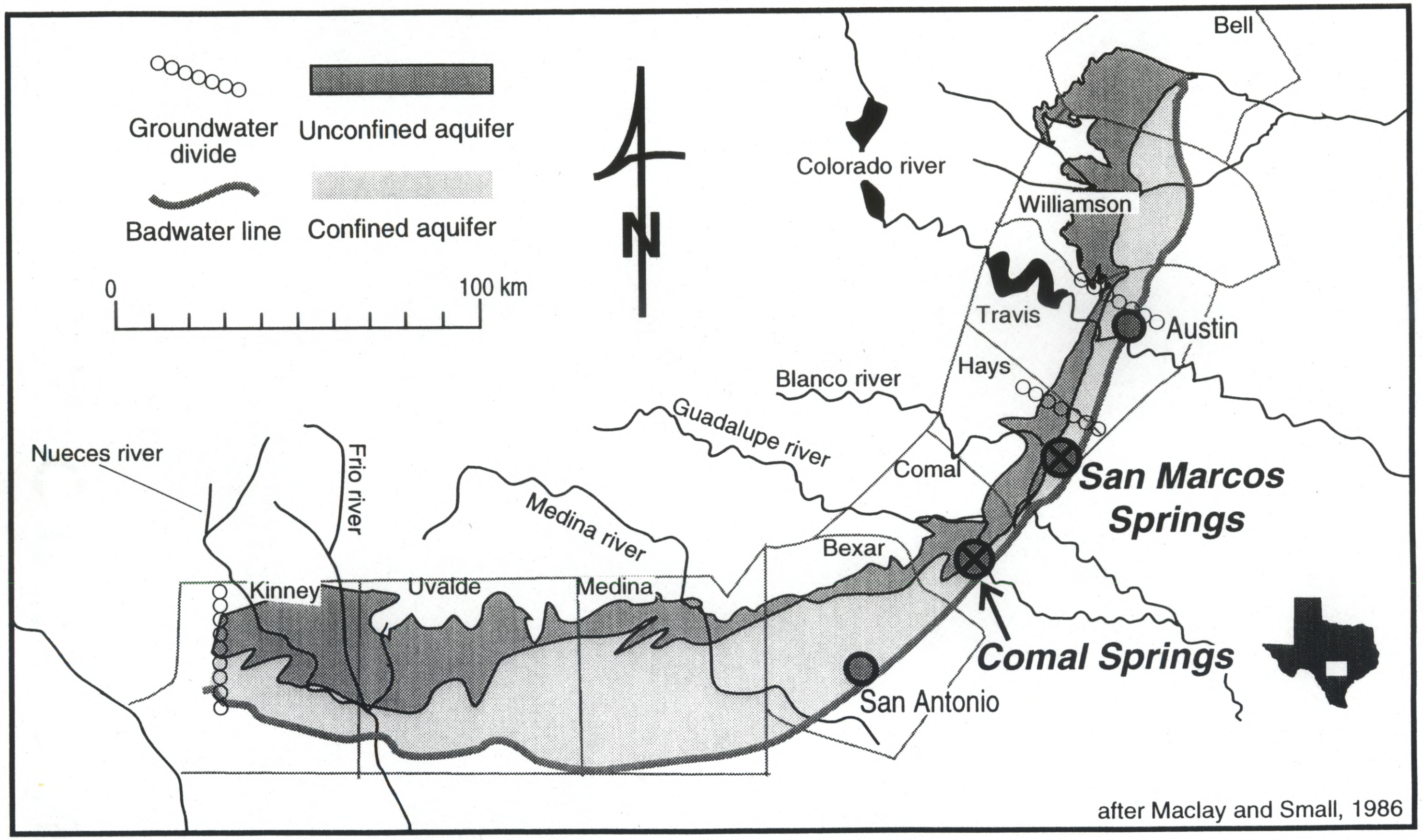

Figure 1.1 The Edwards aquifer, Central Texas

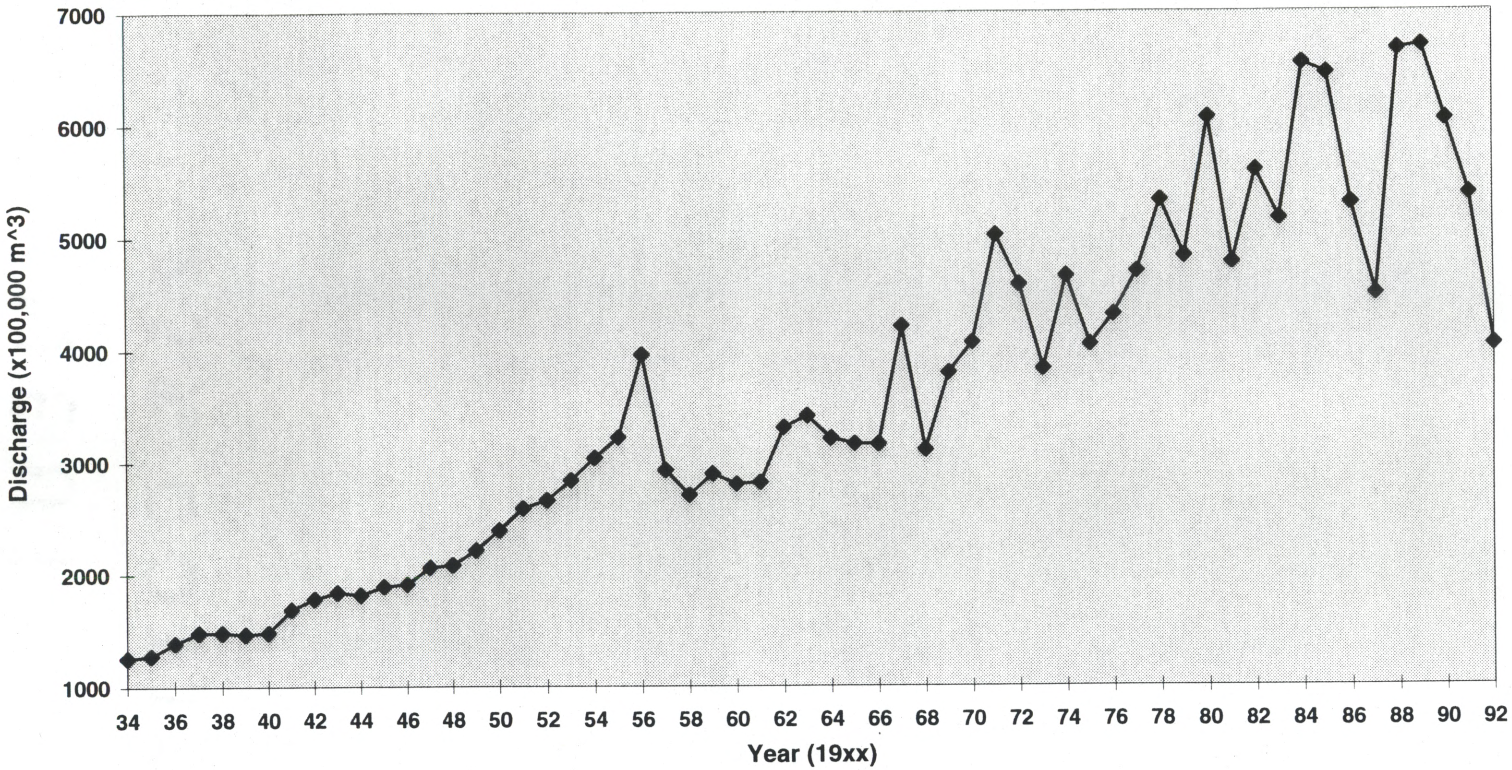

Figure 1.2 Historic annual well discharge from the Edwards aquifer (Data listed in Table 8.1; Brown *et al*, 1992)

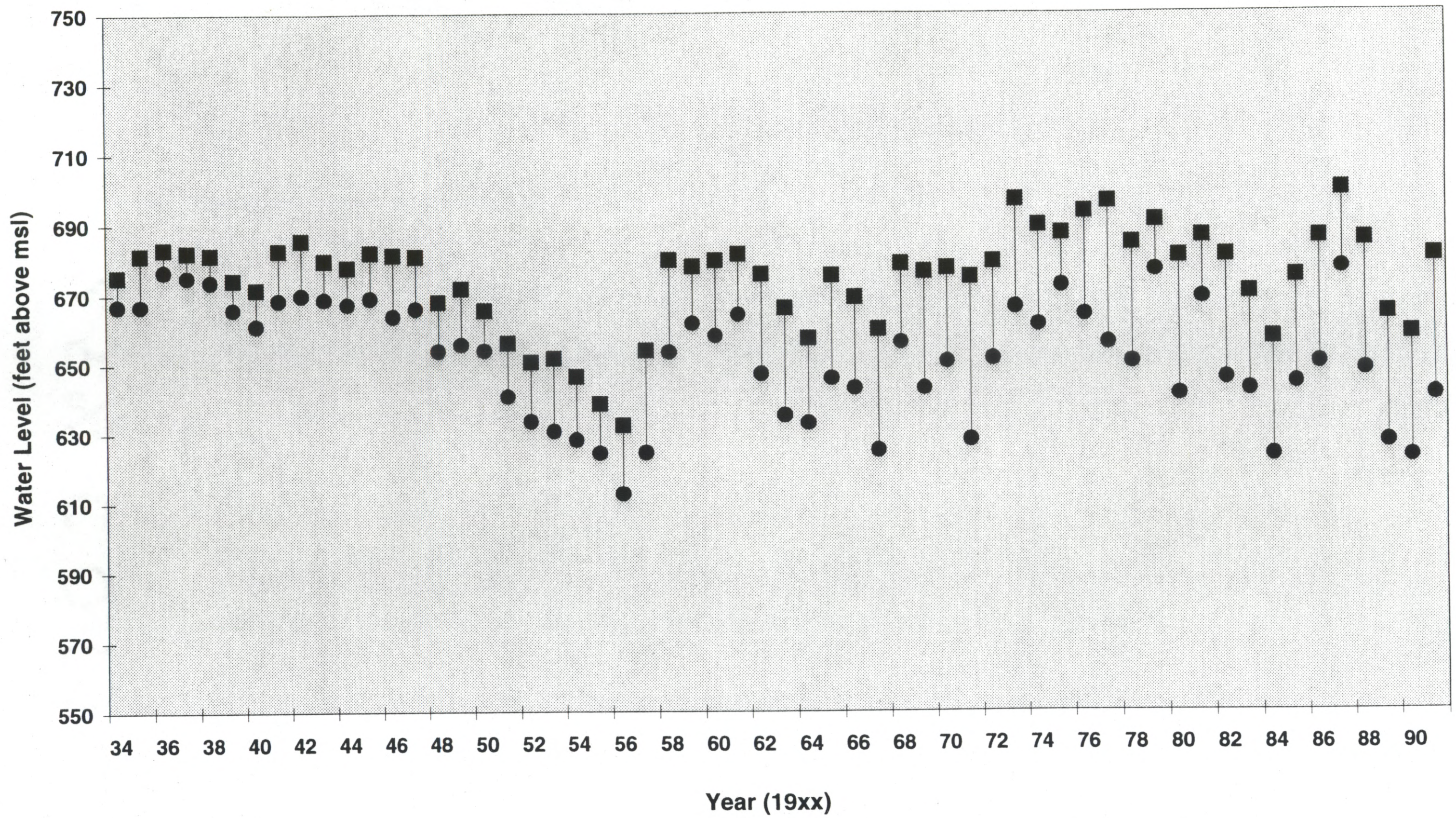

Figure 1.3 Annual high and low water levels in Index Well J-17; Bexar County (Data listed in Table 8.2; Brown *et al* , 1992)

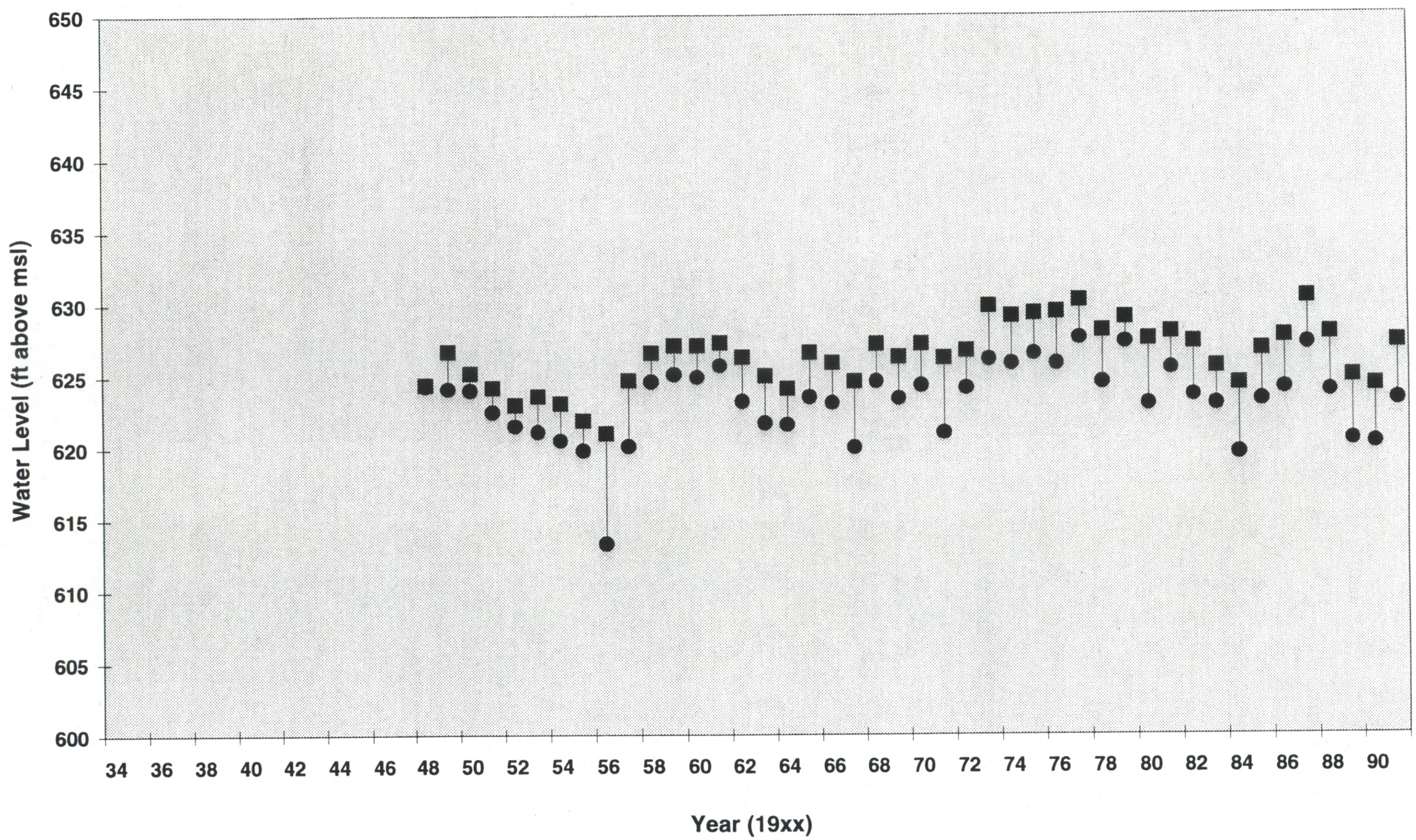

Figure 1.4 Annual high and low water levels in Index Well G-49; Comal County (Data listed in Table 8.2; Brown *et al* , 1992)

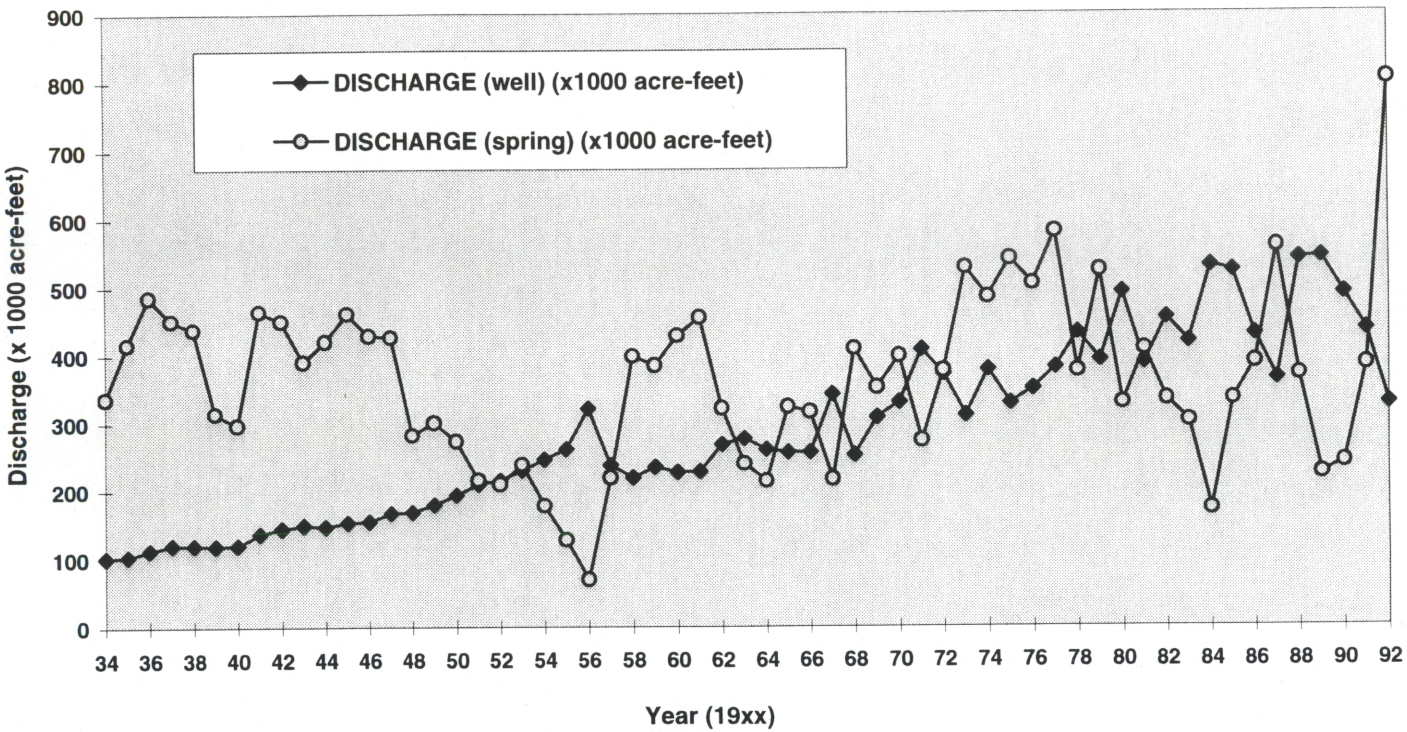

Figure 1.5 Total aquifer well discharge versus spring discharge: Comal Springs (Data listed in Table 8.1; Brown *et al*, 1992)

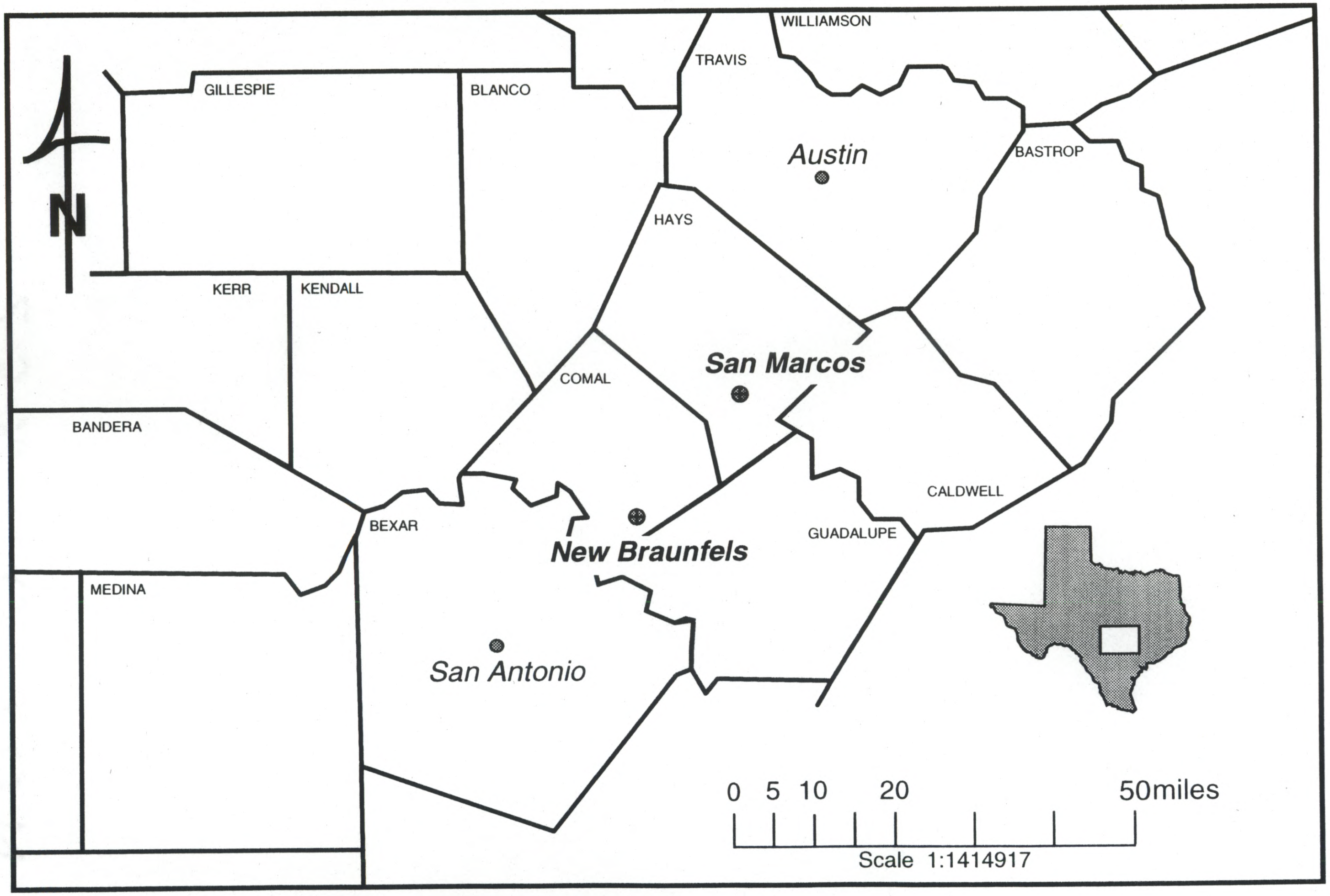

Figure 1.6 Map of Central Texas

1.4 Study Area: Location and Physical Description

1.4.1 Comal Springs

Comal Springs are located at Landa Park in New Braunfels, Texas, at an elevation of 623 ft (190 m) above mean sea level (Figure 1.7). These springs issue from the base of the Balcones Escarpment, a topographic feature in Central Texas that separates the Edwards Plateau from the Gulf Coastal Plain. The springs discharge into Landa Lake, where they form the headwaters of the Comal River. From this point, the Comal River travels a 1.6 km course to its confluence with the Guadalupe River.

Groundwater flows through highly transmissive fractures, solution cavities, and solutioned beds in the Cretaceous Person and Kanier Formations to discharge points in and around Landa Lake. These discharge points occur along a 1500 ft (460 m) section of the Comal Springs Fault, a large normal fault with over 750 ft (230 m) of offset (Figures 1.8 and 1.9). The spring system contains several major spring orifices, four of which are large enough to have spring runs associated with them. In addition to the discrete spring orifices, groundwater discharges through areas of diffuse seepage around and under Landa Lake (Crowe, 1994).

A historical record of discharge from Comal Springs has been kept since 1934 (Figure 1.10). Over this time period, Comal springs has flowed at an average rate of 284 cfs (8 m^3/s). The highest monthly flow rate during the period of record was 534 cfs (15 m^3/s). Comal Springs ceased to flow from 13 June, 1956 to 4 November, 1956, when severe drought conditions dropped water levels in the aquifer to extremely low levels (Brown *et al*, 1992). During this time, water was still present in Landa Lake (McKinney and Sharp, 1995).

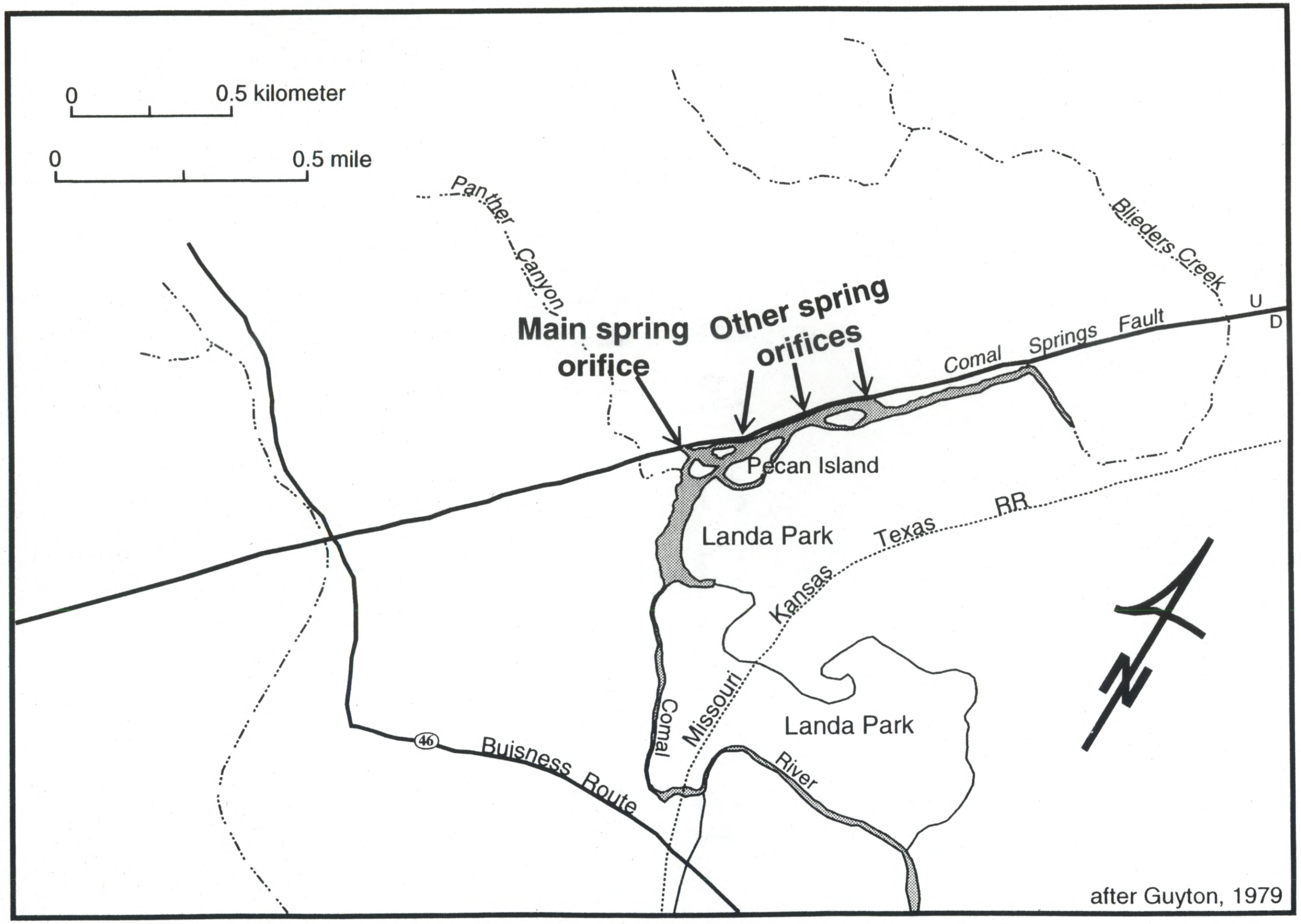

Figure 1.7 Comal Springs at Landa Park in New Braunfels, Texas

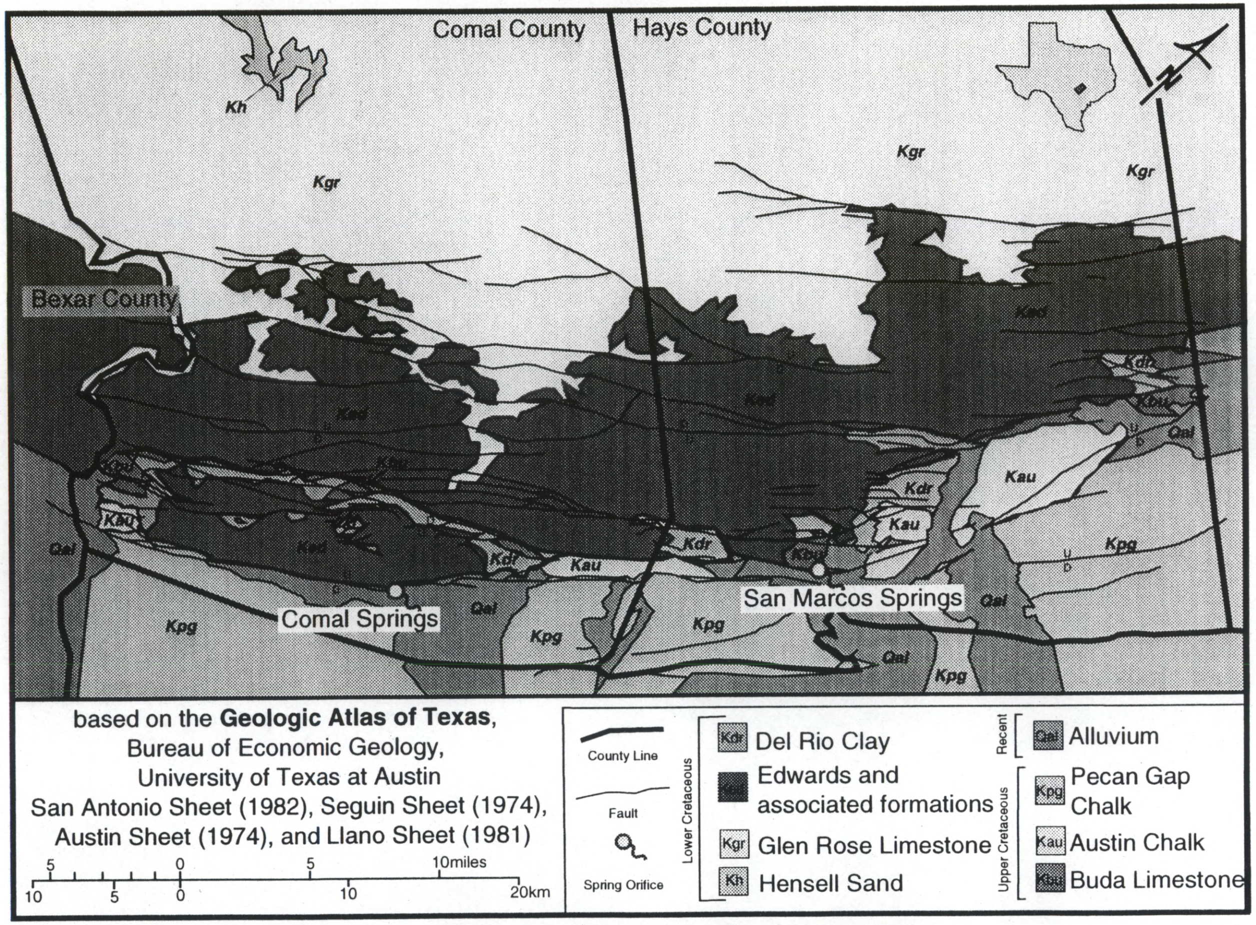

Figure 1.8 Geology of Hays and Comal Counties

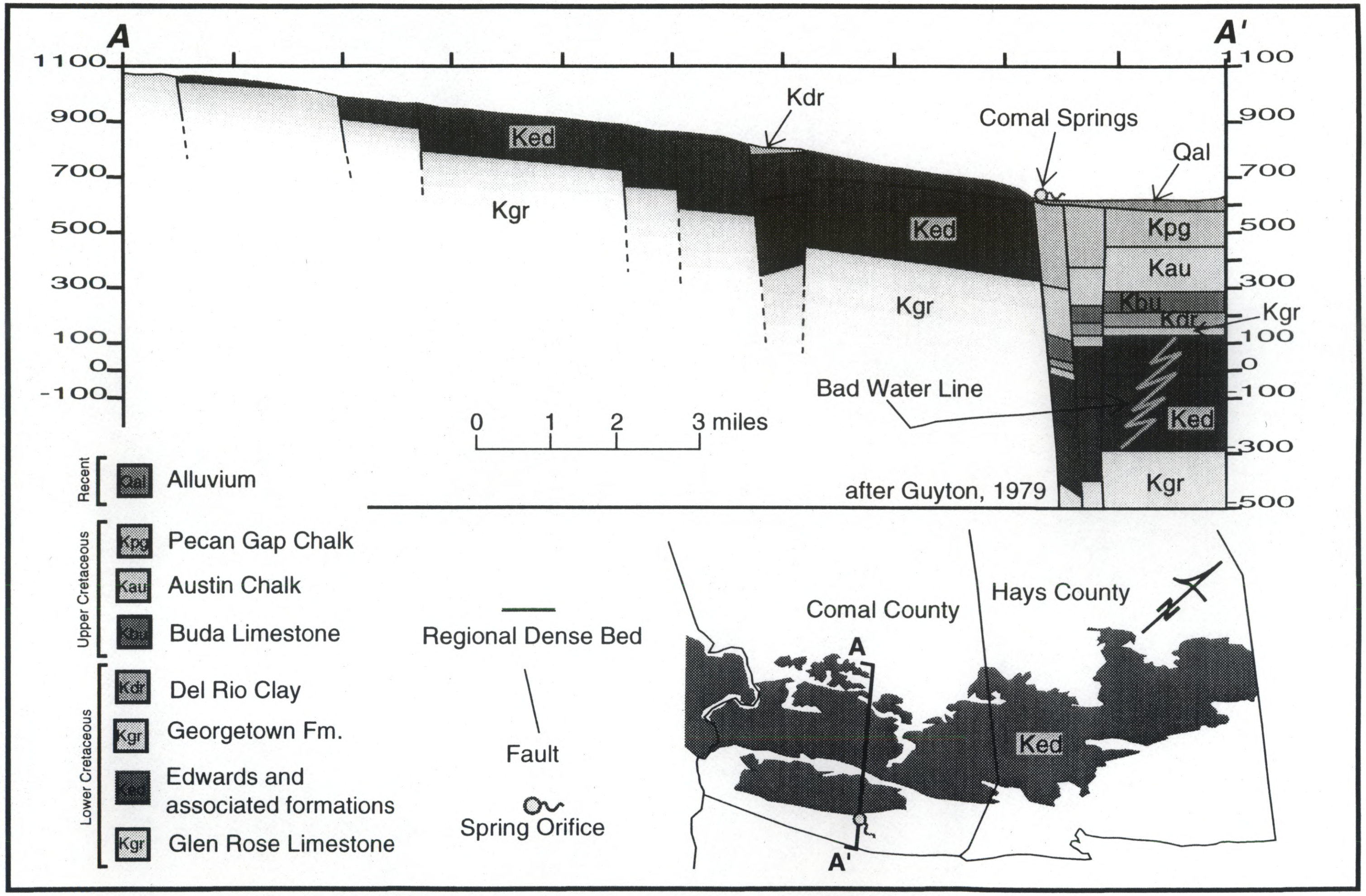

Figure 1.9 Cross section at Comal Springs

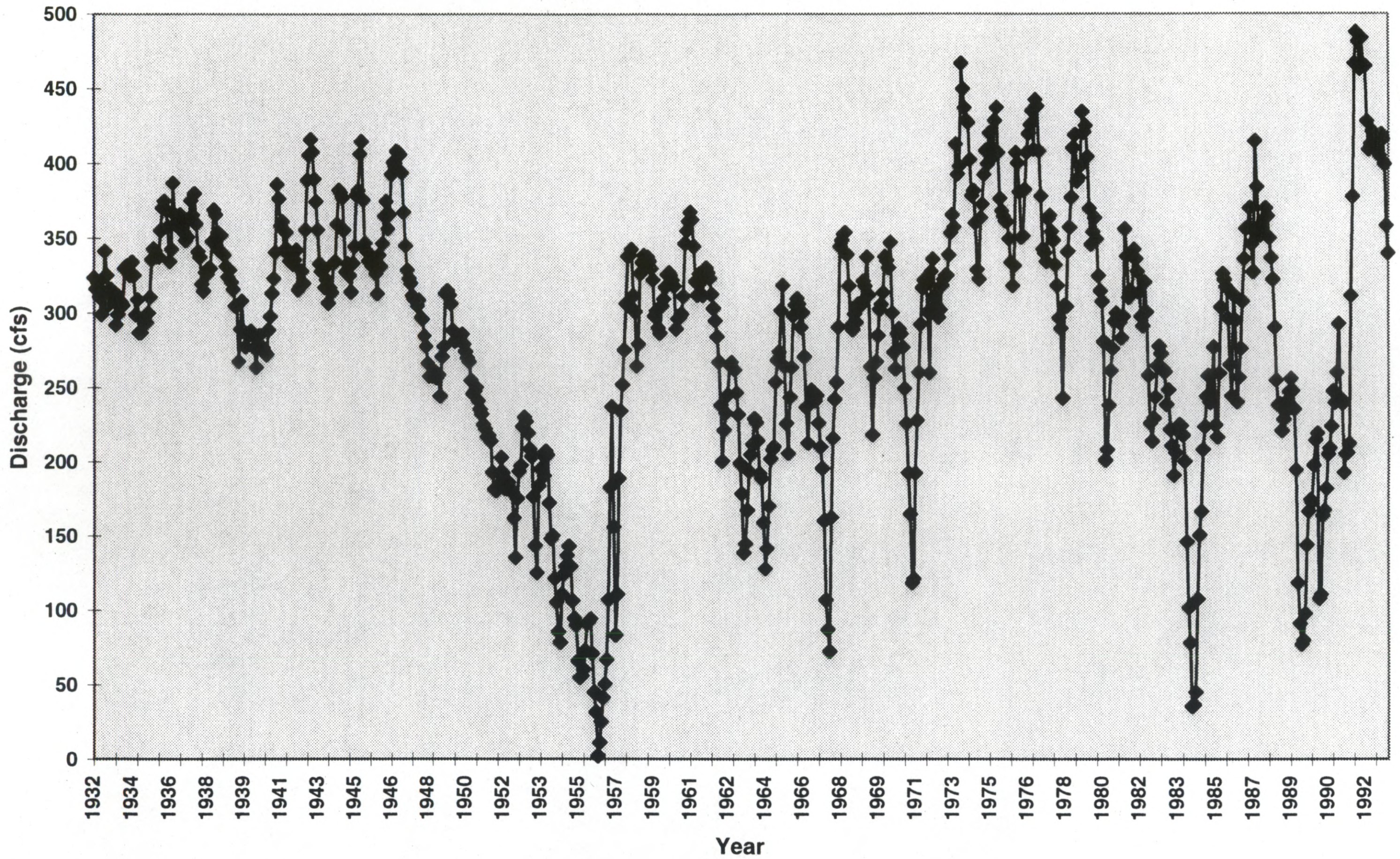

Figure 1.10 Spring discharge versus time; Comal Springs

1.4.2 San Marcos Springs

San Marcos Springs are located at Aquarena Springs in San Marcos, Texas, at an elevation of 574 ft (175 m) above mean sea level (Figure 1.11). These springs also issue from the base of the Balcones Escarpment. The springs at San Marcos discharge into Spring Lake, a man-made surface impoundment that acts as the primary source of the San Marcos River. This river eventually drains into the Blanco River.

Similar to Comal Springs, groundwater flows to the San Marcos spring system through highly transmissive karst channels in the Cretaceous limestone, and the spring orifices occur along the trace of a normal fault (the San Marcos Springs Fault) with significant offset (Figures 1.8 and 1.12). Groundwater discharges through five large fissures and numerous small openings at the bottom of Spring Lake.

A historical record of discharge from San Marcos Springs has been kept since 1956 (Figure 1.13). Over this time period, San Marcos Springs has flowed at an average rate of 170 cfs (4.8 m^3/s). The highest and lowest flow rate during the period of record was 451 cfs (12.7 m^3/s) and 59 cfs (1.7 m^3/s), respectively. Unlike Comal Springs, San Marcos Springs has never ceased to flow during the period of record (Brown *et al*, 1992).

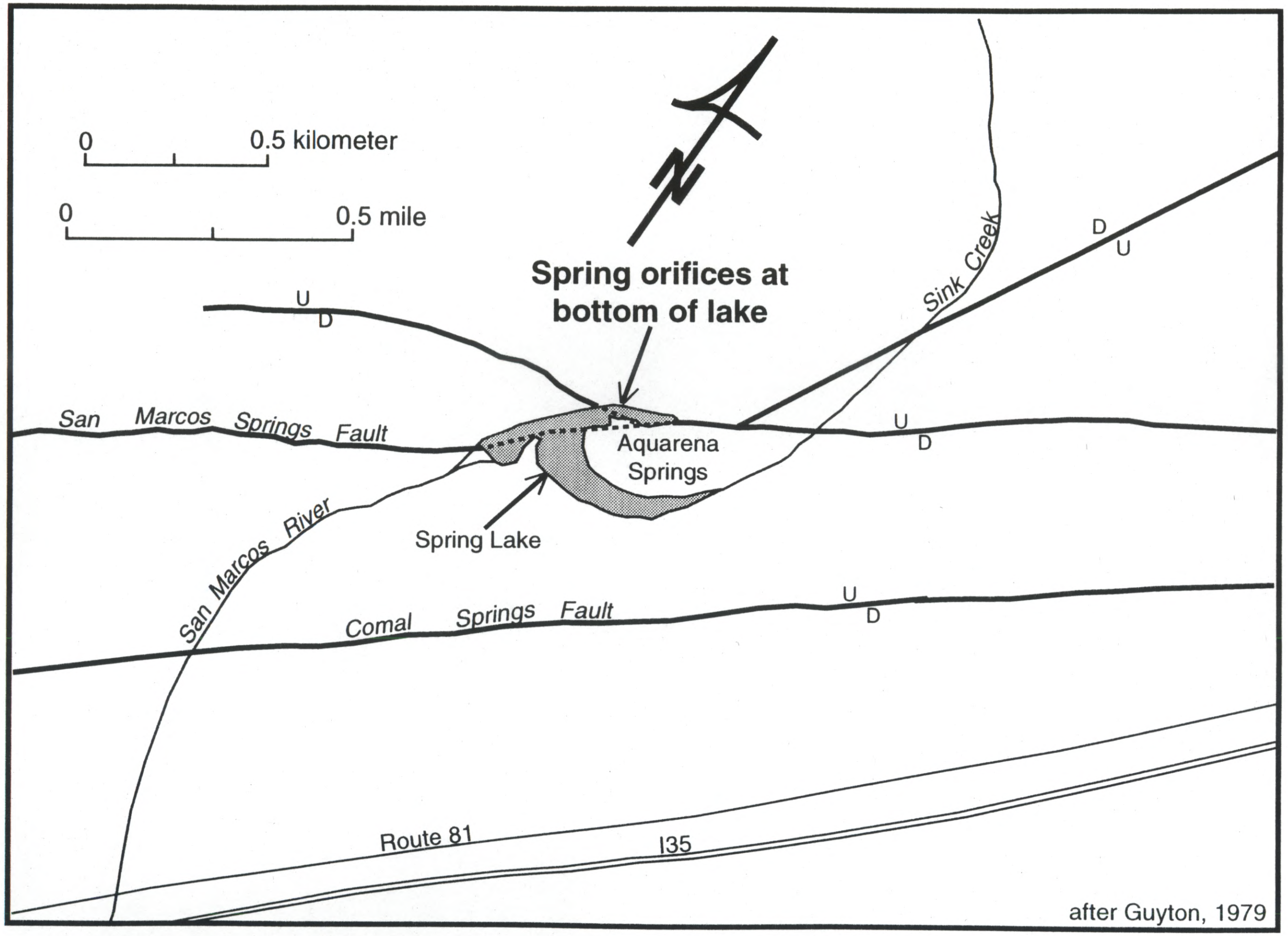

Figure 1.11 San Marcos Springs at Aquarena Springs Park in San Marcos, Texas

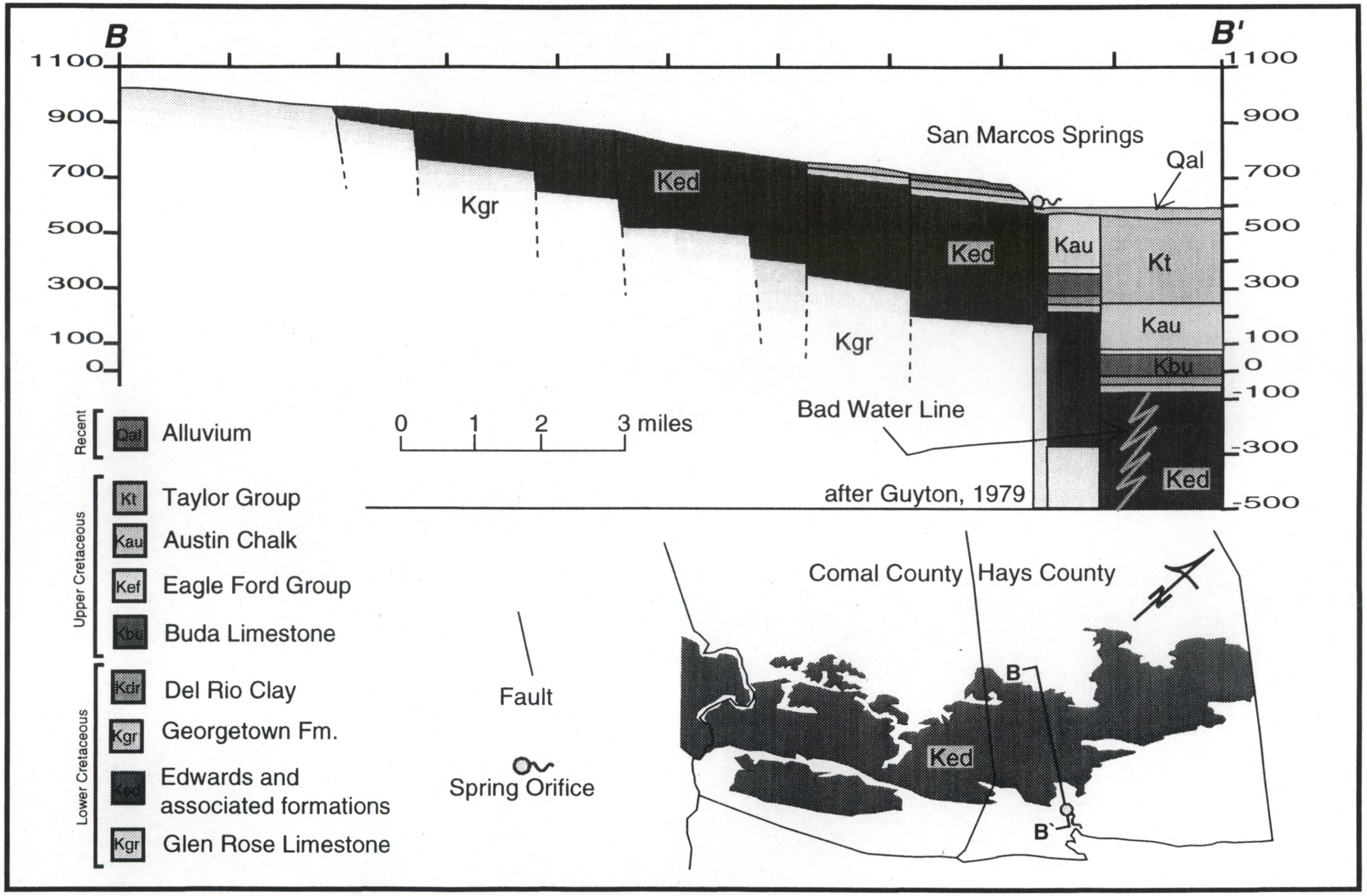

Figure 1.12 Cross section at San Marcos Springs

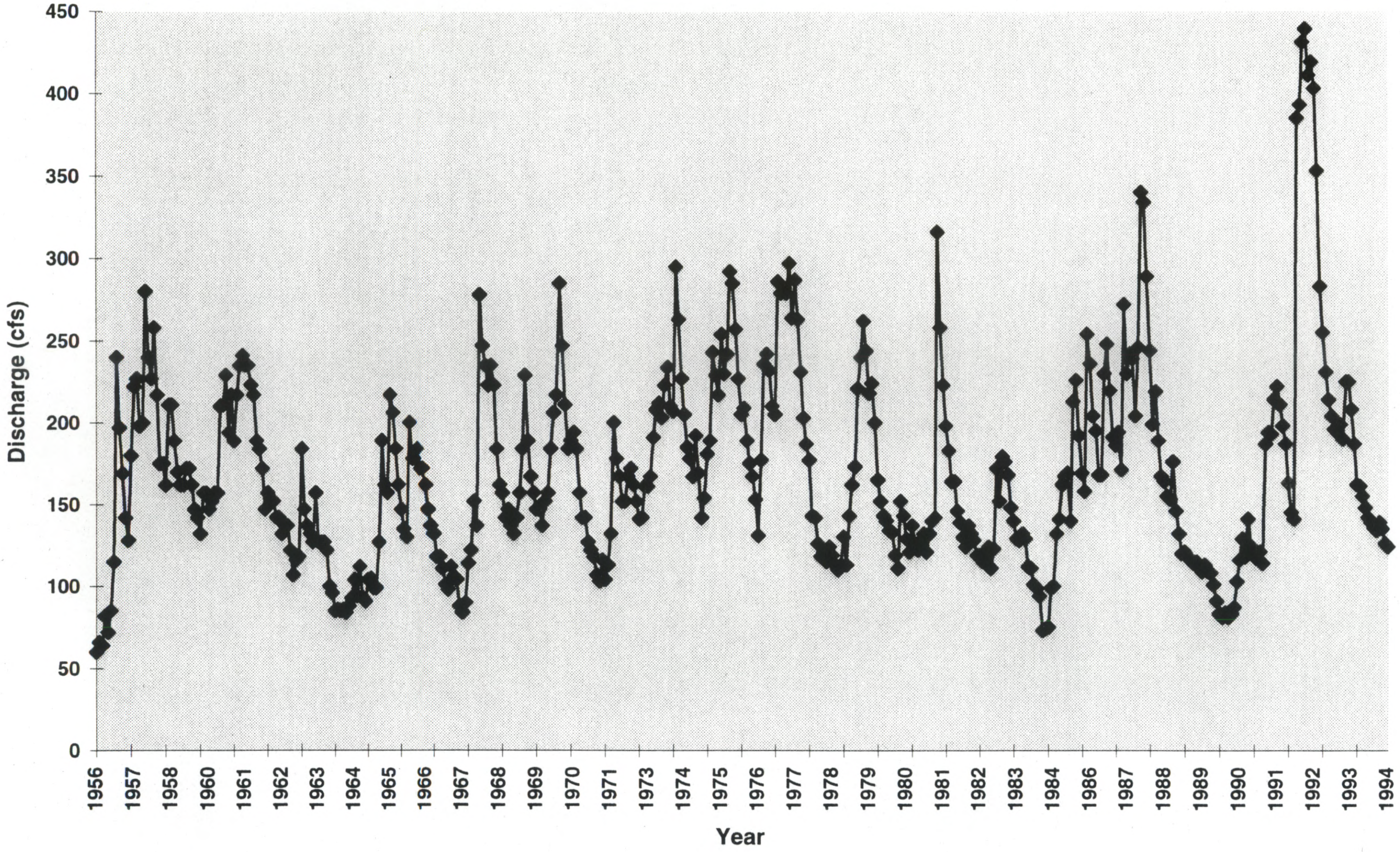

Figure 1.13 Spring discharge versus time; San Marcos Springs

2. THE EDWARDS AQUIFER: GEOLOGY AND HYDROGEOLOGY

2.1 General Description

The Edwards aquifer is located in Central Texas along the Balcones Fault Zone (Figure 1.1). A groundwater divide in Kyle, TX, separates the Austin Region section of the aquifer from the San Antonio Region section; this thesis deals exclusively with the San Antonio Region of the aquifer.

The groundwater resources associated with the Edwards and equivalent limestones can be divided into three parts (Figures 2.1 and 2.2). In the Edwards Plateau, exposure of the porous, flat-lying, relatively undeformed Edwards Group has resulted in the formation of a water-table aquifer. This section is known as the catchment area. Unless discharged by transpiration or pumpage, the water that infiltrates into the Edwards Plateau discharges into streams that drain the Edwards Plateau and run out over the exposed Glen Rose Formation towards the fault zone. Upon reaching the fault zone, these streams begin to lose flow to the Edwards rocks that have been exposed there by faulting and subsequent erosion. In this part of the aquifer, called the recharge zone, surface water infiltrates through the stream beds as streams flow across the fault zone towards the coast. Eventually, streams flow over areas where displacement by the faults has placed the Edwards rocks in the subsurface and below younger strata that act as confining beds. This part is called the confined, or artesian zone. In the confined zone, groundwater is channeled by the faults towards the northeast where, if not captured by a well, it eventually discharges at one of the springs in the area between San Antonio and San Marcos.

The Edwards aquifer in the San Antonio region is about 180 miles (275 km) long and varies in width from about 5 to about 40 miles (8 to 61 km). The total area of this section of the aquifer is approximately 2,500 square miles (3831 square km), of which about 2,000 square miles (3065 square km) is within the fresh water zone of the artesian aquifer (Maclay and Small, 1986). Groundwater divides in Hays County (Kyle, TX) and Kinney County (Brackettville, TX) form the north-eastern and western boundaries of the aquifer, respectively. The aquifer is bounded to the north by the up-dip limits of the Edwards Group outcrops. To the south, the freshwater zone of the Edwards is bounded by the "bad-water" line, a line that separates groundwater with less than 1000 mg/l of total dissolved solids (hereafter referred to as fresh water) from groundwater with greater than 1000 mg/l of total dissolved solids (hereafter referred to as saline or bad water). Comal Springs and San Marcos Springs are near the eastern end of the area and are about 25 miles (38 km) and 8 miles (12 km), respectively, from the Kyle groundwater divide.

Geologic mapping and hydrologic studies show that the Edwards is a complex karstified aquifer that supplies large quantities of water to wells and to large springs like the ones at Comal and San Marcos. The aquifer is intensively fractured, causing the limestone to be porous, permeable and receptive to recharge (Figure 1.8) (Caran *et al*, 1981; Maclay and Small, 1984, 1986; Maclay and Land, 1988). This breakup of the rocks has facilitated the development of karstic features, such as honeycombing, caves, caverns, and other solution channeling over wide areas in the freshwater zone. This karstification is not as extensive in the saline zone of the aquifer, where geochemical conditions favor mineral precipitation over dissolution (Hovorka *et al*, 1995). This results in a significantly lower permeability in the saline zone as compared to the freshwater zone (Hovorka *et al*, 1995).

This extensive fracturing and subsequent karstification in the freshwater zone of the aquifer make it capable of storing and moving large quantities of water. Large, high-discharge springs emerging from underground streams or caves (Lamoreaux *et al*, 1989), rather than small springs and diffuse seepage, are the general rule in regional karst aquifers like the Edwards. Most groundwater flow in these aquifers occurs in large solution openings which are capable of carrying large volumes of water to the springs.

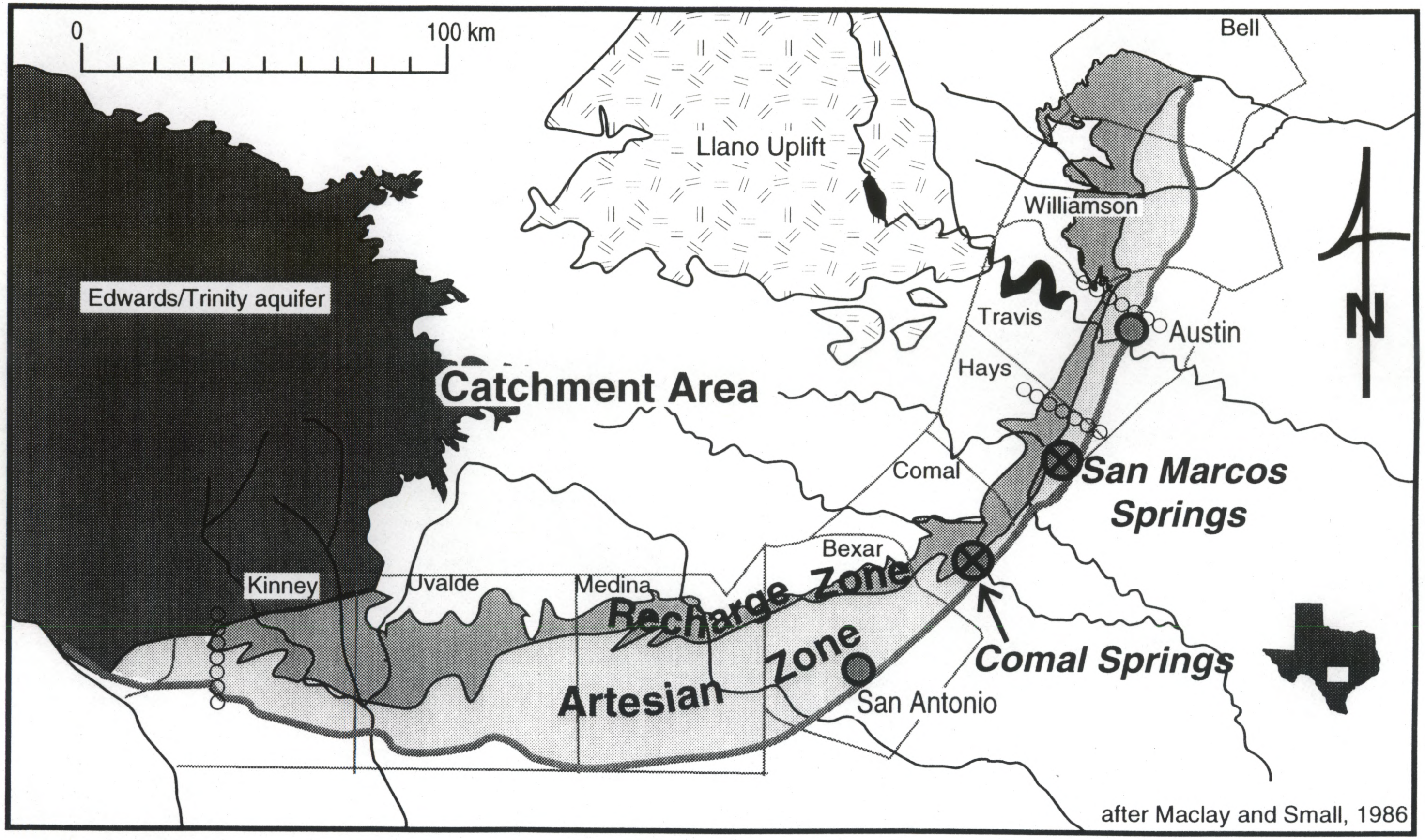

Figure 2.1 Map of the Edwards aquifer, showing the catchment area, the recharge zone, and the artesian zone

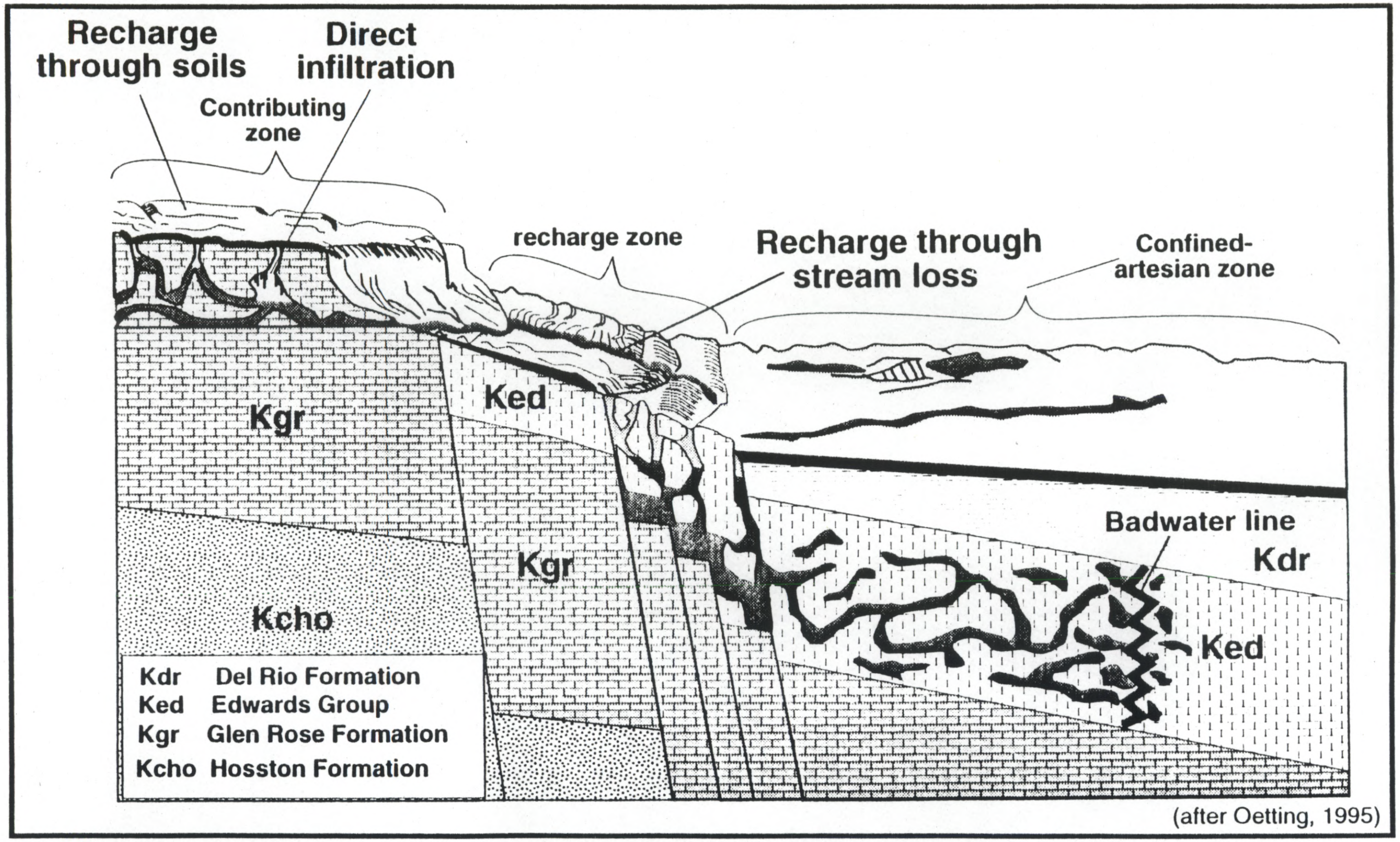

Figure 2.2 Schematic cross-section of the Edwards aquifer, showing the catchment, recharge, and artesian zones

2.2 Stratigraphy

The rocks that make up the Edwards Group extend across the San Marcos Platform, the Devils River Reef, and the Maverick Basin in a wedge which thickens to the south and southwest from about 200 ft (61 m) to about 900 ft (275 m) (Figure 2.3) (Rose, 1972; 1986). During the Early Cretaceous, a shallow marine carbonate shelf similar to the modern Bahama Banks covered most of Texas and deposited the Edwards aquifer formations. A broad rise formed by the Central Texas Platform and its southern extension, the San Marcos Platform, divided the carbonate shelf into shallower tidal flats and deeper basinal depositional provinces. While tidal flats and shallow lagoons alternated with open shelves on the platform, deeper water in the adjacent basins promoted the growth of rudistid and algal bioherms on platform margins, especially in the Devils River Reef north of the Maverick basin and at the shelf edge. The current stratigraphic nomenclature of the aquifer also reflects these different sedimentary environments and resulting lithofacies (Figure 2.4) (Klemt *et al*, 1979).

In the area of the springs, the Cretaceous Edwards Group consists of 400 to 600 ft (122 to 183 m) of thin to massive bedded limestone and dolomite. The lower confining unit of the Edwards aquifer is the upper shaley member of the Glen Rose Formation and, where present, the Walnut Clay. The upper confining unit of the artesian zone of the aquifer is the Del Rio Clay.

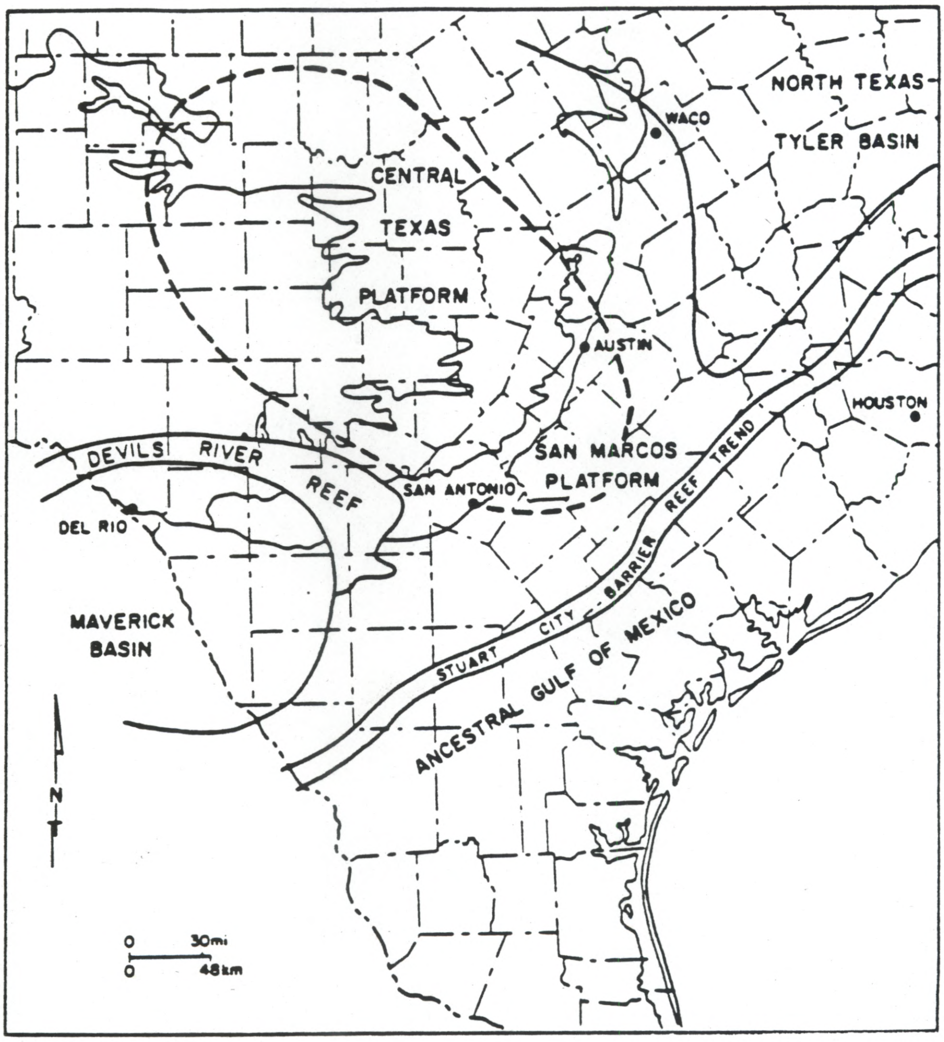

Figure 2.3 Map of the basins and platforms that affected deposition of the Edwards aquifer (after Jacka and Stevenson, 1977)

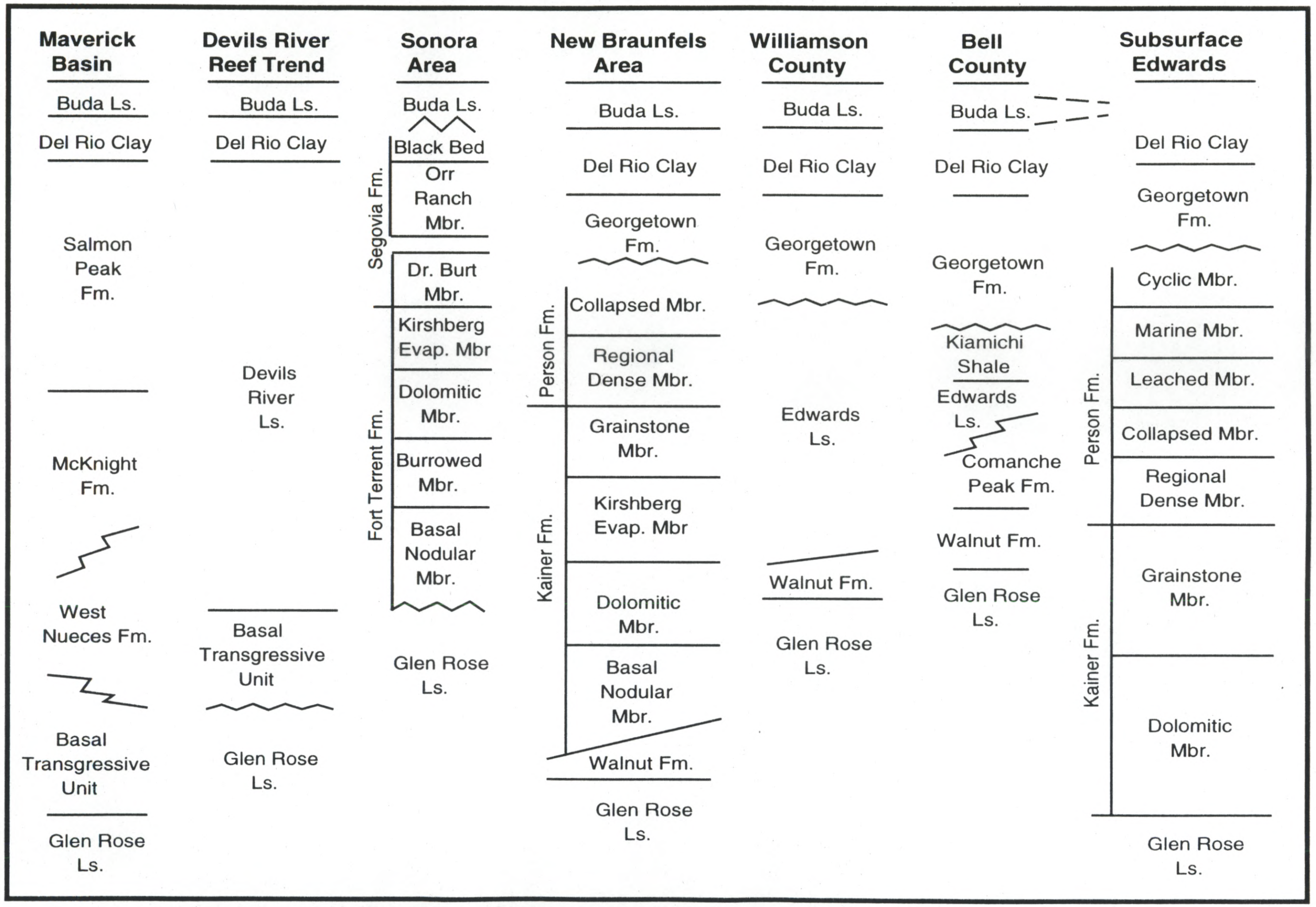

Figure 2.4 Stratigraphic columns of the Edwards aquifer (after Sharp, 1990)

2.3 Structural Features

The Balcones Escarpment is the surface expression of the Balcones Fault Zone, a series of sub-parallel, discontinuous, high-angle, normal faults which strike northeast and generally display a net down-to-the-coast displacement (Figure 2.5). Although most individual faults exhibit less than 200 ft (61 m) of throw, some faults offset the aquifer by as much as 900 ft (275 m) (Small, 1986). The Edwards aquifer is vertically displaced for its entire thickness at several places along several major northeastward-striking normal faults (Small, 1986).

The Luling Fault Zone, located approximately 10-20 miles (15 to 30 km) southeast of the Balcones Escarpment, extends from Caldwell to southeastern Medina County. The Luling Fault Zone is also a belt of sub-parallel normal faults similar to but more narrow than the Balcones Fault Zone. Unlike the Balcones Fault Zone, the individual faults of the Luling Fault Zone are generally downthrown to the northwest rather than to the southeast (Maclay and Land, 1988). Fault displacement within the Luling Fault Zone varies from a few feet to a combined displacement of more than 1,500 ft (457 m).

These features appear to follow persistent zones of weakness in Paleozoic basement rocks deformed during the Pennsylvanian Ouachita-Marathon orogeny. Faults affect and control the movement of groundwater in the aquifer by providing conduits for groundwater flow and by creating flow barriers where high-permeability aquifer units are displaced against low-permeability beds (Maclay and Land, 1988).

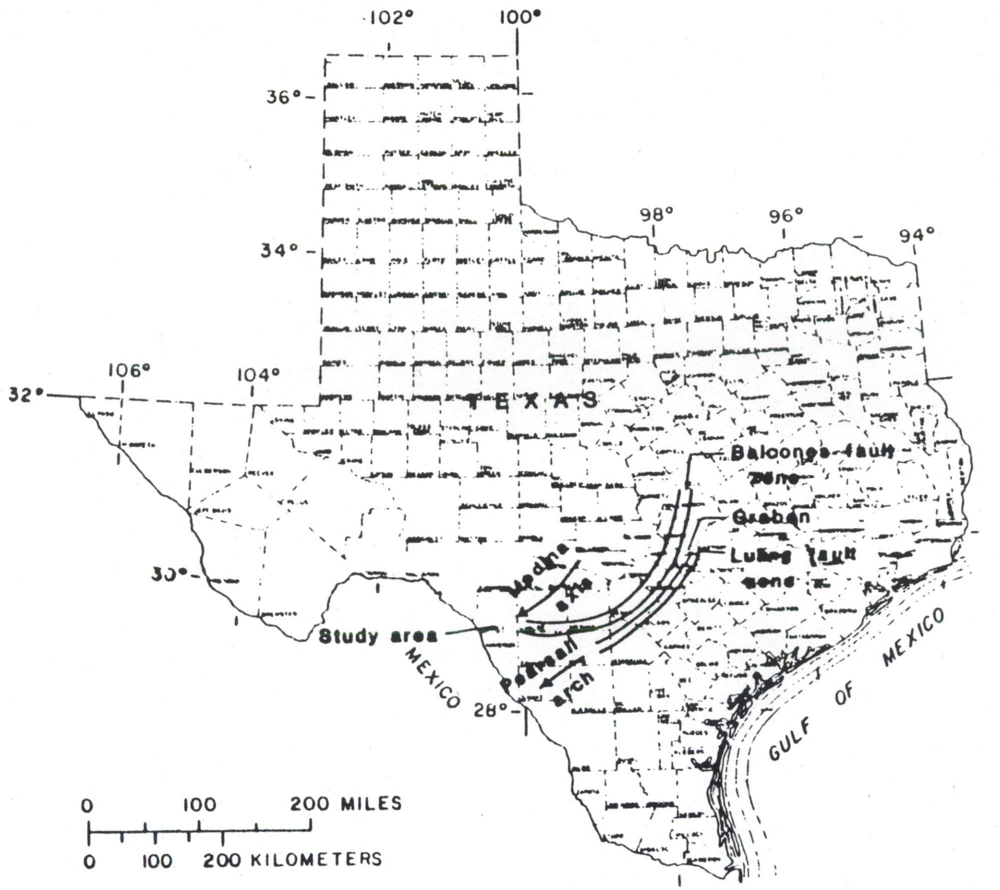

(after Rose, 1972)

Figure 2.5 Structural features in Central Texas

2.4 Hydrogeology: Flow Directions and Hydraulic Parameters

In general, the natural hydraulic gradient of the water in the Edwards points from the updip boundary of the unconfined zone towards the coast (Figure 2.6). However, the faults of the Balcones Fault Zone exert a strong influence on the direction of flow. Flow barriers (formed by the displacement of permeable beds against confining units) and high-permeability subsurface channels (created along the faults by karstification) in the confined zone interrupt the normal flow patterns and channel groundwater sub-parallel to the strike of the faults. The result is a strong east to north-east component of flow in the Edwards (Figure 2.7), with an average velocity of about 27 ft/d (9.5×10^{-5} m/s) (Maclay and Small, 1986). Because of this influence on flow by faults striking sub-parallel to the equipotential lines (Clement, 1989), the flow vectors are generally not perpendicular to the equipotentials. This creates a pattern of flow paths that is not directly inferred from the potentiometric surface.

Low hydraulic gradients, good correlation of water levels among widely spaced wells, large sustained springflows, and uniform temperature and water quality within the aquifer indicate a high transmissivity in the confined zone. However, quantification of transmissivity in a solutioned and heterogeneous carbonate aquifer lacking a uniform distribution of permeability (like the Edwards) is difficult. Klemt *et al* (1979) analyzed pump test and specific capacity information with analytical solutions that assume radial flow, homogeneity, and an laterally extensive aquifer, reasoning as per Eagon and Johe (1972) that the Edwards aquifer follows these assumptions for long-term tests. Klemt *et al* (1979) observed transmissivities ranging from 133 ft^2/d (0.00014 m^2/s) in the Edwards outcrop to over 2.6 million ft^2/d (2.8 m^2/s) in the confined zone in Bexar and Comal Counties. Maclay and Small (1986) created a map of relative transmissivity values for the Edwards (based on specific capacity tests) in which they divided up the aquifer into 21 subareas, each assigned an ordinal rating from 0 to 10. Estimates range from very low values in parts of the recharge area to an ordinal rating of 10 (about 2 million ft^2/d (2.2 m^2/s)) for the most permeable areas of the confined zone (Figure 2.8). Maclay and Small (1988) used previously published transmissivity estimates and a numerical model of the Edwards to estimate transmissivity ranges of 8600 to 1.7 million ft^2/d (0.0092 to 1.8 m^2/s) in the unconfined zone and 1.7 million to 8.6 million ft^2/d (1.8 to 9.2 m^2/s) in the confined zone. Hovorka *et al* (1995) estimated transmissivities ranging from 0.1 to 10 million ft^2/d (0.00000012 to 11.6 m^2/s).

Faults within the Balcones Fault Zone form the main conduits for flow within the Edwards aquifer and are responsible for its very high transmissivity (Sharp, 1990; Woodruff and Abbott, 1979).

Hovorka *et al* (1993) have generated a three-dimensional, cell-based model of the distribution of total porosity in the Edwards. They found that total porosity in the Edwards ranges from low values of 4 to 12 percent in the finer grained highstand facies to high values of 20 to 42 percent in grainstones and leached dolostones. Average total porosity for the entire aquifer is 21.7 percent. If the 1972 potentiometric surface of the unconfined zone is taken as an average water level, the average total volume of water in storage in the aquifer, based on their model, is 215 million af (265.2 billion m^3), with about 27 percent, or 58.5 million af (72.2 billion m^3) in the unconfined zone. The difference in total water volume between the maximum historic water level and the level when Comal Springs became intermittently dry is 6.9 million af (8.5 billion m^3), or approximately 3 percent of the total water in storage (Hovorka *et al*, 1993). Hovorka *et al* (1993) also estimated that the specific retention of the unconfined zone is 58 percent of porosity, which is consistent with Maclay and Small's (1976) estimation of a specific retention of at least 50 percent.

The total volume of the unconfined zone represents 30 to 40 percent of the total volume of the entire aquifer. Maclay and Small (1984) estimated a range of storativity values in the confined zone from 1.0×10^{-4} to 1.0×10^{-5}. Slade *et* al (1985) used a finite difference model of the Edwards aquifer in the Austin area to determine an estimated storage coefficient range of 3.0×10^{-5} to 6.0×10^{-5} for the confined zone and a specific yield range of 8.0×10^{-3} to 6.4×10^{-2} for the unconfined zone. Maclay and Small (1986) calculated a confined storage coefficient of 1.6×10^{-4}. Hovorka *et al* (1993), calculated an average storativity for the confined zone of 2.6×10^{-4}, using barometric efficiency and interpolated porosity.

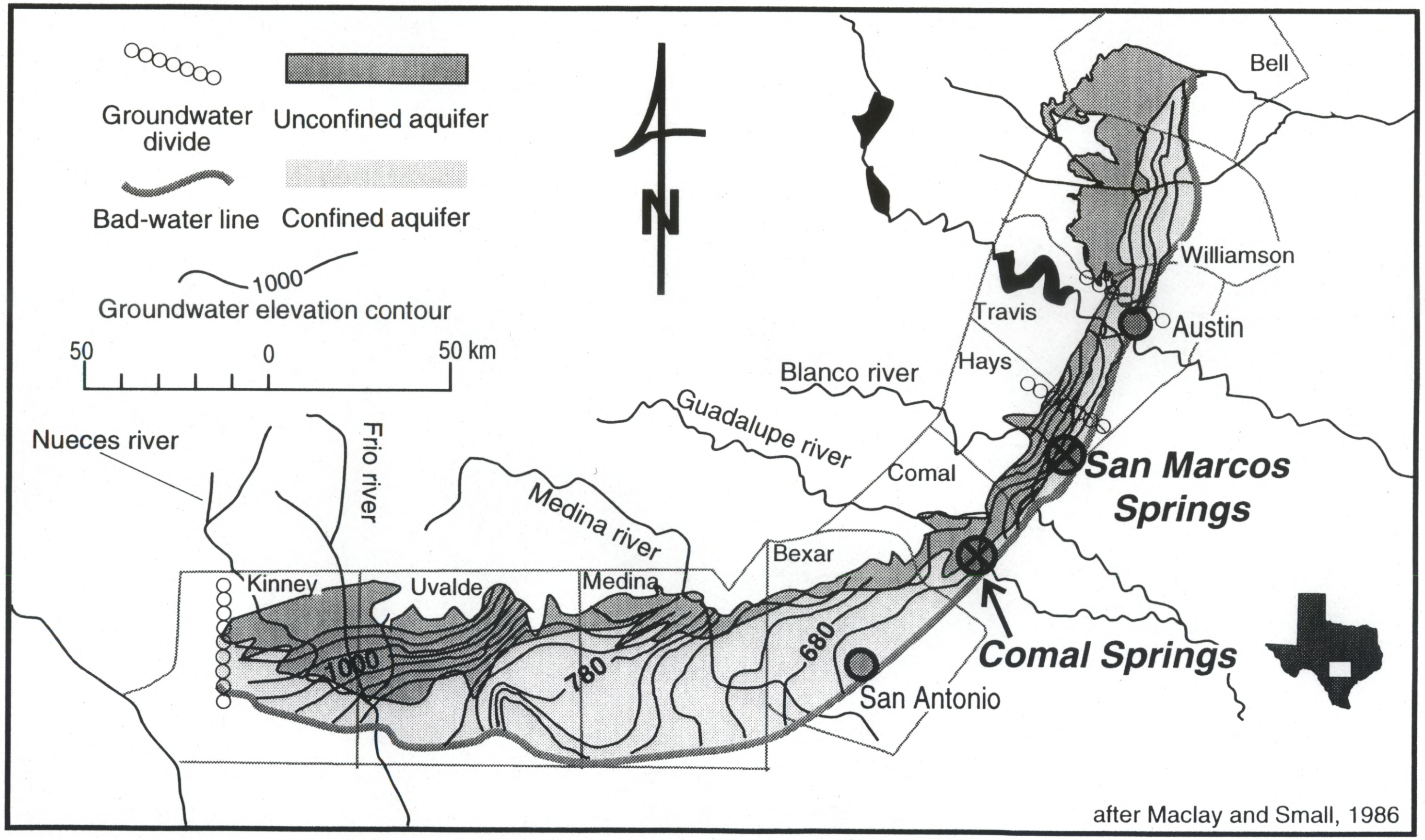

Figure 2.6 Groundwater contour map of the Edwards aquifer

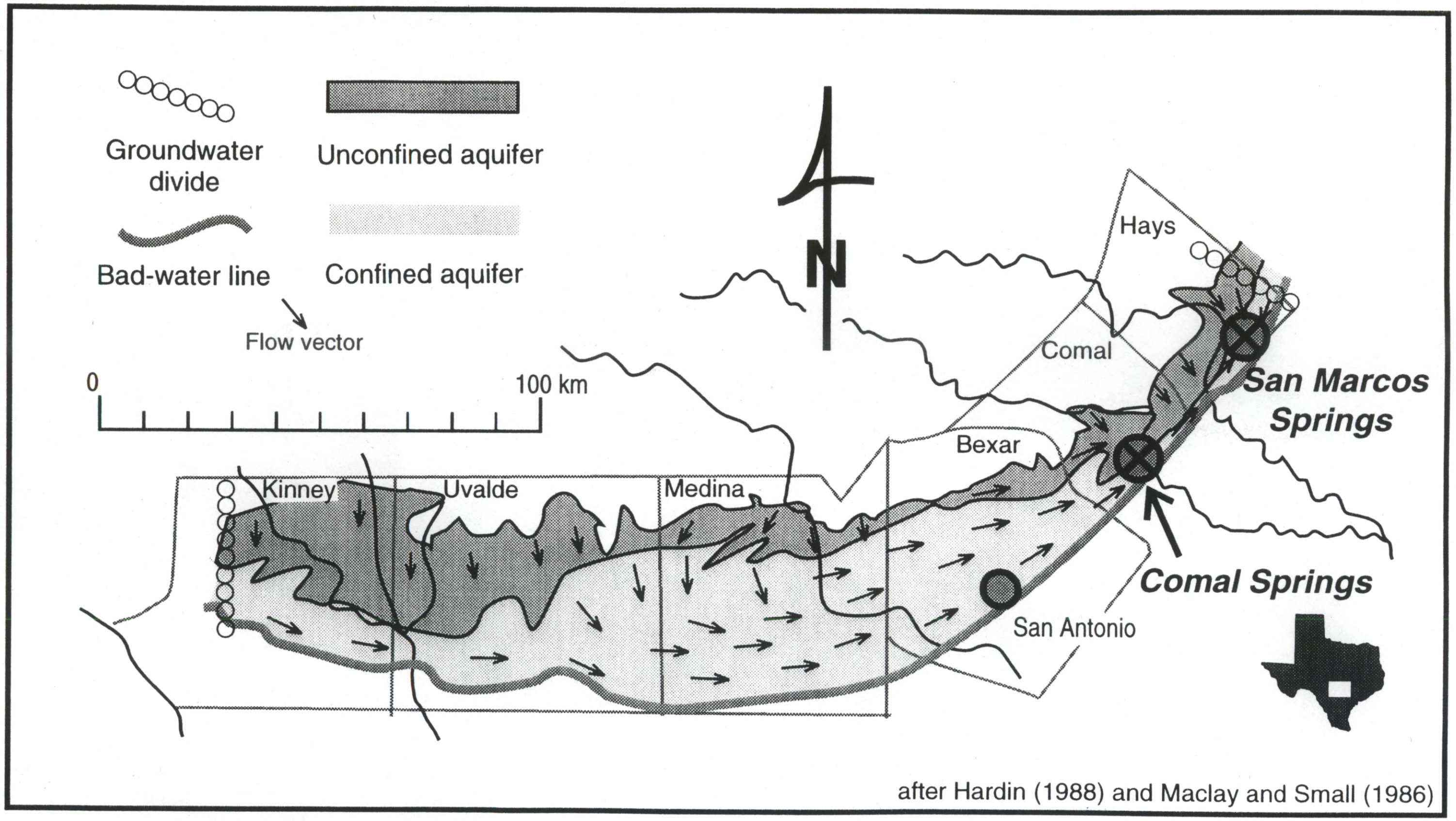

Figure 2.7 Groundwater flow vectors in the San Antonio region of the Edwards aquifer

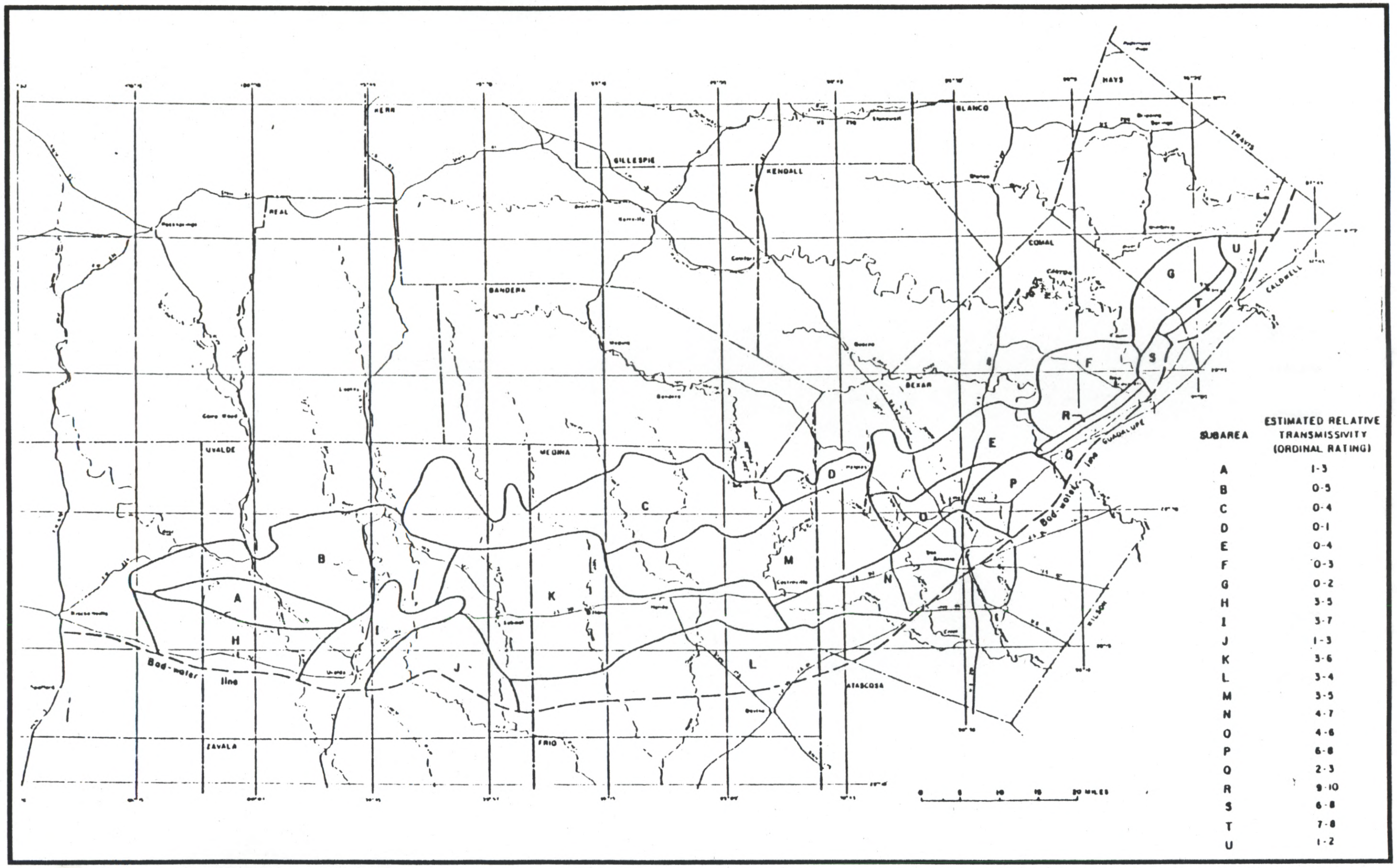

Figure 2.8 Transmissivity zones in the Edwards aquifer (after Maclay and Small, 1986)

2.5 Recharge

Recharge occurs primarily along the northern edge of the Balcones Fault Zone where faulting has exposed the Edwards formation and equivalent rocks. Streams draining the Cretaceous rocks of the Edwards Plateau generally lose all of their base flow and much of their storm runoff by infiltration through the stream beds as they flow over the porous and fractured rocks of the Edwards aquifer. Infiltration through stream beds may account for 60 to 80 percent of the recharge to the Edwards aquifer (Rothermel and Ogden, 1987); the remainder of the recharge is the sum of direct infiltration in the interstream areas and a small amount of cross-formational flow from the Glen Rose Formation. Such interformational flow most likely occurs where faults juxtapose the Glen Rose Formation against the Edwards aquifer. Locations of the major faults within the Balcones Fault Zone are shown in Figure 2.5.

Since 1963 the U. S. Geological Survey has analyzed the tritium content of samples from selected wells, springs, and streams of the Edwards aquifer. The highest tritium concentrations (greater than 20 tritium units (TU)) occur in the updip areas of the Edwards outcrop, along the western border of the aquifer. These high tritium values indicate that groundwater in this area has recently (within the last 50 years) infiltrated and recharged the aquifer. Very low tritium values (less than 1 TU) are present in samples taken from deep in the confined zone of the aquifer, along the aquifer's southern and southeastern boundary. These low values suggest that a significant amount of tritium has not yet penetrated into the deeper parts of the aquifer. In general, tritium distribution within the Edwards aquifer confirms that significant recharge to the aquifer occurs in the outcrop portion of the aquifer, and that groundwater flows from the outcrop area into the confined area (Pearson, Rettman, and Wyerman, 1975).

The amount of recharge to the Edwards is estimated by adding the measured loss of stream flow from streams crossing the Edwards outcrop to estimates of rainfall infiltration in the interstream areas of the outcrop. The average annual recharge for the period 1934-1992 is estimated by the Edwards Underground Water District (EUWD) (Brown *et al*, 1992) to be 682,800 af (842 million m^3) per year. The maximum annual estimated recharge of 2,486,000 af (3,066 million m^3) occurred in 1992, and a minimum estimated annual recharge of 43,700 af (54 million m^3) occurred in 1956 (Brown *et al*, 1992). Average annual discharge for the same period is estimated to be 647,300 af (798 million m^3). Estimates of average annual recharge and discharge for the aquifer over this time period are presented in Table 3 in Appendix D. Discharge includes pumpage from wells in the aquifer as well as springflow from Comal, Hueco, San Marcos, Leona, San Antonio, and San Pedro Springs. The balance of cumulative recharge and discharge over the past 50 years in the San Antonio area (cf., Reeves and Ozuma, 1986) suggests that the aquifer may be approximated by steady-state flow conditions over the long term.

The Edwards aquifer often exhibits seasonal or weather-related variations in well levels of many feet, and in the recharge area water table response to isolated rains can be nearly instantaneous. The reason for this rapid response to precipitation is because the large infiltration capacity of the karst terranes can transmit a large volume of water to the subsurface in a short period of time.

2.6 Summary

The Edwards aquifer, one of the most productive groundwater resources in the world, is a highly faulted, fractured, and karstified aquifer. The fracturing and subsequent karstification has created zones of high transmissivity within the aquifer. This ability of the aquifer to transmit large quantities of water through discrete zones in the subsurface has led to the development of several high discharge springs in Hays and Comal counties. Based on average spring discharge from 1940 to 1985, two of these springs, Comal and San Marcos Springs, are the two largest springs in the state.

The hydraulic gradient in the aquifer is generally downdip, towards the coast. However, faults oriented sub-parallel to the equipotential lines influence the flow of water in the aquifer, so that groundwater flow is primarily from the west to the northeast. Recharge to the Edwards aquifer occurs primarily where the Edwards formation and equivalent rocks are exposed on the upthrown side of the Balcones Fault Zone.

3. THE HYDROGEOLOGY OF THE SPRINGS: LOCAL FLOW SYSTEMS AND RECHARGE AREAS

At each spring site, groundwater discharges through orifices located along major normal faults which have displaced the aquifer against lower permeability beds. The majority of subsurface flow to each spring moves though these faults. However, there are differences between the two spring systems in both the orientation of the flow paths to the springs and in the amount of local recharge versus regional recharge that each spring gets. This chapter describes the flow system and recharge at each site.

3.1 Comal Springs

3.1.1 Local Flow System

Comal Springs (Figure 1.8) issue from the Comal Springs Fault, the most conspicuous fault in the Balcones Fault Zone in this area. At some places along the fault, including at Comal Springs, the Cretaceous Taylor Marl - a 300 ft (91 m) thick confining bed - is faulted into contact with the Edwards aquifer, indicating a stratigraphic displacement of 400 to 600 ft (122 to 183 m) (Figure 1.9). This displacement of the aquifer against the Taylor Marl, coupled with the exceptional karstic development of the Edwards aquifer and the topographic low at the spring site, is responsible for the existence of Comal Springs.

Groundwater flow appears to be concentrated along the strike of the Comal Springs Fault throughout most of its length between San Antonio and New Braunfels. Extensive karstification along the fault has created a highly transmissive zone (subarea R, Figure 2.8) that Maclay and Small (1986) consider the most transmissive zone in the entire aquifer. Subarea R is a two mile wide by 17 mile long (3.1 by 26 km) subsurface corridor that reaches from the Comal-Bexar County line just north of Interstate Highway 35 to Comal Springs at New Braunfels. Well yields in this zone are very large, and geophysical logs indicate that both the Person and Kainer Formations (the formations that make up the Edwards aquifer in this zone) are extremely cavernous.

The surface geology of the Comal Springs area is relatively simple. In the immediate vicinity of Comal Springs, the Edwards aquifer rocks crop out north of the Comal Springs Fault, while the area to the immediate south of the fault is Taylor Marl overlain by Quaternary alluvium (William F. Guyton and Associates, 1979). The subsurface situation is more complex. The Comal Springs fault and two other parallel faults of lesser displacement to the southeast have displaced the beds of the aquifer by as much as 750 ft. Lower permeability beds of the Taylor Group, Austin Group, Eagle Ford Group, Buda Formation, and Del Rio Formation form subsurface barriers to southeastward groundwater flow in the Edwards aquifer (William F. Guyton and Associates, 1979). These flow barriers channel groundwater to the northeast, in the direction of Comal Springs.

3.1.2 Recharge

The majority of water discharging from Comal Springs is from regional recharge areas far from the springs (possibly across several counties). There is only minor local recharge. These two possible areas of recharge are discussed separately.

3.1.2.1 Regional

Most of the water discharging at Comal Springs flows to the springs along routes that parallel the faults and extend westward from the springs across several counties. The flow reach extends westward as far as the Brackettville divide in Kinney County 140 miles (215 km) west of Comal Springs. A significant portion of the total flow to the springs is within the artesian part of the Edwards aquifer, where secondary permeability has been enhanced by faulting, fracturing, and karstification. Much of this flow is within the narrow, 2 mile (3.1 km) wide corridor known as subarea R (Figure 2.8)(Maclay and Small, 1986)

Tritium studies by Pearson, Rettman, and Wyerman (1975) show that Comal Springs had what was probably pre bomb-era tritium only in 1963 and 1964, and from 1967 to 1971 has had a maximum of only 6.7 TU. Tritium concentrations reached a maximum of 7.0 TU in 1975 and 1977 as reported by Maclay, Rettman, and Small (1980). Nalley and Thomas (1990) reported tritium concentrations of only 4.4. TU in 1989. These low tritium values imply that water discharging from Comal Springs has experienced a considerable residence time in the aquifer. Recharge from areas far west of the springs, such as Kinney or Uvalde Counties, would provide longer travel paths and, consequently, greater residence time in the aquifer. Most likely, the majority of the water issuing from Comal Springs originally entered the aquifer in one of these counties on the western side of the Edwards Aquifer. It is also likely that this water has had little opportunity to mix with any recently recharged water (Pearson, Rettman, and Wyerman, 1975).

Water chemistry and dye tracing studies were done in 1982 and 1983 (Rothermel and Ogden, 1986) for Comal Springs. Spring water samples were taken weekly over a 2-year period (more frequently during storm events) from four spring orifices at Comal Springs to determine if any local recharge was affecting water chemistry and discharge volumes. A tritium value of 5.0 TU obtained from Comal Springs by Rothermel and Ogden (1986) indicates a considerable residence time for the spring water. This reinforces the findings of Pearson, Rettman, and Wyerman (1975), who got a maximum of 6.7 TU in 1971, that recharge areas are distant from the springs. In addition to their tritium data, Rothermel and Ogden (1986) noted that water issuing from Comal Springs exhibited a lack of turbidity during and after storms, low coefficients of variation for different chemical constituents, and warmer temperature than the approximate mean annual air temperature. These observations, along with their inability to dye-trace local sink sites in the area of the springs, also indicate that recharge areas for Comal Springs are not, for the most part, local.

3.1.2.2 Local

The average annual water budget shows that Cibolo and Dry Comal Creeks, in the vicinity of Comal Springs, contributed 106,700 acre-ft/yr (132 million m^3/yr) of recharge to the Edwards aquifer (Brown *et al*, 1992). This is approximately 30 percent of annual discharge from Comal Springs. However, water-chemistry studies have shown little variation of water quality and water temperature following storm events (Ogden, Quick and Rothermel, 1986). Spring response to storm events seems to indicate that Comal Springs is not receiving a significant amount of local recharge. In addition, the tritium studies by Pearson, Rettman, and Wyerman (1975) indicate a regional source for the spring water. It is therefore believed that "faulting has hydrogeologically isolated Comal Springs from any large sources of local recharge" (Ogden, Quick and Rothermel, 1986).

3.2 San Marcos Springs

3.2.1 Local Flow System

San Marcos Springs, like Comal Springs, issue from the Edwards aquifer at the base of the Balcones Escarpment. The points of discharge occur where the fault intersects the land surface at topographic lows within Spring Lake, the pool which receives spring flow.

San Marcos Springs Fault is the continuation of the Hueco Springs Fault in Comal County (George, 1952) (Figure 1.8). The San Marcos Springs Fault (including the Hueco Springs Fault continuation) is about 35 miles (54 km) long and extends from a point near the Bexar County - Comal County border, past San Marcos Springs to its termination point in southeastern Hays County. The stratigraphic displacement caused by the San Marcos Springs Fault in the vicinity of San Marcos Springs is greater than 300 ft (91 m) (Figure 1.12) (DeCook, 1956).

Concentrated groundwater flow appears to occur where the Edwards aquifer is cut by the San Marcos Springs Fault. Intense fracturing and extensive karstification in a wide area on both sides of this fault has resulted in a zone of high transmissivity. This zone, referred to as subarea T in Figure 2.8, is a narrow corridor about 3 miles (5 km) wide and 13 miles (20 km) long reaching from 10 miles (15 km) west of San Marcos Springs to 3 miles (5 km) east of the springs. Maclay and Small (1986) described subarea T as a very transmissive zone that has produced large capacity wells.

The surface around San Marcos Springs is more varied geologically than the Comal Springs area. Within a 1 mile (1.6 km) radius of the springs seven geologic formations have been mapped. Surface exposures of the Edwards aquifer rocks (the Person and Kainer Formations and the Georgetown Limestone) are restricted mostly to outcrops along stream channels or along topographic breaks on hillsides. The San Marcos Springs Fault cuts through the San Marcos Springs area and passes beneath Spring Lake. The Comal Springs Fault runs parallel to the San Marcos Springs Fault less than one-half of a mile south of the springs.

Figure 1.12, a geologic cross section through San Marcos Springs, shows the position of the Edwards aquifer in the subsurface. The Georgetown, Person, and Kainer Formations are close to the surface on the upthrown side of the fault in the vicinity of the springs. There is over 300 ft (91 m) of displacement along the fault, bringing massive confining beds, such as the Austin

Chalk, Eagle Ford Shale, Buda Limestone, and Del Rio Clay, adjacent to the Edwards aquifer on the downthrown side of the fault. Similar to the situation at Comal Springs, these tight confining beds form a subsurface barrier to normal groundwater flow southeastward, forcing groundwater to flow to the northeast as well as vertically upward along the fault plane to the surface.

A map of the potentiometric surface around San Marcos Springs by Ogden, Quick, and Rothermel (1986) suggests that flow lines in the aquifer around San Marcos Springs are converging on the springs (Figure 3.1). In addition, San Marcos Springs is the lowest discharge point in the San Antonio Region of the aquifer. This would indicate that San Marcos Springs is the final discharge point in this segment of the aquifer.

3.2.2 Recharge

San Marcos Springs, unlike Comal Springs, has both significant regional and significant local sources of recharge.

3.2.2.1 Regional

Some of the flow of San Marcos Springs may recharge in the western part of the aquifer, as far away as Kinney, Uvalde, and Medina Counties. Because the orifices at San Marcos Springs are 49 ft (15 m) lower in altitude than the Comal Springs orifices, water flowing in Comal County that does not discharge through Comal Springs will most likely flow past Comal Springs to discharge at San Marcos Springs (Guyton & Associates, 1979). Highly transmissive subsurface corridors, (subareas R and T on Figure 2.8), are present in the Edwards aquifer from west of San Antonio to San Marcos. These two subareas could convey groundwater in the Edwards past Comal Springs to the springs at San Marcos.

It may be possible that flow towards San Marcos Springs from recharge areas to the west may diverge from those conveying water to Comal Springs. This divergence might be caused by structural controls (i.e., faulting) in Comal and Hays Counties. More specifically, flow to Comal Springs is channeled in the subsurface by the Comal Springs Fault, whereas flow toward San Marcos Springs is channeled largely along the San Marcos Springs Fault which is sub-parallel to the Comal Springs Fault. These structures are a major influence in determining the recharge areas for San Marcos Springs (Ogden, Quick and Rothermel, 1986).

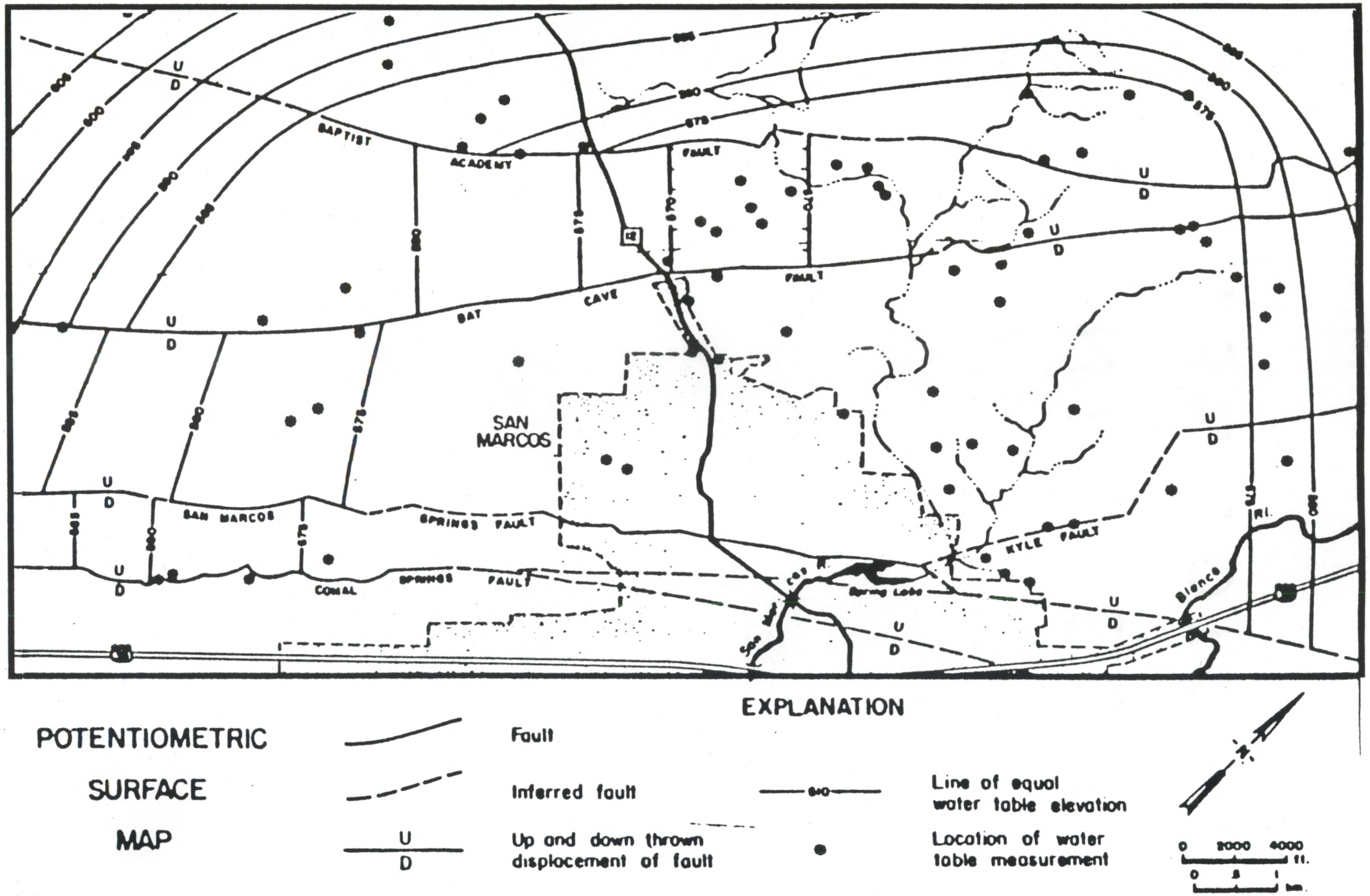

Figure 3.1 Potentiometric surface map of the San Marcos area (after Ogden et al, 1986)

Recharge areas for San Marcos Springs are probably closer to the springs than are the respective recharge areas for Comal Springs. This inference is based on the geographic location of the San Marcos Springs Fault, the eastward continuation of the Hueco Springs Fault. This 35 mile (54 m) long fault has its western extremity in a more northerly portion of the Edwards aquifer outcrop (recharge area) in Comal County and eastern Bexar County than does the Comal Springs fault. The latter is more closely associated with the artesian portion of the Edwards aquifer. Consequently, a possibly significant portion of the total discharge at San Marcos Springs may recharge in Comal County and eastern Bexar County at distances of 10 to 30 miles (15 to 46 km) west from San Marcos Springs. Substantiating this possibility were the tritium studies by Pearson *et al* (1975) who concluded that water recharging in northern Bexar and Comal Counties does not mix with water from further west in the Edwards, but rather flows to the east in a subsystem of its own and discharges at Hueco Springs and primarily at San Marcos Springs.

3.2.2.2 Local

Hydrographs from wells near San Marcos Springs show poor correlation with well levels in Comal, Bexar, Medina, and eastern Uvalde counties. This indicates that there is a component of local recharge to San Marcos Springs in addition to the regional recharge component. Because the groundwater flowpaths leading to San Marcos Springs are well-developed along the San Marcos Springs Fault, it is reasonable to expect that multiple recharge areas exist on the Edwards outcrop along and in close proximity to this fault.

West of San Marcos Springs, Purgatory Creek and York Creek cross the San Marcos Springs Fault and contribute significant recharge to the aquifer (Figure 3.2). Purgatory Creek has its headwaters in eastern Comal County but flows across the San Marcos Springs Fault in western Hays County at a point 2.5 miles (3.8 km) southwest of San Marcos Springs. York Creek is mostly in eastern Comal County, but enters Hays County in its lower reaches. York creek crosses the San Marcos Springs Fault just north of Interstate Highway 10 near the easternmost tip of Comal County, 10 miles (15 km) southwest of San Marcos Springs. In addition to these creeks, the Blanco River contributes a significant amount of recharge to the aquifer in Hays County. These sites probably contribute a relatively small amount to the total spring discharge. Pearson *et al* (1975) suggest that recharge in the immediate vicinity of San Marcos Springs accounts for less than 35 percent of springflow. They conclude that the remainder must be from areas further south and west in the Edwards aquifer. San Marcos Springs had tritium levels of 30 TU or more in 1964-71 compared to the Comal Springs maximum tritium level of 6.7 TU in 1971. This implies that much of San Marcos Springs discharge is locally recharged from areas east of Bexar County.

A hydrochemical and artificial tracer test study of San Marcos Springs by Ogden *et al* (1986) suggests that San Marcos Springs receives water from two distinct flow regimes. Tracer tests in the vicinity of the springs imply that a large percentage of the water discharging from San Marcos is moving northward from Comal and northern Bexar County along a narrow fault block created by the San Marcos Springs Fault. This water primarily discharges from the southern group of orifices at San Marcos (Ogden *et al*, 1986).

Dye-tracing studies in the vicinity of San Marcos Springs by Ogden *et al* (1986) also revealed a direct flow path to San Marcos Springs. Sodiumfluorescein green dye was injected into a deep lake at the bottom of a cave about 2 miles (3 km) west of San Marcos Springs. This injection site is along the San Marcos Springs Fault and is about 1 mile east of the Purgatory Creek crossing of the fault. Of the six orifices of the springs that were monitored, two (Deep Spring and Catfish Spring) were positive. The velocity of the dye travel was approximately 1,500 ft (457 m) per day. Water from none of the other four spring orifices monitored produced any dye. The conclusion drawn by Ogden *et al* (1986) is that water from San Marcos Springs is not from a single discrete pathway, but that the springs receive water from two distinct flow regimes.

3.3 Summary

Much of the groundwater flowing to Comal Springs flows along the Comal Springs Fault from southwest to northeast. The majority of recharge to Comal Springs is regional; only a small percentage is local. Similar to Comal Springs, a large portion of the flow to San Marcos Springs moves along the San Marcos Springs Fault. However, San Marcos Springs does receive a considerable amount of local recharge. In addition, flow lines in the area of the spring appear to converge on the spring orifices.

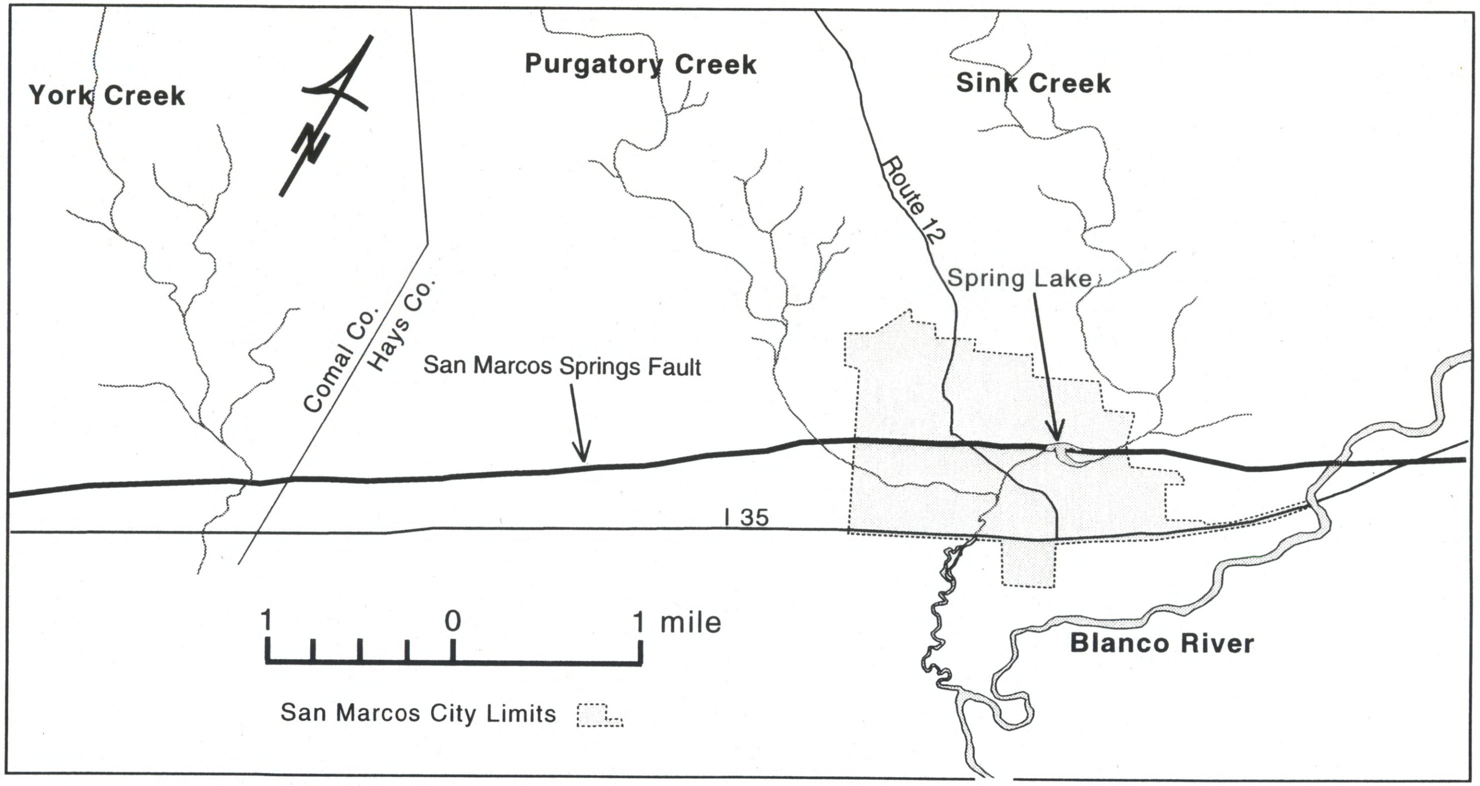

Figure 3.2 Locations of streams crossing the San Marcos Springs Fault

4. POTENTIAL METHODS OF SPRINGFLOW AUGMENTATION

4.1 Introduction

Augmentation of springflow for the purpose of maintaining discharge from Comal and San Marcos Springs during low flow periods is proposed. Five possible methods of springflow augmentation, two that involve modifications of the natural system (enhanced recharge and subsurface flow barriers) and three that involve the introduction of water into the aquifer (direct addition of water to the spring lakes, injection wells, and infiltration galleries) are presented. The advantages, disadvantages, and uncertainties associated with each method are discussed, and each method is evaluated for its appropriateness and effectiveness at each site.

4.2 Possible Methods of Augmenting Springflow

4.2.1 Enhanced Surface Recharge.

The majority of the total recharge to the Edwards aquifer (approximately 60 - 80%) is via infiltration through the beds of losing streams that flow over the Edwards outcrop (Sharp, 1990). Groundwater recharge through these streams can be enhanced up-potential from the springs, either on a regional scale (i.e., on a basin-wide or aquifer-wide scale), or an a local scale (i.e., in the immediate vicinity of each spring). Two methods for increasing surface recharge are:

a) Creating surface impoundments (i.e., reservoirs) on intermittent losing streams that flow over the recharge area of the spring. These reservoirs have been classified as two types: type-I and type II (HDR, 1993). A type-I reservoir would be placed upstream from the recharge area, where it would hold surface runoff from periods of high precipitation and release it into the stream during drought conditions, thereby allowing water to infiltrate into the aquifer through the stream bed. The type-II reservoirs would be placed directly over the recharge area, allowing the impounded water to constantly recharge the aquifer. The Edwards Underground Water District has been operating a series of four type-II recharge structures since 1974 (EUWD, 1993).

b) Increasing the infiltration capacity of the recharge area. The volume of water that losing streams in the recharge area contribute to the springs can be increased by increasing the infiltration capacity of the substrate that they flow over. Because groundwater flow in the recharge zone of the Edwards Aquifer is generally through solution-enlarged fractures in the bedrock, drilling vertical boreholes in the stream beds could create hydraulic connections between the individual fractures and the stream bed to permit greater recharge.

4.2.2 Man - made subsurface flow barriers.

If the plumbing of the system bringing water to the springs can be known with confidence, it may be possible to modify the flow system through the installation of subsurface flow barriers. These barriers would be constructed by pumping grout into the ground through several boreholes. The injected grout fills the void spaces in the aquifer and hardens, creating a low permeability zone in the subsurface. Flow barriers may be used to increase their effectiveness of injection wells and infiltration galleries by isolating or semi-isolating the spring orifices so that injected water will not bypass the springs. Or, flow barriers could be constructed in such a way that they would divert a fraction of the groundwater that normally would flow around or under the spring discharge points towards the spring orifices.

4.2.3 Direct Addition of Water to Spring Lakes.

Instead of augmenting springflow through the enhancement of natural recharge or by the introduction of water to the aquifer, water could be added directly to the spring lakes that the springs feed into. While this will not actually augment discharge from the spring orifices, it will maintain flow in the rivers that are directly fed by the springs.

4.2.4 Injection Wells.

A well or set of wells can be drilled presumably near and up-potential from spring orifices. Water from an outside source is imported and injected into the well, creating a groundwater mound around the orifice area. Keeping groundwater levels locally elevated will keep the springs flowing even if overall aquifer levels are low.

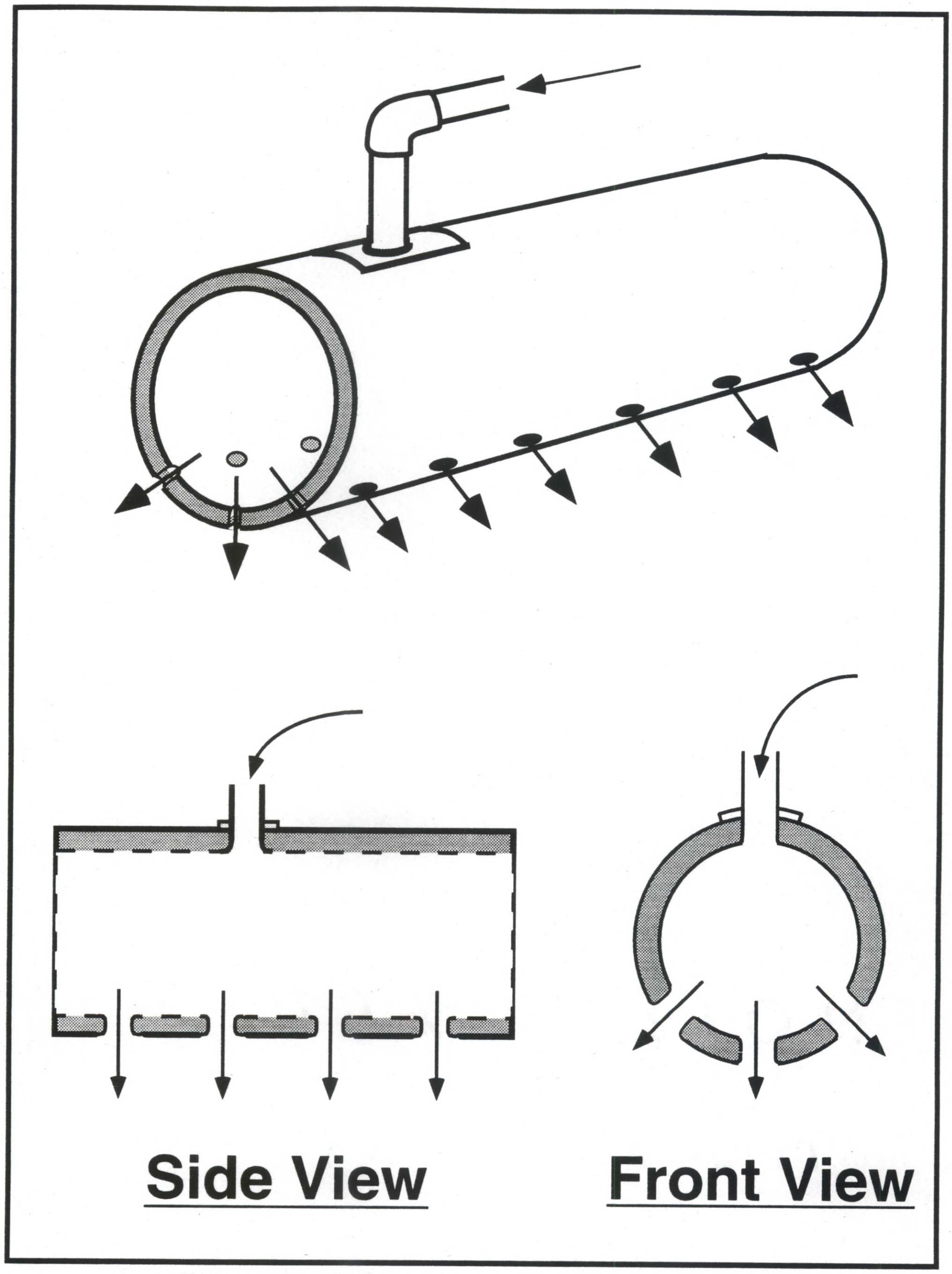

Figure 4.1 Infiltration gallery design schematic

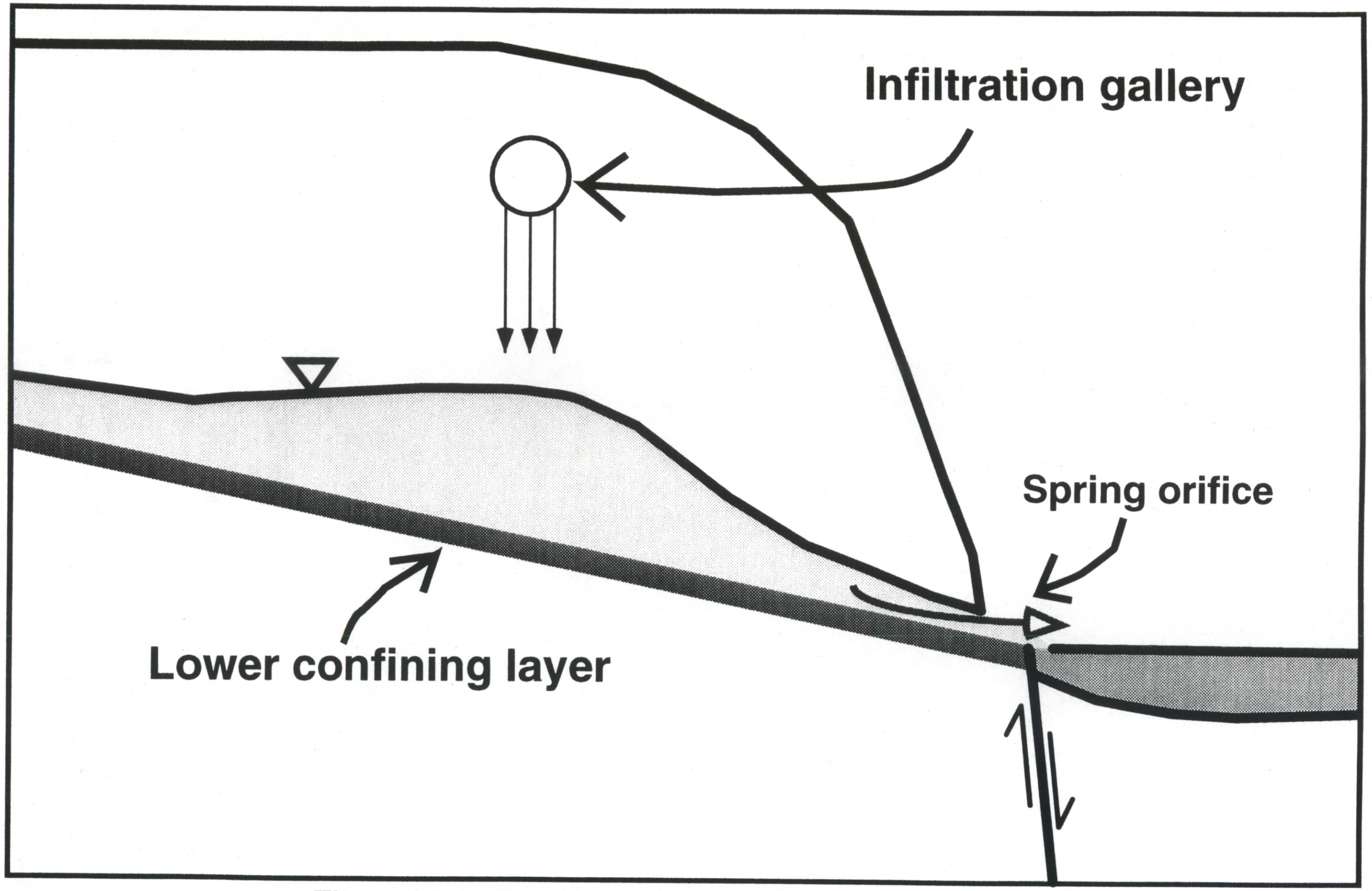

Figure 4.2 Infiltration gallery installation schematic

4.2.5 Infiltration Galleries.

Rather than injecting water at a point, water is allowed to infiltrate into the subsurface through a trench or tunnel constructed in the bluffs which parallel the lines of the springs at both sites (Figures 4.1 and 4.2). As in the injection well, an infiltration gallery creates a mound of groundwater above the springs that would maintain flow in the spring runs even if aquifer levels were low.

4.3 Discussion of Augmentation Technologies.

The feasibility of augmenting springflow from Comal and San Marcos Springs via the methods outlined above was investigated by McKinney and Sharp (1995). McKinney and Sharp (1995) evaluated each of these methods based on already existing data and computer simulations. The final results of their study categorized the feasibility and the current uncertainty in the performance of the various augmentation methods. The following is a brief summary of their results.

Enhanced surface recharge: Enhanced recharge of the Edwards aquifer is a technology that is being used today. Recharge structures like the ones described above already exist in the Edwards aquifer recharge zone. The Edwards Underground Water District has operated a number of these structures since the mid 1970's (EUWD, 1993). This would imply that enhanced recharge is not only feasible, but is probably a practical means of augmenting spring flow.

Regionally enhanced recharge appears to be a feasible method for augmenting flow from both springs. The possibility of regionally enhancing recharge in the Nueces, Guadalupe, and San Antonio River Basins was studied by HDR Engineering, Inc. (HDR, 1991, 1993). Their estimates, calculated under a number of different water allocation and aquifer level scenarios, implied that recharge to the aquifer in these basins can be enhanced by up to 19% over natural recharge.

Locally enhanced recharge is not a feasible alternative at Comal Springs, due to the fact that local natural recharge at Comal Springs appears to be insignificant (Ogden, Quick and Rothermel, 1986). San Marcos Springs, on the other hand, receive a significant volume of local recharge. Enhancement structures in the vicinity of San Marcos Springs could be constructed on the Blanco River or on other losing streams in that area. Ogden, Quick and Rothermel (1986) suggest that a recharge dam placed on the Blanco River could provide up to 80,000 af (98.7 million m^3) per year of enhanced recharge.

Increasing the infiltration capacity of the recharge areas would be an effective means of enhancing surface recharge to the aquifer. However, increasing recharge to the aquifer by opening direct conduits to the subsurface reduces the degree of attenuation of contaminants that occurs when recharging water infiltrates through the natural porosity of the system. This would increase the potential impact of contamination from surface runoff, especially runoff from impervious cover like roads and parking lots. For this reason, this alternative should be avoided unless steps can be take to reduce the risk of surface runoff contaminating the aquifer.

Engineered subsurface flow barriers: The unpredictable nature of the occurrence and orientation of void spaces in extensively fractured and karstified aquifers severely complicates the type of precision grouting necessary to construct this type of flow barrier. Once injected, it might be difficult to control or predict the paths that the grout slurry will take in the subsurface, creating the possibility of closing off flow paths that were intended to be left open. In addition, increased pore water pressures created by the flow barrier might open up silt-plugged cavities in the limestone, creating new conduits for groundwater flow and further altering the flow system. Furthermore, it is difficult to determine how much grout will be needed to construct an adequate barrier, as large caverns and voids are common in aquifers like the Edwards. Finally, it is speculated that the injection of grout into the subsurface may adversely affect the habitats of the troglodytic fauna residing in the aquifer.

In general, it is difficult to predict the effect that grouting in a karst aquifers will have on the flow paths in the subsurface. Considering the unpredictability of this method, the potential for adversely affecting the subsurface flow paths, and the fact that a primary reason for pursuing this research is the desire to maintain species that depend on the springs, McKinney and Sharp (1995) have concluded that this method is infeasible, except as a measure of last resort.

Direct addition of water to spring lakes: The main advantage of this technique over injection wells and infiltration galleries is that this method maintains control of the water during the augmentation process. This effectively eliminates the possibility of losing a percentage of the injected water and assures a near 100% efficiency rate for augmentation ("efficiency rate" is defined as the percentage of water introduced onto the system that actually augments spring flow). The disadvantage of this method is that, while it will maintain flow in the spring runs and lakes that are fed by the springs, it will not augment the actual discharge from the spring orifices. There is some consensus among the biological experts that the San Marcos salamander requires upwelling flow in order to reproduce, although no documented evidence to support this consensus could be found. If it can be shown that the fauna at the springs do not require upwelling flow to propagate, this method would be a feasible means of maintaining flow in the spring runs and lakes into which the springs discharge.

Injection wells: Construction of wells for injection is not a new technology. Injection wells for the disposal of petroleum-related brines and other wastes have been in use for decades. For the purpose of maintaining flow from a spring, an injection well can be placed directly up-potential from the spring orifices, so that injected water creates a localized mound of ground water that will maintain spring flow as water levels in the aquifer drop. Locating a potential site for an injection well, therefore, requires an understanding of 1) the geometry of the potentiometric surface of the aquifer surrounding the spring, 2) the main flow paths leading to the springs, and 3) the hydraulic characteristics of the flow system (i.e., hydraulic conductivity, transmissivity, effective porosity, etc.) This implies that the placement and design of injection wells in relatively homogeneous and isotropic aquifers, in which the potentiometric surface and the hydraulic parameters can be readily determined, is fairly simple.

The Edwards aquifer, however, is a complex system. The extensive faulting in the Balcones Fault Zone, and the subsequent karstification of the aquifer formations, gives rise to a flow system that is highly transmissive, heterogeneous, and anisotropic. In this type of aquifer, flow velocities and transmissivities may be so high that a significant amount of the water pumped in through an injection well may disperse before it has a chance to mound. This means that, of the total volume of water that would be pumped into an injection well, only a small amount might ever reach the spring. Proper design of an injection well in the Edwards requires that the flow systems around Comal Springs and San Marcos Springs be characterized in as much detail as possible, so the possibility of bypassing the springs can be anticipated and minimized. This should not cause much of a problem at San Marcos Springs; the fact that it is the lowest discharge point in the aquifer coupled with the geometry of the groundwater potential lines surrounding the springs suggests that the flow lines in the area converge on the springs (Ogden *et al*, 1986). In this case, an injection well could be placed in the immediate vicinity of the spring orifices, on the upthrown side of the San Marcos Springs Fault, with a high degree of confidence that nearly 100% of the injected water would eventually discharge at the springs.

Comal Springs, however, is a different situation. It is known with a good deal of confidence that the main flow lines leading to Comal Springs are roughly parallel to the Comal Springs Fault, moving from the southwest to the northeast. Therefore, the likely place to construct an injection well or wells would be southwest of the springs, along the Comal Springs Fault (Figure 4.3). What is not known in any certainty is how much of the water injected in a well placed along the fault would bypass the springs. To further complicate matters, it appears that a significant amount of the water discharging from Comal Springs is moving upward along the Comal Springs Fault from the confined portion of the aquifer (Maclay, 1989). Proper design of an injection well at Comal Springs requires a more complete understanding of the flow paths.

One way to gain a better understanding of the flow system is through chemical analysis of the waters issuing from the springs. Concentrations of naturally occurring dissolved constituents in the water discharging from the springs can be compared to the concentrations in the groundwater surrounding the springs. These concentrations can then be used to model groundwater mixing and rock-water interactions in the subsurface, thereby tracing out potential flow paths in the aquifer. In addition to the natural chemistry, artificially introduced chemical tracers can be used to infer flow paths leading to the springs. Tracer studies and chemical analyses have been performed at both springs (Rothermel and Ogden, 1986, Ogden, Quick and Rothermel, 1986, Pearson, Rettman, and Wyerman, 1975). These studies indicate that the flow lines at San Marcos Springs are converging on the springs and that the main flow lines at Comal Springs are moving along the fault. However, these studies have not fully addressed the question of injection well efficiency at Comal Springs.

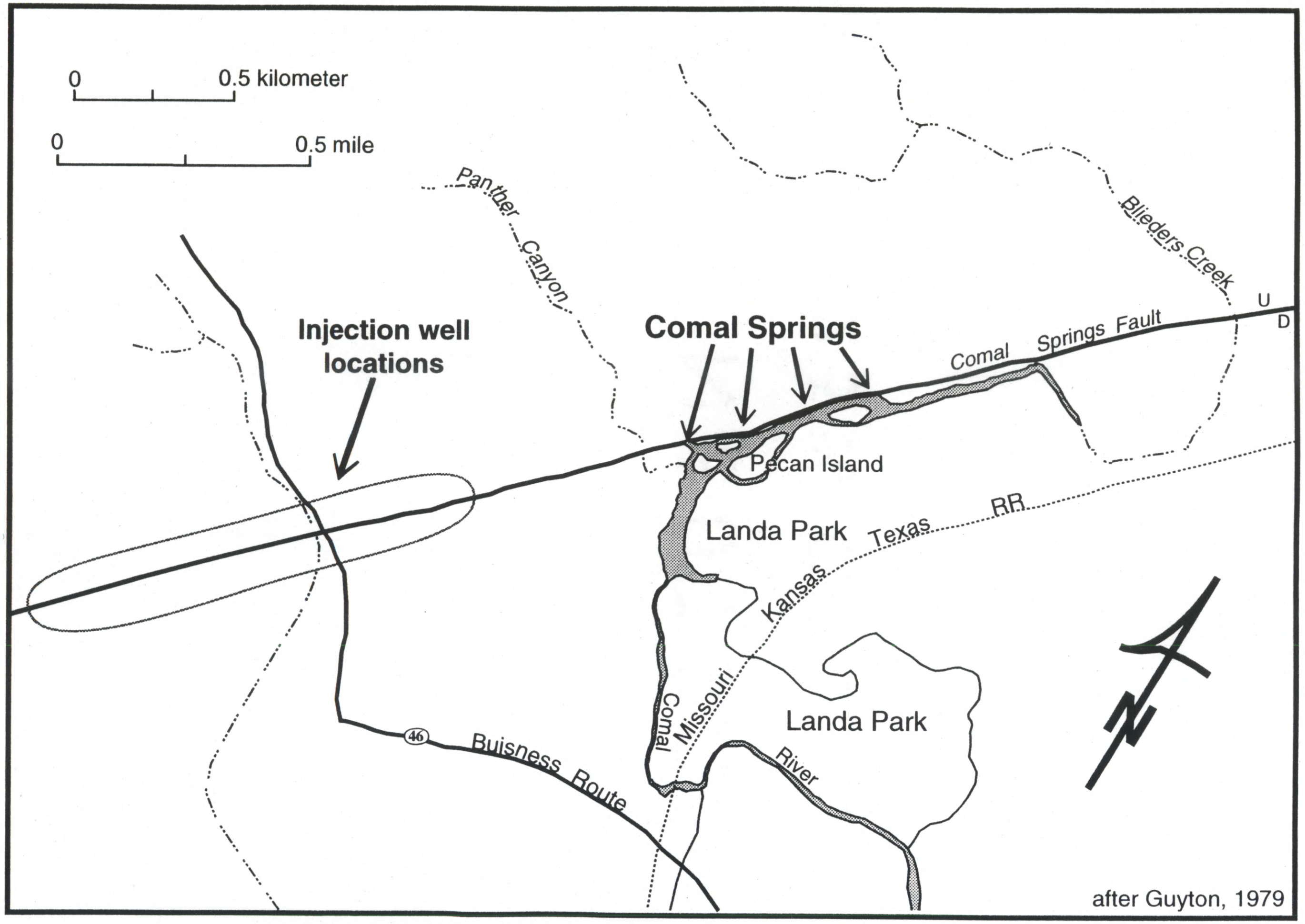

Figure 4.3 Potential injection well locations at Comal Springs

A second way to increase the understanding of the flow system at Comal Springs is through the use of computer modeling. Computer simulations of the aquifer surrounding the springs can be used to establish potential flow paths in the aquifer and to estimate injection efficiencies. Extensive modeling of the entire Edwards aquifer has been done (Klemt *et al*, 1979; Maclay and Land, 1988, Kuniansky, 1995). However, detailed models of the aquifer in the immediate vicinity of Comal and San Marcos Springs have not been constructed. In order to model the effect of injection wells on discharge from these springs, more detailed modeling of the aquifer needs to be done.

Infiltration Galleries: Infiltration galleries, like injection wells, are not a new technology. Infiltration galleries have been used in contaminated aquifers to collect free product and contaminated water for treatment, as well as at other sites to drain water from aquifers for the purpose of controlling the water table elevation. As a means of augmenting springflow, an infiltration gallery in the form of a horizontal pipe or tunnel can be constructed above the water table in the bluffs on the upthrown side of the spring faults, running parallel to the faults (Figures 4.4 and 4.5). In this location, water introduced into the gallery would percolate down towards the water table, creating a mound of groundwater that would maintain discharge from the springs.

This method of augmenting discharge has advantages over injection wells. First of all, an infiltration gallery would most likely have a greater efficiency than an injection well because introduction of water closer to the springs reduces the risk of a large volume of the water bypassing the spring orifices. This is a more significant concern at Comal Springs than at San Marcos Springs, where flow lines converge on the springs. An advantage that this method has at Comal Springs is the fact that the formation outcropping at the base of the bluff (the Regional Dense Member (RDM) of the Edwards group) may be a local confining layer in this part of the Edwards (John Hanson, personal communication; Gregg Oetting, personal communication). If this is the case, the RDM could act as a vertical control on water percolating down through the subsurface below the infiltration gallery. This would increase the likelihood that infiltrating water would flow towards, and eventually discharge from, the springs.

Nevertheless, it is not known with certainty if the RDM at Comal Springs would act as a confining layer on the scale of an infiltration gallery. The area on the upthrown side of the fault is fractured; the small fractures do not show in the resolution of existing maps. It is not known if these fractures would allow significant vertical flow through the RDM, thereby reducing its effectiveness as a vertical control on infiltrating water. Before a gallery is constructed at Comal Springs, it is important that the capacity of the RDM to act as a confining layer be investigated, through detailed mapping of the fractures, dye trace and natural chemical trace studies (if possible), and computer modeling to determine the sensitivity of the system to the conductivity of the RDM.

Another concern with infiltration galleries deals with the chemical compatibility of the infiltrating water with the natural water discharging from the springs. At present, it is not known how sensitive the ecosystems or the endangered species in and around the spring orifices are to changes in water chemistry. It is important, for the sake of these ecosystems, that the chemical parameters (e.g., temperature, pH, salinity, etc.) of water introduced into the aquifer for the purpose of springflow augmentation be similar to those of the natural spring water by the time it discharges through the spring opening. Springflow augmentation via injection wells allows the augmentation water to equilibrate with the ambient water in the aquifer, an advantage that is less significant for the infiltration gallery method because of the close proximity of the infiltration points to the spring discharge points. If this method is implemented, there may be a need to treat the augmentation water before it is introduced into the gallery.

A final possible disadvantage deals with the potential impact of gallery construction on the subsurface around the springs. Invasive work, like drilling, tunneling, and excavating, always disrupts the subsurface to a certain degree. There has been some concern that any construction near the springs may have a detrimental impact on the fauna living in and around the aquifer, although no data have been presented to document this assertion. This impact is more significant in the case of an infiltration gallery, where construction would entail horizontal drilling and possibly excavation, than it would for an injection well drilled vertically one or more kilometers from the springs. Before construction of an infiltration gallery is undertaken, the potential impact of construction must be investigated.

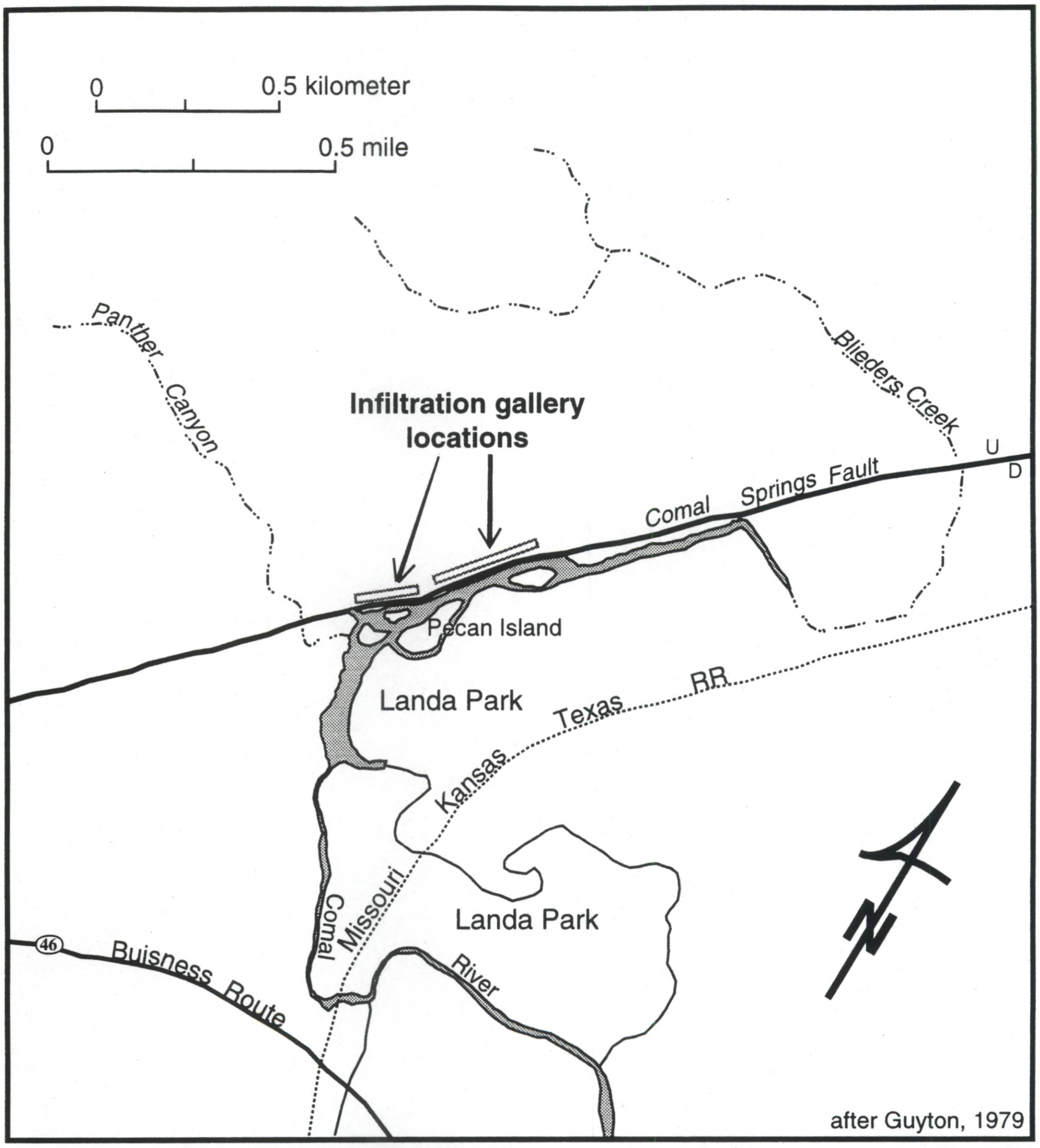

Figure 4.4 Potential infiltration gallery locations at Comal Springs

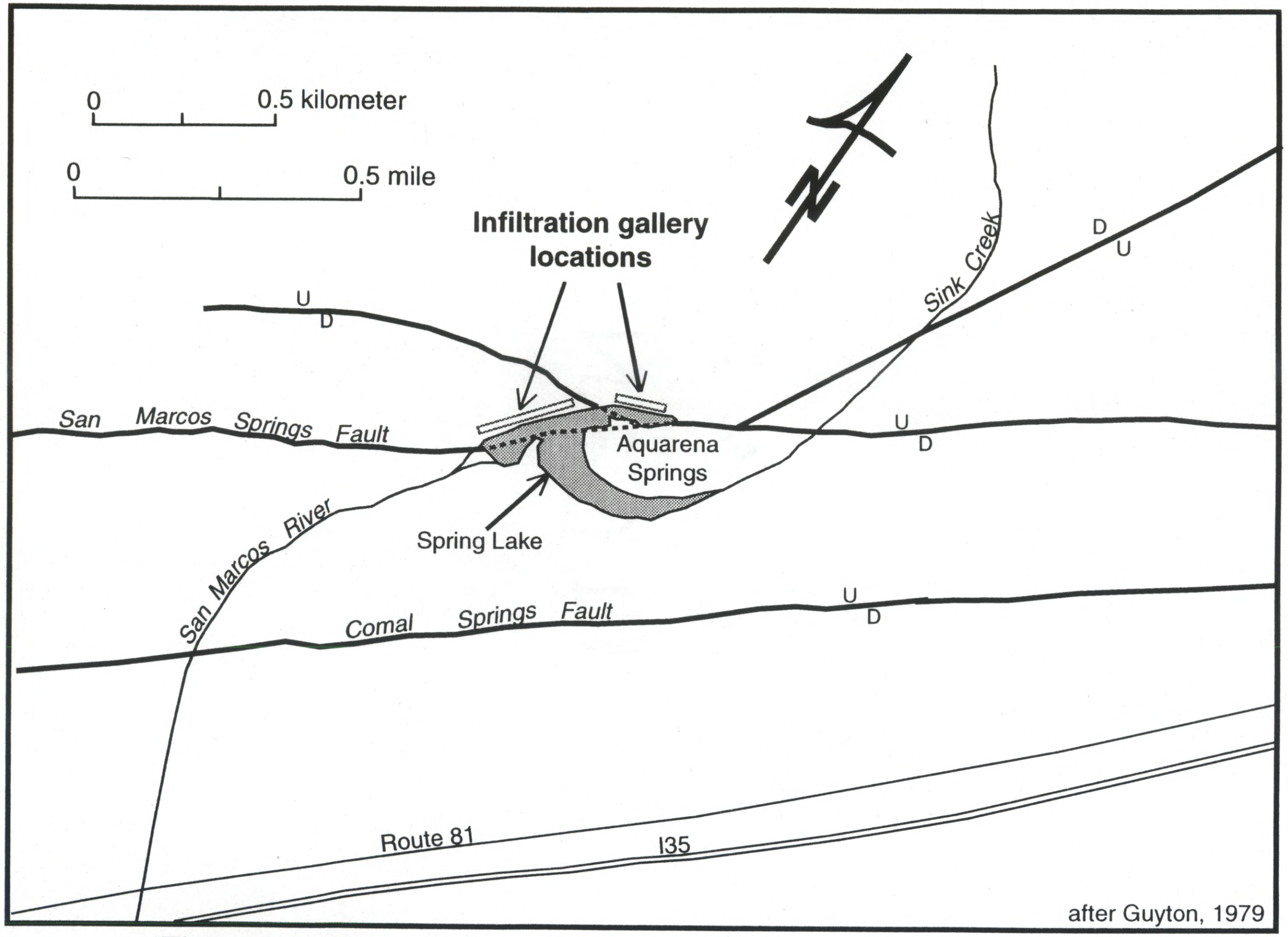

Figure 4.5 Potential infiltration gallery locations at San Marcos Springs

Infiltration galleries are a possible method for augmenting discharge at either spring. However, based on the advantages (better efficiency than injection wells) and disadvantages (chemical compatibility of the infiltrating water, impact of construction on the aquifer), infiltration galleries are not as appealing an option at San Marcos Springs, where injection efficiency is not as great a concern. While the potential risks associated with this method are similar at each site, the nature of the flow systems are such that the use of an infiltration gallery at San Marcos may not be necessary.

4.4 Conclusions

Five methods of augmenting springflow from Comal and San Marcos Springs are proposed and discussed. These methods are 1) enhancement of natural recharge, 2) subsurface flow barriers, 3) direct addition of water to the spring lakes and spring runs, 4) injection wells, and 5) infiltration galleries. Enhancement of natural recharge to the Edwards, in the form of impoundment structures on and above the recharge zone, are presently in place. On a local scale, recharge to the aquifer may be enhanced near San Marcos Springs, where local recharge contributes a significant amount of water to the springs, but not at Comal Springs, where local recharge is insignificant. Sub-surface flow barriers are not recommended at this time because they are difficult to construct in karst aquifers. Direct addition to the spring lakes is a viable, low risk option for maintaining water in the spring lakes and spring runs, but it does not address the question of the need for upwelling flow from the springs for propagation of certain species (if such a need exists).

Injection wells installed along the spring faults upgradient from the springs are a possible method for augmenting flow from the springs. However, there are uncertainties concerning the potential efficiency of this technology. At Comal Springs, there is a possibility of a significant volume of water bypassing the springs after it is injected. This possibility is not great at San Marcos Springs, where the flow lines converge toward the springs. In order to properly design and locate injection wells at Comal Springs, dye tracer tests and more detailed modeling of the aquifer needs to be done.

Infiltration galleries installed in the bluffs on the upthrown side of the spring faults are another possible method of introducing water into the flow systems. Infiltration galleries would probably be more efficient than injection wells because they would be constructed much closer to the springs and that they would introduce water to the system along a line parallel to the line of spring orifices rather than at a point in the aquifer. However, the proximity of infiltration galleries to the springs requires that the water used for augmentation be chemically compatible with natural spring water, so that the ecosystems in and around the springs are not adversely affected. In addition, the potential impact of construction of an infiltration gallery on the subsurface needs to be investigated and factored into the decision to build.

Comal Springs

Alternative	Hydrological	Geological	Biological	Technical	Average
Injection Wells	3	2.5	2.5	4	3
Infiltration Galleries	3	2	1	2	2
Enhanced Recharge (Regional)	4	4	3	5	4
Enhanced Recharge (Local)	0	0	3	1	1
Subsurface Flow Barriers	1	1	0	2	1
Direct Addition to Lakes	4	5	3	4	4

San Marcos Springs

Alternative	Hydrological	Geological	Biological	Technical	Average
Injection Wells	3	2.5	2.5	4	3
Infiltration Galleries	3	3	2	4	3
Enhanced Recharge (Regional)	4	4	3	5	4
Enhanced Recharge (Local)	4	4	3	5	4
Subsurface Flow Barriers	1	1	0	1	1
Direct Addition to Lakes	4	5	3	4	4

Scale: 0 = infeasible 2.5 = uncertain, 5 = feasible

Table 4.1 Feasibility-uncertainty rankings of the springflow augmentation alternatives at Comal and San Marcos Springs (McKinney and Sharp, 1995).

5. MODEL CONSTRUCTION AND CALIBRATION

5.1 Introduction

The effects of an injection well placed up-potential from the spring orifices at Comal Springs is simulated by a three dimensional numerical computer model, hereafter referred to as the "injection well response (IWR) model". This model, created using **MODFLOW/EM** (the Maximal Engineering Software, Inc. version of the U. S. Geologic Survey's Modular Three-Dimensional Finite-Difference Ground-Water Flow Model (MODFLOW) (McDonald and Harbaugh, 1988)) and **Processing MODFLOW** (**PM**) (a MODFLOW pre-processor developed by Chiang and Kinzelbach, 1992), calculates discharge from Comal and San Marcos Springs as a function of aquifer heads. Injection wells with varying injection rates are placed in this model upgradient from Comal Springs, at distances ranging from 0.25 to 2.0 miles (0.4 to 3.2 km). The increase in spring discharge that results from injection is used to calculate the efficiency of the injection wells, in terms of how much of the injected water actually ends up discharging from the springs.

In addition to the numerical model, a steady-state analytical model that simulates the effects of an infiltration gallery was created. This model, hereafter referred to as the "infiltration gallery model", calculates the dimensions and the time of formation of a saturated ground-water mound forming on a sloping, leaky lower confining layer below a finite, constant infiltrating source. It also calculates flux rates of infiltrating water as it moves down the slope and as it seeps through the confining layer. The infiltration gallery model is used to estimate the time of formation of a steady-state groundwater mound under a gallery at Comal Springs. It is also used to estimate the infiltration rate and the efficiency for galleries of various diameters, given a range of conductivities for the aquifer and for the confining layer.

5.2 Injection Well Response Model

Spring flow response to injection of water into the aquifer via injection wells was simulated by a three-dimensional, steady-state finite difference model created using the MODFLOW/EM version of MODFLOW and the PM pre-processor. Spring discharge was calculated using the Water Balance analysis option included with the PM software. Final head distributions were imported into SURFER™ for contouring. Injection efficiencies were calculated on EXCEL™ spreadsheets. Details on model construction, simplifying assumptions, data used in determining model parameters (such as hydraulic conductivity and areal recharge), and model output processing are given below.

5.2.1 MODFLOW Description.

MODFLOW models groundwater flow by numerically solving the equation

$$\frac{\partial}{\partial x}\left(K_{xx}\frac{\partial h}{\partial x}\right)+\frac{\partial}{\partial y}\left(K_{yy}\frac{\partial h}{\partial y}\right)+\frac{\partial}{\partial z}\left(K_{zz}\frac{\partial h}{\partial z}\right)-W=S_s\frac{\partial h}{\partial t} \qquad (1)$$

where

x, y, and z ≡ Cartesian coordinates aligned along the major axes of hydraulic conductivity (K_{xx}, K_{yy}, K_{zz})

K ≡ hydraulic conductivity [L/t]

h ≡ potentiometric head [L]

W ≡ sources and sinks of groundwater [1/t]

S_s ≡ specific storage of the aquifer materials [1/L]

t ≡ time [t]

Aquifer dimensions (areal extent and thickness) are discretized on two-dimensional or three-dimensional block-centered grids with user-specified variable grid spacing. The finite-difference approximation of Equation 1 is placed at each node in the grid and solved iteratively. Hydrogeologic parameters, such as hydraulic conductivity and effective porosity, are input into a model on a cell - by - cell basis. Individual layers of a model grid are designated as either confined or unconfined. The modeling software contains several independent subroutines, called "packages", that model the effects of various groundwater-related processes, such as injection/pumping wells, drains, stream-aquifer interraction, areal recharge, evapotranspiration, and general head boundaries.

The PM preprocessor used allows for graphic input of model dimensions and model parameters. It also processes model output for direct transfer of the output files into SURFER™ for contouring, and it has an intrinsic function that calculates the water balance through user-specified zones in the model grid.

5.2.2 Boundary Conditions.

The model domain covers a large part of Hays County, roughly half of Comal County, a small portion of northeastern Bexar County, and the eastern corner of Guadalupe County (Figure 5.1). The northwestern and northeastern borders of the aquifer in the model area are defined by the updip limit of the Edwards Group outcrop and a groundwater divide near Kyle, Texas, respectively. These boundaries are treated in the model as no-flow boundaries. The southeastern border of the aquifer in the study area is delineated by the "bad-water line", a line that separates waters with greater than 1000 mg/l total dissolved solids ("saline water") from waters with less than 1000 mg/l total dissolved solids ("freshwater"). High hydraulic heads in the saline zone would be expected to inhibit the downdip movement of freshwater into the zone of high salinity while driving the updip movement of saline water from the Stuart City Reef. However, flow from the saline zone into the fresh zone is restricted by the low transmissivity of the saline zone and by the density difference along the "bad-water line" interface (Maclay and Land, 1988). Because of the significant transmissivity and density differences between the freshwater zone and the saline zone, there is relatively little flow across this boundary. Therefore, this boundary is also treated in the model as a no-flow boundary.

The southwestern boundary of the model runs through northeast Bexar County roughly parallel to the border between Bexar and Comal counties. This boundary is treated as a constant head boundary, under the assumption that it is far enough upgradient from the injection well locations that injection of water will not affect the potentiometric surface at this distance. Model boundaries are shown on Figure 5.2.

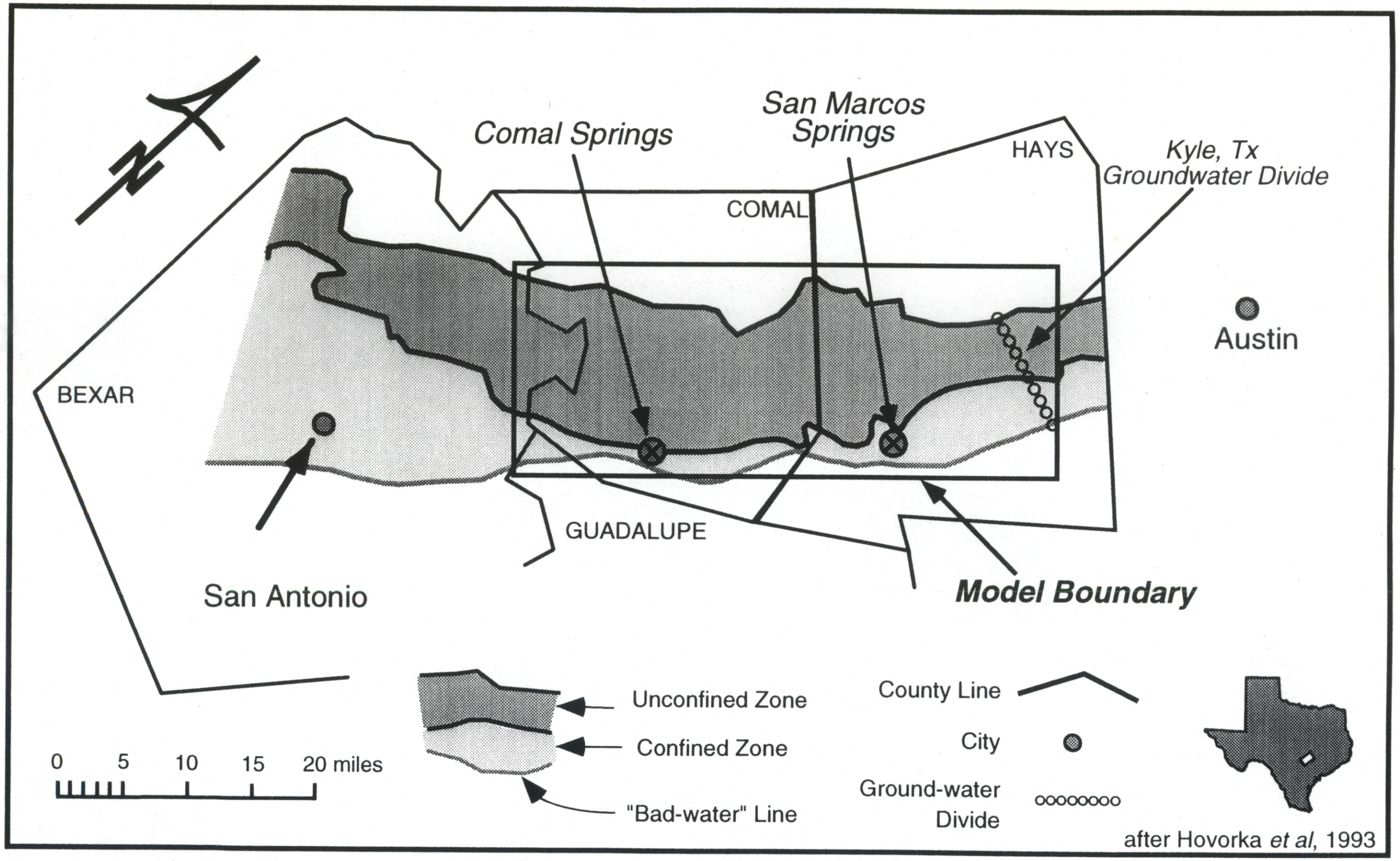

Figure 5.1 Model area

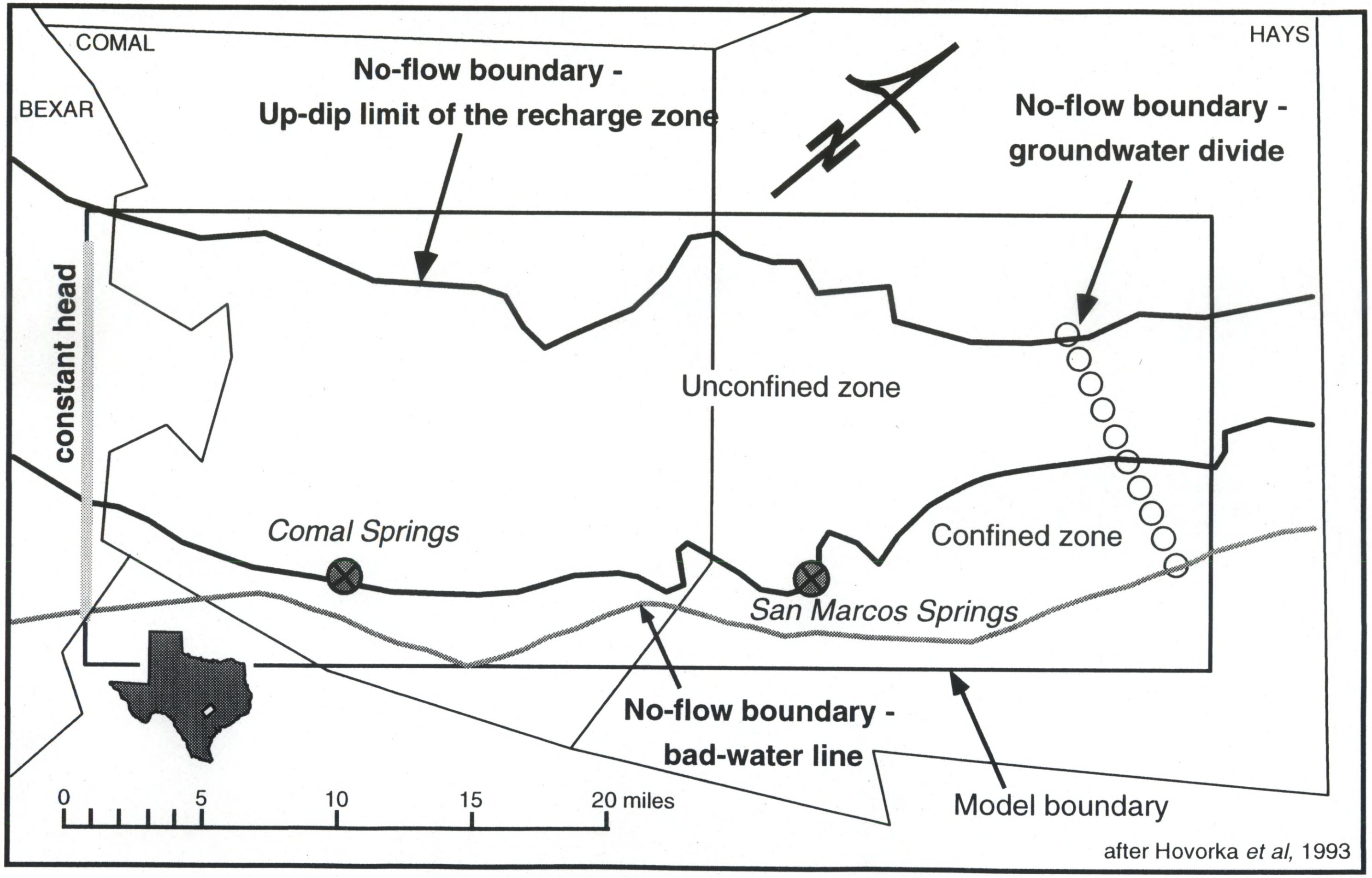

Figure 5.2 Model boundary conditions

5.2.3 Model Grid Dimensions.

The dimensions of the model are based on the actual dimensions of the aquifer units, as shown on Figures 1.8 and 1.9. The study area is modeled on a block-centered node finite-difference grid of 35 rows and 87 columns. The majority of the rows and columns are 0.5 miles (0.8 km) wide, with the following exceptions: rows 29 and 30 are 0.25 miles (0.4 km) in width and columns 18 through 25, 61, and 62 are also 0.25 miles (0.4 km) wide (Figure 5.3).

In order to model both the unconfined outcrop zone and the confined artesian zone, the model was constructed with two layers, an unconfined upper layer and a confined lower layer, connected by a 0.5 mile (0.8 km) wide strip (hereafter called the "model fault zone") that simulates the main faults displacing the aquifer units in the study area. The top of the upper layer is set at an elevation of 800 ft (243.8 m) above the model datum, which is meant to represent mean sea level. The bottom of the active cells in this layer range from 750 ft (228.6 m) along the northeast border of the model to 400 ft (121.9 m) along the model fault zone, giving this part of the layer a thickness that ranges from 50 ft (15.2 m) to 400 ft (121.9 m). The bottom of the fault zone in the upper layer, as well as the bottom of the inactive cells adjacent to this zone, is set at an elevation of 100 ft (30.5 m). The top of the cells in the lower layer are in contact with the bottom of the upper layer, meaning that the top of the active cells in the lower layer are at an elevation of 100 ft (30.5 m). The bottom of this layer is set at a constant elevation of -300 ft (-91.5 m), giving the active cells in this layer a thickness of 400 ft (121.9 m). Map views of the upper and lower layers of the model grid are shown in Figure 5.3. A cross section of the model, along line A - A`, is shown in Figure 5.4.

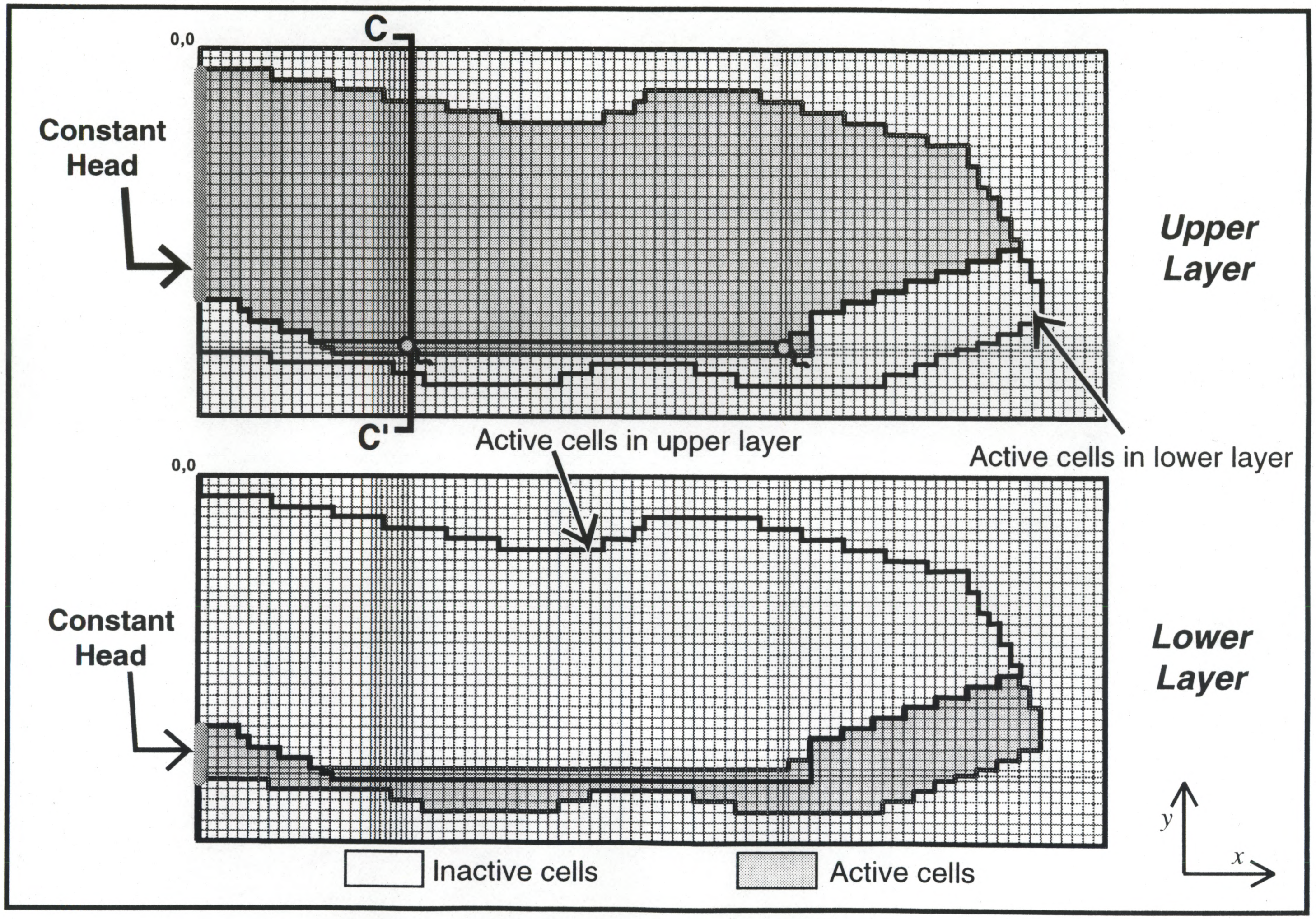

Figure 5.3 Model grid boundaries and active cell zones

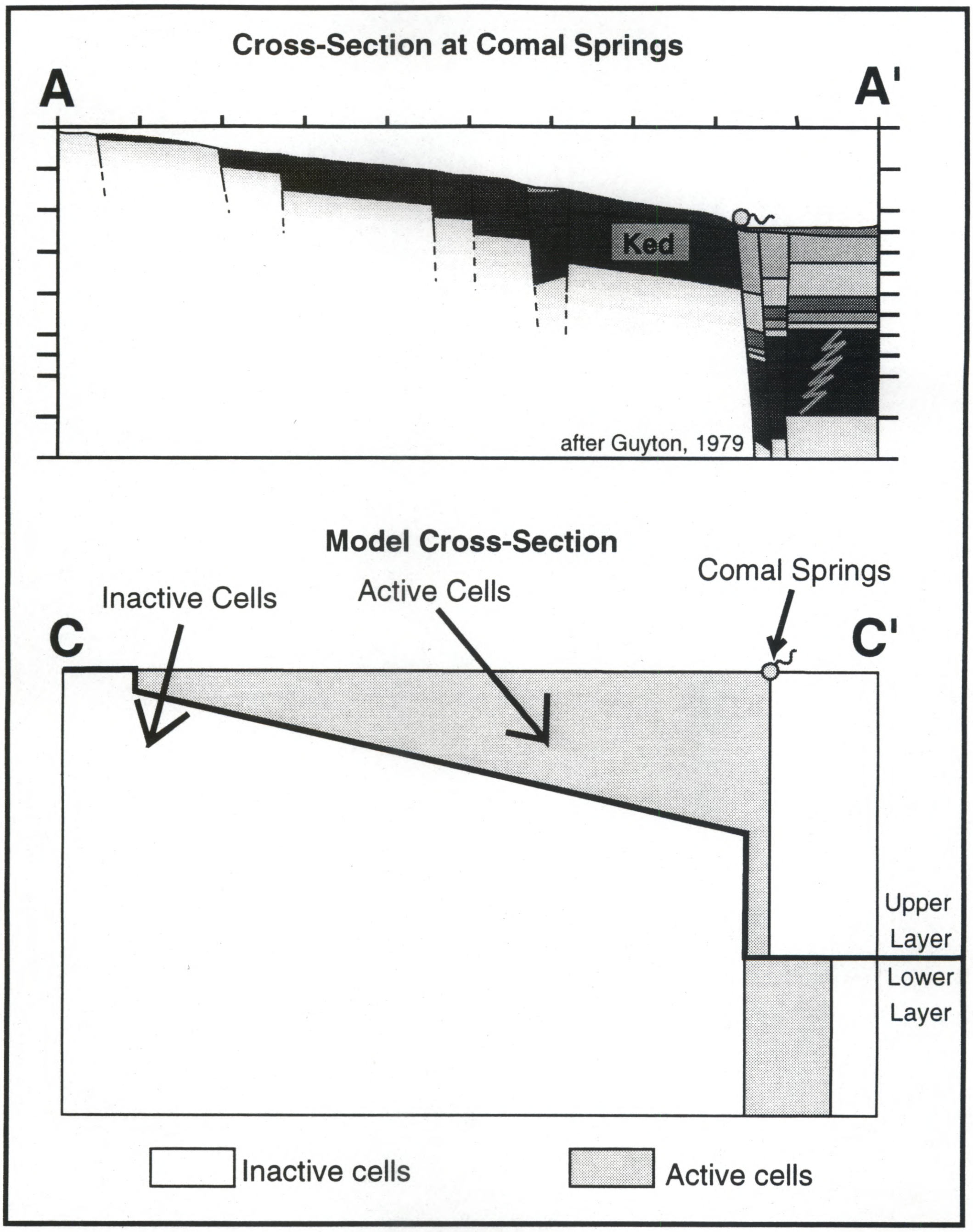

Figure 5.4 Cross section of model grid

5.2.4 Hydraulic Heads Along the Constant Head Boundary.

Constant head boundary values for the IWR model are based on water levels in three wells - two unconfined and one confined - located in Bexar County (Figure 5.5). These wells were chosen because they are the only wells close to the model boundary that had sufficient historical water level data available to estimate constant head boundary values under different flow conditions. Water level data from each well is plotted against the corresponding discharge from Comal Springs to develop a linear relationship between head value at the well and spring discharge (Figure 5.6). This relationship is used to calculate a head value for each boundary well at "average-flow" conditions (i.e., Comal Springs discharge = 284 cfs (8.0m^3/s)) and at "low-flow" conditions (Comal Springs discharge = 78 cfs (2.2 m^3/s)). Each well is assigned to a single node along the constant head boundary in the model. In addition to the three Bexar County wells, a fourth well is used to estimate water levels near the northern end of the constant head boundary. This well (DX-68-22-401, located in Comal County) has a recorded water elevation of 850 ft (259 m) in December of 1970. At this time, Comal Springs was flowing at approximately average discharge (286 cfs (8.0 m^3/s)), so this value is used as a constant head value for "average-flow" conditions. There is, however, not enough historical data for this well to develop a linear relationship that could be used to calculate head for the corresponding node under "low-flow" conditions. The well numbers, the corresponding node coordinates, and the head values at average and low flow conditions are given in Table 5.1.

For the initial simulations, all of the constant head boundary nodes in the lower layer of the model were assigned the same head value as the "average-flow" value for well AY-68-30-807 (i.e., 660 ft (201 m)). Nodes (1,23) and (1,18) were assigned head values corresponding to the "average-flow" values for the wells that they represent (665 ft (203 m) and 750 ft (229 m), respectively). Node (1,8) was assigned a value of 850 ft (259 m), corresponding to the "average-flow" value for well DX-68-22-401. All values in between node (1,8) and node (1,18), as well as the nodes above node (1,8), were interpolated by a 10 ft (3.1 m) drop in head per node. The same was done with 15 ft (4.6 m) drop in head per node between node (1,18) and node (1,23).

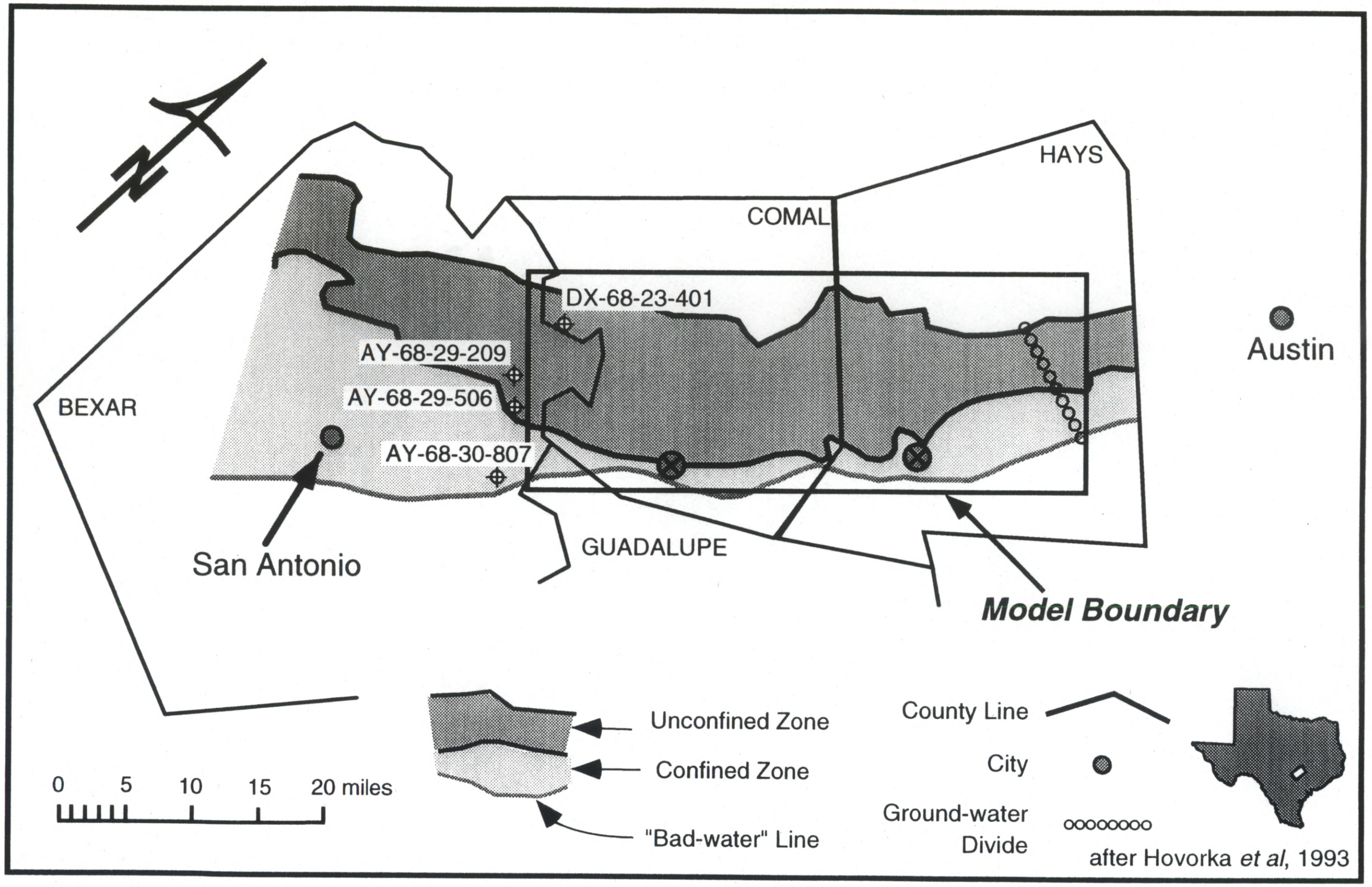

Figure 5.5 Locations of the constant head boundary wells

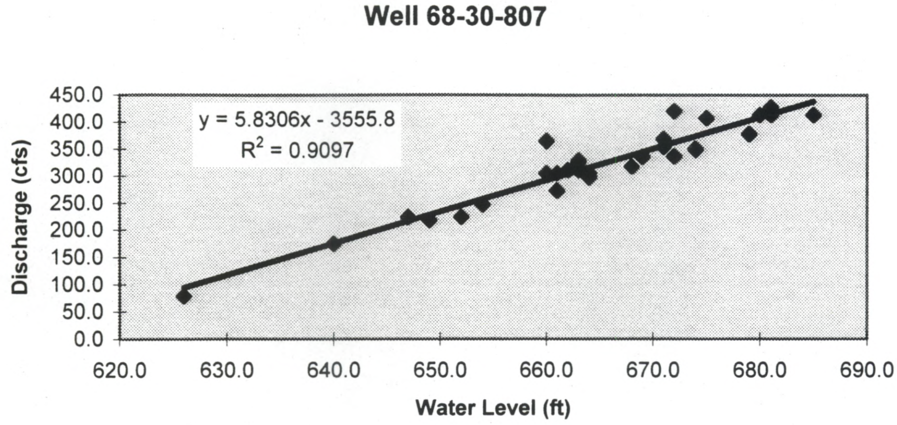

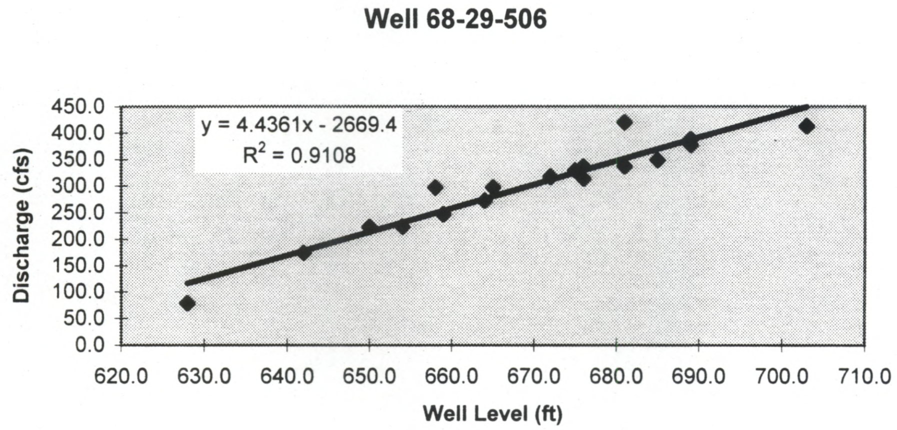

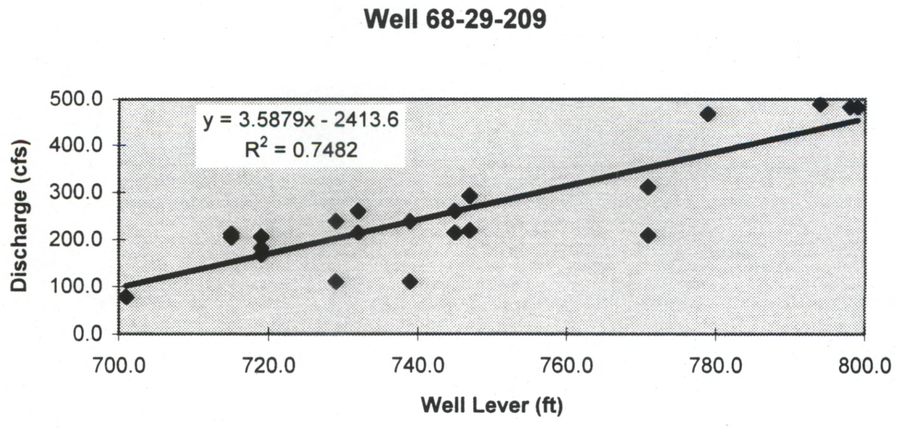

Figure 5.6 Comal Springs discharge versus well levels in the constant head boundary wells

Well Number	Corresponding Node Coordinates	Head under average flow conditions	Head under low flow conditions
DX-68-22-401	**1,8 (upper layer)**	**850 ft (251 m)**	**N/A**
AY-68-29-209	**1,18 (upper layer)**	**750 ft (229 m)**	**700 ft (213 m)**
AY-68-29-506	**1,23 (upper layer)**	**665 ft (203 m)**	**628 ft (191 m)**
AY-68-30-807	**1, 30 (lower layer)**	**660 ft (201m)**	**625 ft (190 m)**

Table 5.1 Node coordinates and head values for constant head boundary wells.

Node coordinates	Head under "average-flow" conditions (ft)	Head under "low-flow" conditions (ft)	Comments
			Upper Layer (unconfined)
1, 1	-	-	inactive cell
1, 2	-	-	inactive cell
1, 3	900	850	
1, 4	900	840	
1, 5	890	830	
1, 6	880	820	
1, 7	870	810	
1, 8	860	800	corresponds to well DX-68-22-401
1, 9	850	790	
1, 10	840	780	
1, 11	830	770	
1, 12	820	760	
1, 13	810	750	
1, 14	800	740	
1, 15	790	730	
1, 16	780	720	
1, 17	760	710	
1, 18	750	700	corresponds to well AY-68-29-209
1, 19	735	685	
1, 20	710	660	
1, 21	695	645	
1, 22	680	630	
1, 23	665	628	corresponds to well AY-68-29-506
1, 24	665	628	
1,25 - 1,35	-	-	inactive cells

Table 5.2 Head values along IWR model constant head boundary for "average-flow" and "low-flow" conditions (upper layer)

Node coordinates	Head under "average-flow" conditions (ft)	Head under "low-flow" conditions (ft)	Comments
			Lower Layer (confined)
1, 1 - 1, 24	-	-	inactive cells
1, 25	660	625	
1, 26	660	625	
1, 27	660	625	
1, 28	660	625	
1, 29	660	625	
1, 30	660	625	corresponds to well AY-68-30-807
1, 31 - 1, 35	-	-	inactive cells

Table 5.3 Head values along IWR model constant head boundary for "average-flow" and "low-flow" conditions (lower layer)

In addition to the "average-flow" constant head boundary values, a set of "low-flow" constant head boundary values were determined, based on the "low-flow" head values in the three Bexar County wells listed in Table 5.1. The "low flow" head values were later used in the calibration of the model to check the response of the springs to lowered water levels, and all injection simulations were run with the constant head boundary set at "low flow" conditions.

Head values of all constant head boundary nodes under "average" and "low-flow" conditions are presented in Tables 5.2 and 5.3.

5.2.5 Spring Simulation.

The MODFLOW Drain package was used to simulate spring discharge. This module approximates the rate at which water discharges through a drain using the equation

$$Q_d = C_d(h - d) \tag{2}$$

where:

Q_d ≡ discharge through the drain $[L^3/t]$

h ≡ elevation of the drain [L]

d ≡ hydraulic head in the aquifer at the drain [L]

C_d ≡ conductance of the interface between the drain and the aquifer $[L^2/t]$

In other words, this equation states that the model assumes flow through the drain to be proportional to the head of the aquifer above the drain. Discharge through the drain equals zero when aquifer levels are below the elevation of the drain.

In the IWR model, the nodes which represent Comal and San Marcos Springs are designated as aquifer drains, with a specific elevation (h) and a spring conductance (C_d) assigned to each one. After MODFLOW solves for the hydraulic head at the spring node (d), it uses these values and Equation 2 to solve for discharge from the spring. The method used to determine values for h and C_d is described in the next section.

5.2.6 Spring Elevations and Spring Conductance.

Historic spring discharge data from Comal and San Marcos Springs and well levels from nearby observation wells were used to develop regression equations that relate spring discharge to aquifer levels (Figures 5.7 and 5.8). Spring discharge was plotted as the independent variable, and the corresponding water levels were plotted as the dependent variable. The equation for the least squares fit to the data was calculated, and used to determine the spring elevation. The resulting spring elevation, an arbitrarily chosen water level in the observation well, and the corresponding spring discharge were then plugged into equation 2 and used to calculate C_d, which was used in the model as the spring conductance. A sample calculation is given in Appendix A.

For Comal Springs, monthly average discharge over the interval January, 1980 to December, 1989 was plotted versus the corresponding monthly average water levels in the Landa Park Observation Well (DX-68-23-302). A linear least-squares trend line was fit to the data on the graph, and the equation for the line was determined. This equation for the linear least-squares fit to the data has an R^2 coefficient of 0.972. Based on this equation, the spring elevation and spring conductance for Comal Springs are 617.5 ft (188.2 m) and 3,195,417.6 ft^2/d (13.0 m^2/s), respectively. The values 617.5 ft and 3,200,000 ft^2/d are used in the model.

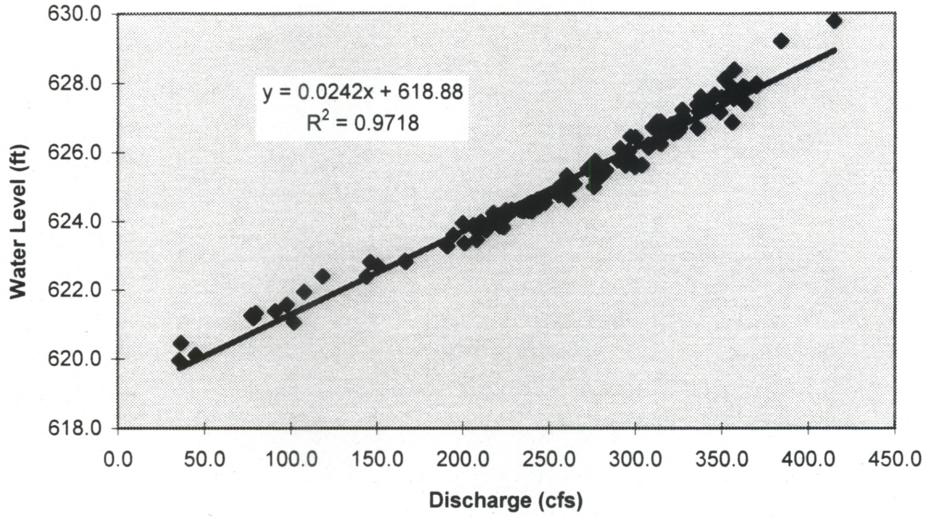

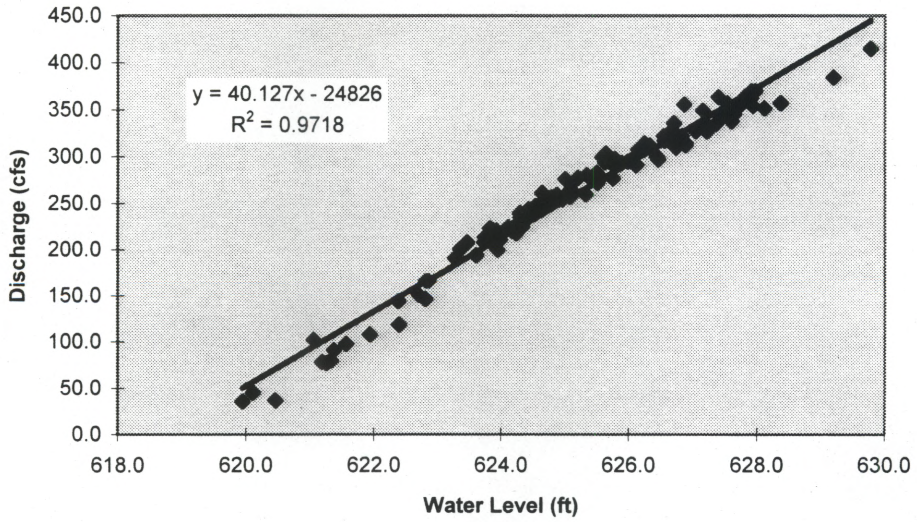

Figure 5.7 Comal Springs discharge versus water level in Landa Park Well

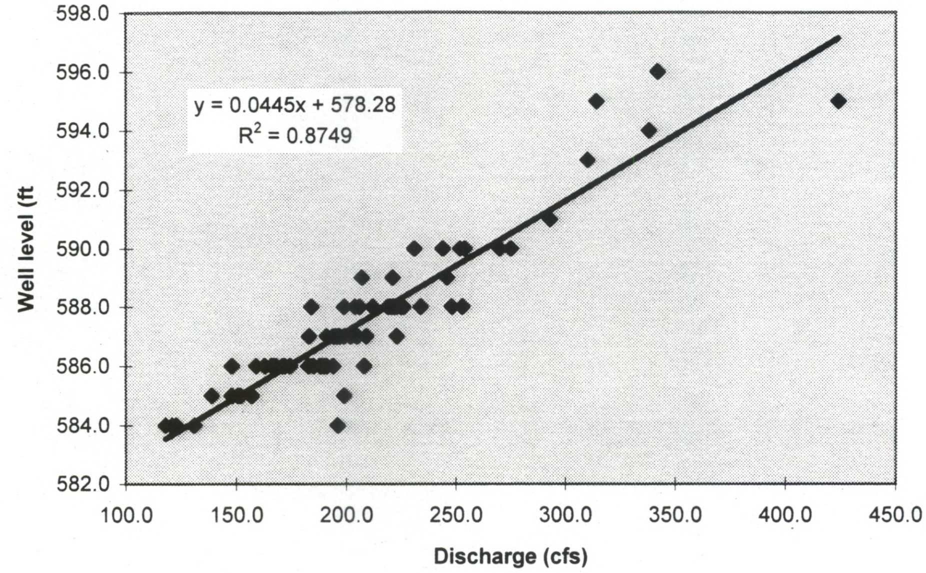

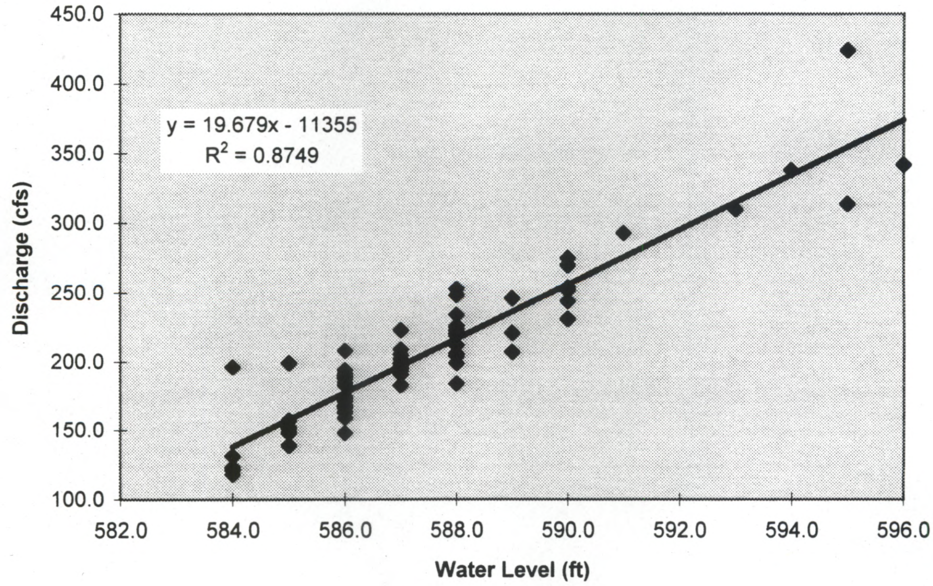

Figure 5.8 San Marcos Springs discharge versus water level in well 67-09-110

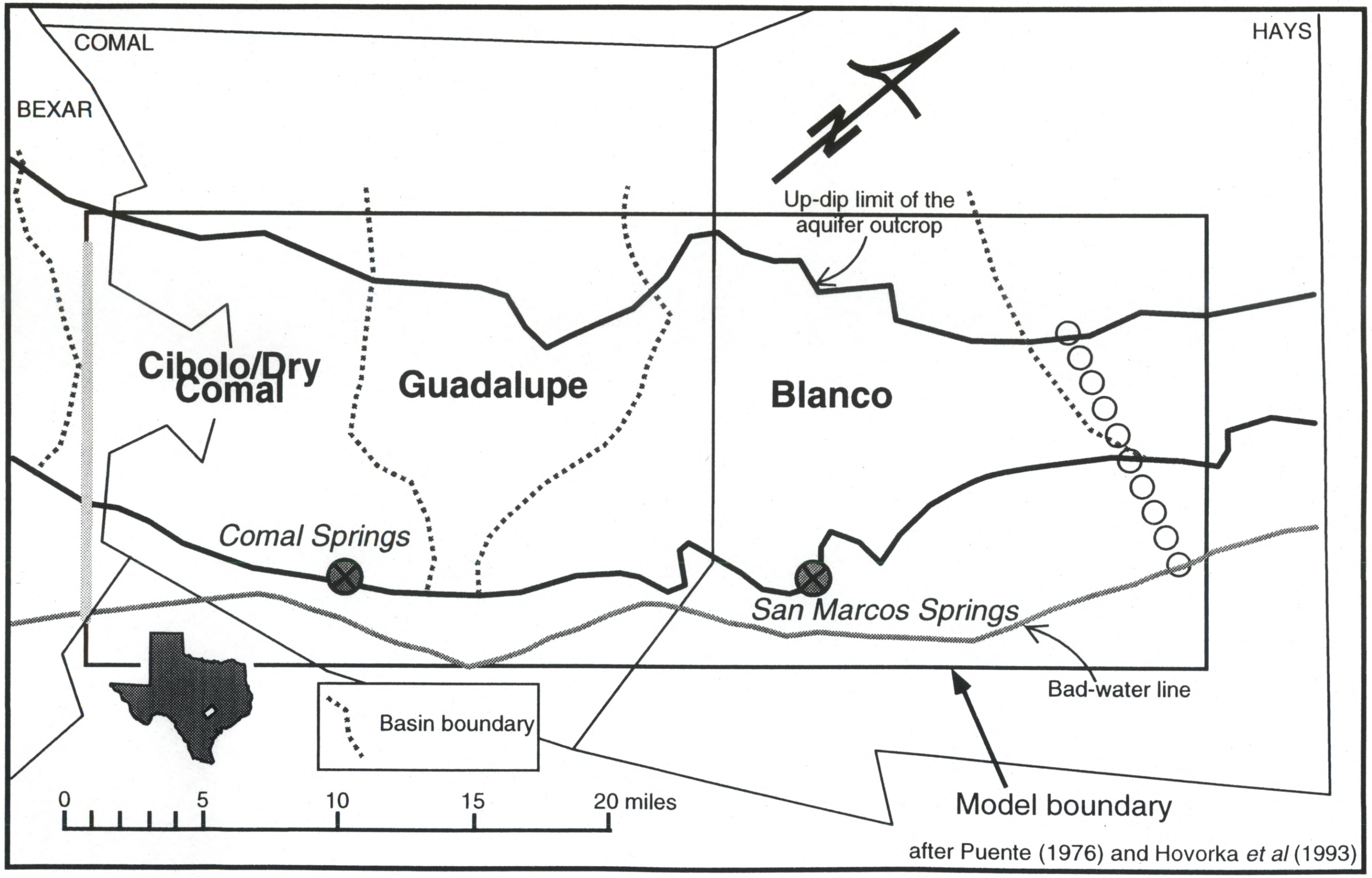

Figure 5.9 Recharge basins in the model area

For San Marcos Springs, discharge values were similarly plotted versus water levels in well LR-67-09-110 taken sporadically over the interval January, 1986 to December, 1993. The equation for the linear regression fit to the data has an R^2 coefficient of 0.875. Based on this equation, the spring elevation and spring conductance for San Marcos Springs are 578.3 ft (176.3 m) and 1,970,739.5 ft^2/d (6.9 m^2/s), respectively. The values 578.3 ft and 2,000,000 ft^2/d are used in the model.

5.2.7 Areal Recharge.

Areal recharge in the IWR model is treated as a single, one-dimensional term with the units [L/t] applied to every active node in the upper (unconfined) layer. In other words, recharge to the aquifer in the model is applied evenly over the entire area of the unconfined layer.

The recharge value used in the IWR model was calculated using historical recharge data from the three river basins in the model area. The model area is covered by the Cibolo - Dry Comal River Basin, the Guadalupe River Basin, and the Blanco River Basin (Figure 5.9) (Puente, 1976). Estimations of annual recharge to the Edwards through each of the major river basins in the aquifer have been recorded over the period 1934 to 1992 (EUWD, 1993). The annual recharge data over the period of record was used to determine an average annual recharge value for each of the three basins in the model area. The average annual recharge for each basin is then divided by the area of the basin to get a one dimensional term of [L/t] for each basin. These values were converted to the proper units and averaged over the entire area of the model recharge zone to get a single value that was applied to every unconfined node in the model. These calculations resulted in a recharge value of 0.00136 ft/d ($3.91\text{x}10^{-9}$ m/s). The value 0.001 ft/d ($3.52\text{x}10^{-9}$m/s) was used for the IWR model.

5.2.8 Hydraulic Conductivity and Anisotropy.

Hydraulic conductivity values were assigned to each node in the IWR model. A single anisotropy value was then assigned to the whole model area. Since no specific values for these parameters exist, hydraulic conductivity and anisotropy values were estimated by "trial and error" calibration of the IWR model. This calibration involved varying model conductivity and anisotropy values while monitoring the resulting spring discharge and aquifer heads, until discharge matched the real aquifer discharge values and the model head distribution matched the real aquifer pootentiometric surface. Model calibration is discussed in detail in section 5.2.10.

Before the IWR model was calibrated, a preliminary two-dimensional finite difference model of the study area (hereafter referred to as the "preliminary model") was constructed (see Appendix B for a discussion of the construction and results of the preliminary model). This simplified approximation of the model area was used to estimate the initial values of hydraulic conductivity and anisotropy that were applied to the IWR model before calibration. Results of the preliminary model simulations indicated that a homogeneous aquifer with a conductivity of 5000 ft/d (0.0176 m/s) and an anisotropy of $K_x = 15K_y$ matched the real aquifer potentiometric surface and resulted in a Comal Springs discharge value (170 cfs (4.8 m^3/s)) that falls within the same order of magnitude as the period-of-record average of 284 cfs (8.0 m^3/s). This conductivity value, when assigned to the IWR model and multiplied by the saturated thickness of the model (i.e., 400 ft (122 m) for the confined zone and 50 to 400 ft (15.2 to 121.9 m) for the unconfined zone), results in transmissivity values of 2 million ft^2/d (2.15 m^2/sec) for the confined zone and 250,000 to 2 million ft^2/d (0.27 to 2.15 m^2/sec) for the unconfined zone. It was therefore decided that the values 5000 ft/d and $K_x = 15K_y$ would be the initial values used in the calibration of the IWR model.

Previous studies of the Edwards aquifer have published estimated ranges of aquifer transmissivity that verify the preliminary model results. The most recent research on the Edwards aquifer in the Bexar, Comal and Hays County area suggests that transmissivities in this region range from 0.1 ft^2/d (0.00000012 m^2/sec) in parts of the unconfined zone to as high as 10 million ft^2/d (11.6 m^2/sec) in the confined zone (Hovorka *et al*, 1995). Other researchers have published the following estimated transmissivity ranges: from 133 ft^2/d (0.00014 m^2/s) in the Edwards outcrop to over 2.6 million ft^2/d (2.8 m^2/s) in the confined zone (Klemt *et al*, 1979); from very low values in parts of the recharge area to about 2 million ft^2/d (2.2 m^2/s) for the most permeable areas of the confined zone (Maclay and Small, 1986); and from 8600 to 1.7 million ft^2/d (0.0092 to 1.8 m^2/s) in the unconfined zone and 1.7 million to 8.6 million ft^2/d (1.8 to 9.2 m^2/s) in the confined zone (Maclay and Small, 1988).

5.2.9 Heterogeneities in Conductivity.

The preliminary model, used to estimate the initial conductivity and anisotropy values for the IWR model, treated the system as a homogeneous and anisotropic aquifer. These conditions, with the final conductivity and anisotropy values of 5000 ft/d (0.0176 m/s) and $K_x = 15K_y$, respectively, resulted in discharge from the Comal Springs node (170 cfs (4.8 m^3/s)) that closely matched the period - of - record average value of 284 cfs (8.0 m^3/s). However, the calculated discharge from the San Marcos Springs node (406 cfs (11.4 m^3/s)) under these model conditions was more than 2 times the volume of discharge from the Comal Springs node (170 cfs (4.8 m^3/s). This is not a surprising result; in a homogeneous groundwater model with two unequal elevation drains, similar drain conductances, and no other discharge, the lower elevation drain should have a greater discharge than the higher elevation drain. However, this result is contrary to the true situation. Over the period - of - record, the average discharge from San Marços Springs (170 cfs (4.8 m^3/s)) is approximately 60% of the average discharge from Comal Springs (284 cfs (8.0 m^3/s)). This is most likely due to the presence of a heterogeneous system that is resulting in lower hydraulic heads near San Marcos Springs.

One scenario that could account for this would be a situation where the transmissivity in the vicinity of San Marcos Springs is lower than the transmissivity near Comal Springs. Groundwater flow is governed by the equation

$$Q = K\nabla h\, A \tag{3}$$

where

$Q \equiv$ discharge through cross sectional area A $[L^3/t]$

$K \equiv$ hydraulic conductivity [L/t]

$\nabla h \equiv$ hydraulic gradient [L/L]

$A \equiv$ cross sectional area of aquifer $[L^2]$.

If we break the area term into the width times the saturated thickness, and then take a unit width of aquifer, the equation becomes

$$Q_u = T\nabla h \tag{4}$$

where

$$T = Kb \tag{5}$$

and

Q_u ≡ discharge through a unit width of aquifer $[L^2/t]$

T ≡ transmissivity $[L^2/t]$

∇h ≡ hydraulic gradient [L/L]

b ≡ saturated thickness of the aquifer [L].

Under steady-state conditions, water flowing from a higher transmissivity zone into a zone of lower transmissivity would result in a higher hydraulic gradient in the low transmissivity zone. A higher hydraulic gradient would mean lower hydraulic heads in the low transmissivity zone, resulting in reduced discharge from any springs in that zone (as per Equation 2 in section 5.2.5). Therefore, if we assume that the transmissivity near San Marcos Springs is lower than the transmissivity near Comal Springs, we would expect the discharge from San Marcos to be lower than it would if transmissivity was homogeneous. This assumption is consistent with the map of transmissivity zones in the Edwards aquifer constructed by Maclay and Small (1986). This map depicted subarea R (the zone surrounding Comal Springs) as having a greater relative transmissivity than subareas S and T (the zones surrounding San Marcos Springs) (Figure 2.8).

The preliminary model was used to investigate the effects of transmissivity heterogeneities on discharge from Comal and San Marcos Springs. Since transmissivity is a function of hydraulic conductivity and saturated thickness, both factors were independently varied through a series of simulations in an attempt to estimate which one is controlling the transmissivity distribution in the aquifer. In the first set of simulations, hydraulic conductivity was held constant at K = 5000 ft/d (0.0176 m/s) while aquifer thickness was increased in the zone around Comal Springs and decreased in the zone around San Marcos Springs. These simulations indicate that variations in aquifer thickness in the zones around the springs, plus or minus up to 75% of the original thickness of the preliminary model (350 ft (107 m)), did not affect the relative discharges from the springs (within 10 cfs). Based on these simulations, it was concluded that aquifer thickness variations were not significant enough to control the distribution of transmissivity in the aquifer.

In the second set of simulations, thickness was held constant and hydraulic conductivity was varied. Based on Maclay and Small's (1986) transmissivity map, the model was broken up into three main zones: zone A (the area updip from the spring faults), zone B (the area around San Marcos Springs), and zone C (the area around Comal Springs) (Figure 5.10). The results of this set of simulations indicate that a conductivity of 5000 ft/d (0.0176 m/s) in zones A and C (i.e., the updip zone and the Comal Springs zone, respectively) and a conductivity of 2000 ft/d (0.00706 m/s) in zone B (i.e., the San Marcos Springs zone) resulted in spring discharges (290 cfs (8.2m^3/s) at Comal; 181 cfs (5.1 m^3/s) at San Marcos) that fell within 5% of the true period-of-record averages.

5.2.10 Model Calibration

Once the IWR model was set up with the dimensions, boundary conditions, and spring parameters described previously, the conductivity values in the three zones (zones A, B, and C described in section 5.2.9) and in the lower layer of the model (hereafter referred to as zone D) were varied until discharge values from the springs matched the period - of - record averages at both springs. Once a set of conductivity values were determined, the head values at the constant head boundary were changed to match the head levels at low flow conditions (78 cfs (2.2 m^3/s) at Comal Springs; see section 5.2.4), and the simulations were run again to check the response of the springs to changing water levels in the aquifer. The conductivity values in the three zones and in the lower layer were then varied until model spring discharge matched the low flow discharge value. The constant head boundary values were then returned to the average condition levels, and the process was repeated until a set of conductivity values were determined that result in spring discharges that match flow conditions under the appropriate constant head boundary values.

Model calibration determined that a model with the following conductivity values:

zone A - 6000 ft/d (0.0212 m/s)

zone B - 1250 ft/d (0.0044 m/s)

zone C - 6000 ft/d (0.0212 m/s)

zone D - 7000 ft/d (0.0247 m/s)

resulted in a model with spring discharge and aquifer heads that closely matched the true values under average and low flow conditions (a comparison of model results and real aquifer data is given in Table 5.2).

1) Spring discharge			
		Model Results	**Real Aquifer Data**
Average flow	*Comal Springs*	**289.1 cfs (8.2 m^3/s)**	**284 cfs (8.0 m^3/s)**
	San Marcos	**181.4 cfs (5.1 m^3/s)**	**170 cfs (4.8 m^3/s)**
Low flow	*Comal Springs*	**80.8 cfs (2.3 m^3/s)**	**78 cfs (2.2 m^3/s)**
	San Marcos	**69.1 cfs (2.0 m^3/s)**	**62 cfs (1.8 m^3/s)**

2) Aquifer heads at the springs			
		Model Results	**Real Aquifer Data**
Average flow	*Comal Springs*	**625.8 ft (190.7 m)**	**626 ft (191 m)**
	San Marcos	**586.3 ft (178.7 m)**	**586 ft (179 m)**
Low flow	*Comal Springs*	**620.8 ft (189.2 m)**	**620 ft (189 m)**
7	*San Marcos*	**581.3 ft (177.1 m)**	**581 ft (177 m)**

Table 5.4 A comparison of IWR model calibration results and real aquifer data (aquifer heads for Comal and San Marcos Springs are based on head values in the Landa Well and well LR-67-09-110, respectively. Both wells are located within 0.25 kilometers of their respective springs).

A summary of the IWR model parameters is presented in Table 5.3.

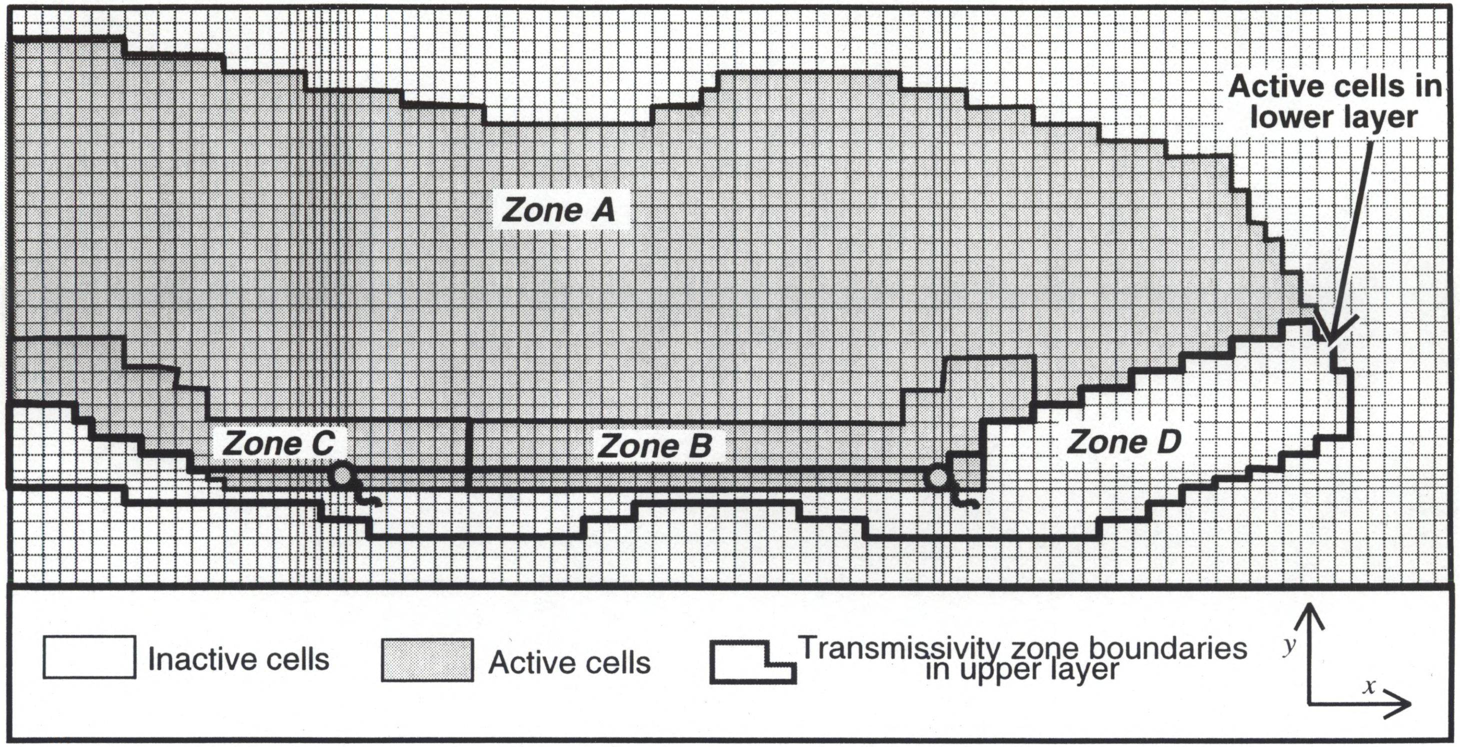

Figure 5.10 Model grid with transmissivity zones

Model Dimensions	**Grid dimensions**: 35 x 87 block-centered nodes **Δx** = 0.5 miles (0.8 km) except columns 18 through 25, 61, and 62 = 0.25 miles (0.4 km) **Δy** = 0.5 miles (0.8 km) except rows 29 and 30 = 0.25 miles (0.4 km) **Number of Layers**: 2 **Thickness**: Upper layer - from 50 to 400 ft (15 to 122 m) Lower layer - 400 ft (122 m)
Spring Parameters	**Conductance**: Comal Springs - 3,200,000 ft^2/d (13 m^2/s) San Marcos Springs - 2,000,000 ft^2/d (7 m^2/s) **Elevation**: Comal Springs - 617.5 ft (188.2 m) San Marcos Springs - 578.3 ft (176.3 m)
Hydraulic Parameters	**Anisotropy**: $K_x = 15K_y$ **Hydraulic conductivity**: zone A - 6000 ft/d (0.0212 m/s) zone B - 1250 ft/d (0.00441 m/s) zone C - 6000 ft/d (0.0212 m/s) zone D - 7000 ft/d (0.0247 m/s)
Areal Recharge	**Recharge** = 1.0×10^{-3} ft/d (3.52×10^{-9} m/s)

Table 5.5 Injection well response model parameters.

5.3 Infiltration Gallery Model

The formation of a steady-state groundwater mound on the Regional Dense Member (RDM) under an infiltration gallery at Comal Springs is simulated by a two-dimensional computer model based on an analytical solution presented by T. H. Filley in **Ground Water** (Filley, 1992). The original solution, which solved for the formation of a steady-state groundwater mound on a sloping, semipervious layer (SPL) under a percolation pond, was adapted for use in an analytical model that simulates infiltration at Comal Springs.

This analytical solution models the system as a two-dimensional slice of the aquifer in the vicinity of Comal Springs (Figure 5.11). Because it is a two-dimensional model, all volumetric flux rates are given area units [L^2/t] rather than volumetric units [L^3/t]. These area flux rates actually imply volumetric flux rates per unit width of aquifer, i.e., [$L^3/t/L$]. In this thesis, all infiltration gallery flux rates will be assigned area units rather than volume per unit width units.

Since ground truth data on the parameters necessary to run the model is limited, the intent of this model is not to create an exact simulation of the aquifer. Rather, the intent is to use the model to investigate the sensitivity of the system to ranges of values for the unknown parameters.

The infiltration gallery model requires the following values for input (all units in meters and days; see Figure 5.11):

- α - the angle of the sloping layer (i.e., the RDM)
- **M** - the thickness of the RDM [L]
- ϕ - the porosity of the subsurface above the RDM (i.e., the Grainstone Member (GM) of the Person Formation) [ ]
- **E** - the evapotranspiration rate [L/t]
- **D** - the width of the infiltration gallery [L]
- $\mathbf{K_{RDM}}$ - the hydraulic conductivity of the RDM [L/t]
- $\mathbf{K_{GM}}$ - the hydraulic conductivity of the subsurface above the RDM [L/t]

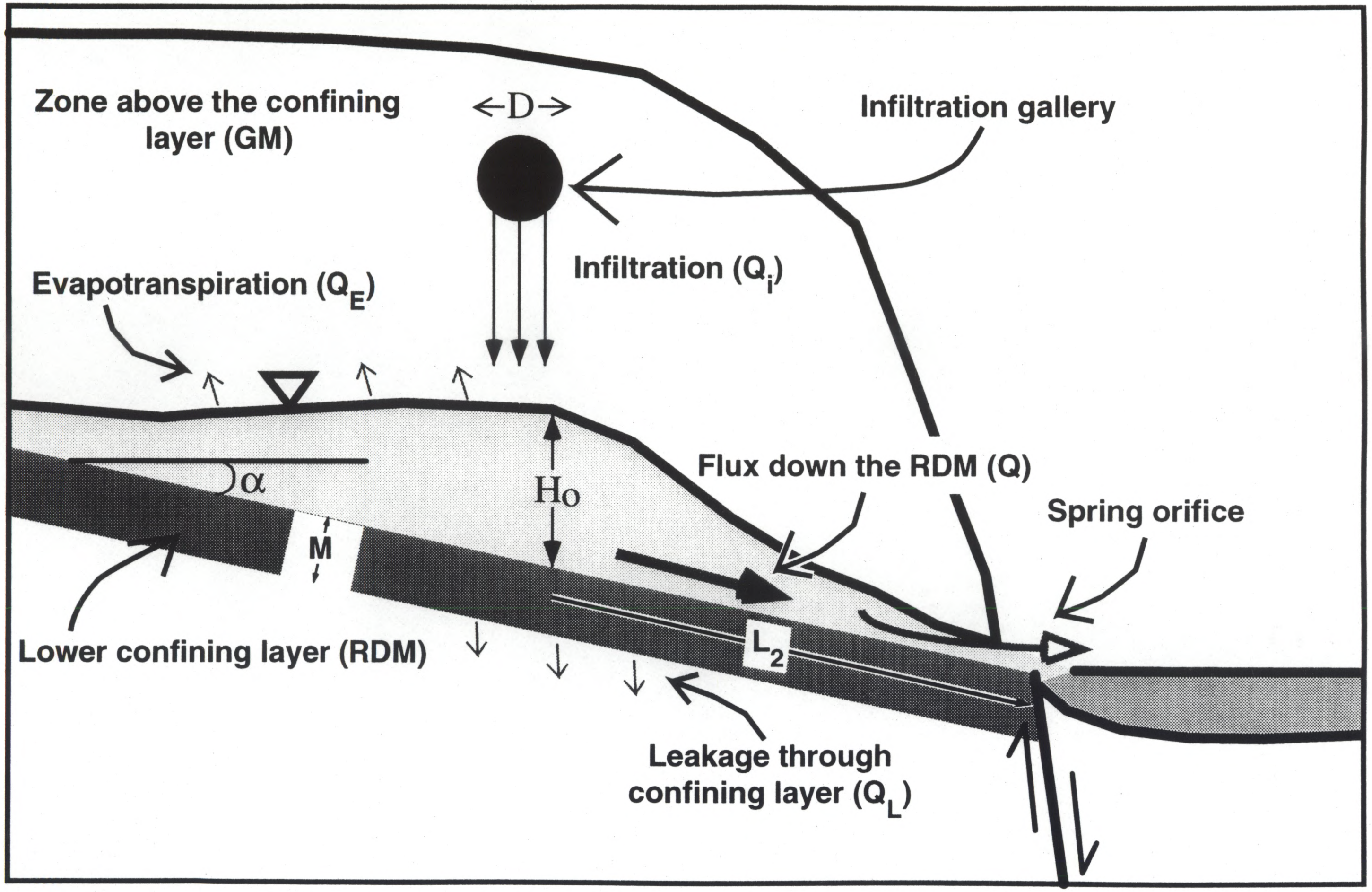

Figure 5.11 Infiltration gallery model cross-section

It uses these data to solve for the dimensions of the mound (more specifically, the head of the mound above the lower confining layer at the point directly below the infiltration gallery (Ho) and the distance from the point of origin of the mound to the leading edge of the mound (L2)), the rate of infiltration through the gallery, the rate of evapotranspiration from the mound, the flux rate of water moving down the slope, the flux rate of water through the RDM, and time of formation of the mound.

5.3.1 Model Theory and Model Derivation

Refer to Figure 5.12 for a graphic representation of the variables discussed in this section. All variables are listed and described in section 5.3.1.2.

The mathematical development of this analytical solution requires that the following assumptions be made:

- The aquifer is of infinite lateral extent.
- The rate of infiltration from the gallery into the subsurface is constant (i.e., the infiltration gallery is provided with a constant source of water).
- The vertically averaged flow is one-dimensional and parallel to the SPL.
- Elevation head gradients are much larger than pressure head gradients.
- The zone above the sloping SPL is homogeneous, continuous, and isotropic.

In reality, the zone above the SPL in the model area is not homogeneous, continuous, or isotropic. However, at this time, the degree of heterogeneity, discontinuity, and anisotropy present in this part of the aquifer is not known, and cannot be accounted for in the model. It was therefor decided to follow these assumptions, with the understanding that these results are preliminary results that may change with the gathering of more detailed data and the development of more sophisticated models.

The governing equations for the system are the steady state continuity equation:

$$\nabla \cdot q_s = \frac{\partial}{\partial x} q_x + \frac{\partial}{\partial z} q_z = 0 \tag{6}$$

where

x and z $\equiv$ Cartesian coordinates aligned horizontal and vertical, respectively

q_s ≡ specific discharge [L/t]

q_x ≡ horizontal specific discharge [L/t]

q_z ≡ vertical specific discharge [L/t],

and Darcy's Law:

$$q_s = -K\nabla h \tag{7}$$

where

K ≡ hydraulic conductivity [L/t]

∇h ≡ hydraulic gradient [L/L].

The model boundary conditions (evaporative flux E [L/t] across the phreatic surface of the mound (F_1) and leakage Q_{cf} [L/t] through the lower confining layer (F_2)) are represented by the following equations:

$$E \nabla F_1 = qb_1 \nabla [z-b_1(x)] \tag{8}$$

$$Q_{cf} \nabla F_2 = qb_2 \nabla [z-b_2(x)] \tag{9}$$

where

qb_1 ≡ flux through the phreatic surface at position $b_1(x)$

qb_2 ≡ flux through the lower confining layer at position $b_2(x)$

Integrating equations (6) and (7) along the vertical between $b_1(x)$ and $b_2(x)$ (making use of the Lebintz rule and after assuming the potential along the vertical is approximately constant) yields

$$-K\left\{\frac{d}{dx}\{[b_1(x)]\frac{d}{dx}H\}\right\} + qb_1\nabla[z - b_1(x)] - qb_2\nabla[z - b_2(x)] = 0 \tag{10}$$

Equation (10) incorporates the continuity and velocity equations (equations (6) and (7), respectively) and the boundary conditions into one equation. The total head in equation (10) is defined as the sum of the pressure head (Hp) and the elevation head (He); that is

$$H = Hp + He \tag{11}$$

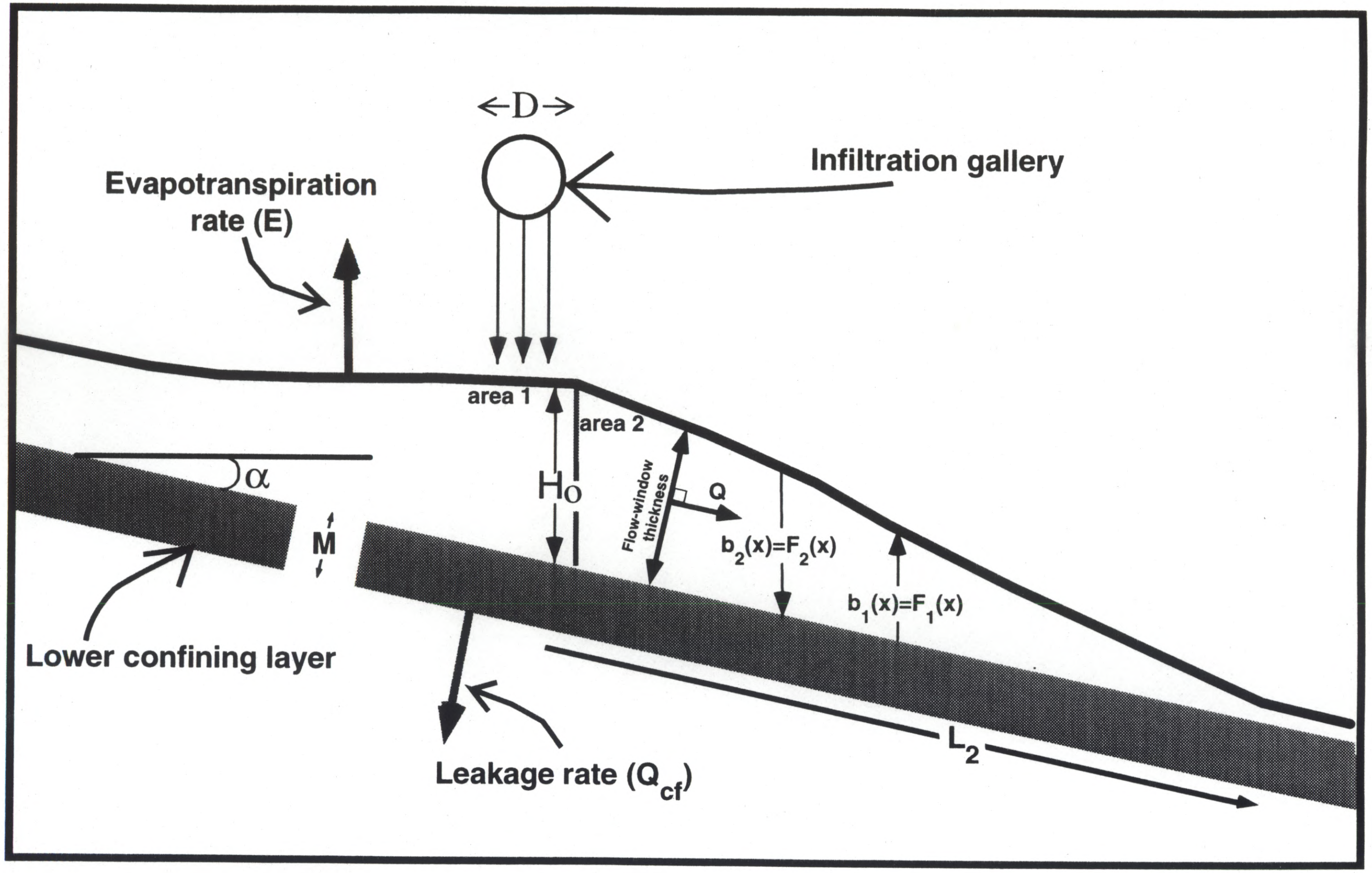

Figure 5.12 Cross-section of infiltration gallery model domain

Using the chain rule, the rotation of the coordinate for the sloping angle α is accomplished as

$$X = L \cos\alpha \tag{12}$$

$$d/dX = (d/dL)(dL/dX) = (d/dL)(1/\cos\alpha) \tag{13}$$

Substitution of equations (11), (12), and (13) into equation (10) results in

$$-\frac{K}{\cos\alpha}\frac{d}{dL}\left\{[b_1(L)]\frac{1}{\cos\alpha}\frac{d(Hp+He)}{dL}\right\} - Q_{cf}\nabla F_2 + E\nabla F_1 = 0 \tag{14}$$

where $b_1(L)$ is the saturated thickness available for groundwater flow at some point along the length of the sloping layer, hereafter referred to as the flow-window thickness.

Equation (14) represents flow parallel to and down the slope of the lower confining layer. Since it is assumed that the elevation head gradient is much higher than the pressure head gradient, the pressure head part of the gradient term is ignored, and the equation becomes

$$-\frac{K}{\cos\alpha}\frac{d}{dL}\left\{[b_1(L)]\frac{1}{\cos\alpha}\frac{dHe}{dL}\right\} - Q_{cf}\nabla F_2 + E\nabla F_1 = 0 \tag{15}$$

The term describing leakage through the SPL assumes that leakage travels through the shortest distance across the SPL. The equation describing the SPL surface is

$$F_2 = -L \sin\alpha \tag{16}$$

and the equation for the gradient across this surface is represented by

$$\nabla F_2 = \hat{\imath}(\partial F_2/\partial x) + k(\partial F_2/\partial z) = \hat{\imath}(\sin\alpha/\cos\alpha) + k \tag{17}$$

where $\hat{\imath}$ and k are the unit vectors. Leakage across a sloping layer can be resolved into its components as

$$Q_{cf} = \hat{\imath}(Q_x) + k(Q_z) = \hat{\imath}(\sin\alpha + k\cos\alpha)(K_{SPL}/M)(Hp + M\cos\alpha) \tag{18}$$

where the last term on the right side of equation (18) is the sum of the pressure head and elevation head difference across the sloping layer. Multiplying equation (18) by the gradient across the SPL

$$Q_{cf} \cdot \nabla F_2 = -\{\hat{\imath}(\sin\alpha)(K_{SPL}/M)+[Hp + M(\cos\alpha)] + k(\cos\alpha)(K_{SPL}/M)[Hp + M(\cos\alpha)]\}\cdot(\hat{\imath}\tan\alpha + k) \tag{19}$$

$$Q_{cf} \cdot \nabla F_2 = ((K_{SPL}/M)\{[(\sin^2\alpha)/(\cos\alpha)] + (\cos\alpha)\}Hp + K_{SPL}) \tag{20}$$

results in the equation for leakage across the SPL. If ($Hp\cos\alpha$) is substituted into equation (14) for the flow window thickness ($b_1(L)$), and equation (20) is then substituted into equation (14), equation (14) becomes

$$K\frac{d}{dL}\left(Hp\frac{d}{dL}L\tan\alpha\right) = -E - \frac{K_{SPL}}{M}\left[(\sin^2\alpha)/(\cos\alpha) + \cos\alpha\right]Hp - K_{SPL} \tag{21}$$

where K is the saturated hydraulic conductivity of the aquifer above the SPL. This equation is the equation for phreatic flow with a dominant elevation gradient along a sloping semipervious layer with leakage and a spatially constant rate of evapotranspiration (hence the scalar E substituted in for $E\cdot\nabla F_1$).

This equation can be used to derive an equation that determines L2, the length of the steady state groundwater mound that forms below the infiltration gallery (assuming an aquifer of infinite lateral extent). First, equation (21) is divided by $\tan\alpha$, and the following substitutions are made:

$$B = (K_{SPL}/M)\,[(\sin^2\alpha)/(\cos\alpha) + \cos\alpha]\,(1/\tan\alpha) \tag{22}$$

$$A = (K_{SPL} + E)\,(1/\tan\alpha) \tag{23}$$

resulting in the equation

$$-K\frac{dHp}{dL} = BHp + A \tag{24}$$

When integrated, this equation yields

$$Hp = \frac{1}{B}\left\{e^{(\frac{B}{K}[C-L])} - A\right\} \tag{25}$$

where C is an arbitrary constant. This constant is evaluated by recognizing that, at the leading edge of the groundwater mound on the sloping confining layer (i.e., at L=L2), flux parallel to the sloping layer is equal to zero. This may be stated as

$$Q|_{L2} = \text{-K Hp } (\cos\alpha) \text{ dHe/dL} = 0$$

or

$$Q|_{L2} = K\frac{1}{B}\{[e^{B(C-L2)/K}] - A\}(\cos\alpha)(\sin\alpha) = 0 \tag{26}$$

Solving for C and substituting into equation (25) yields

$$Hp = \frac{A}{B}\left(\left\{e^{\left[\left(\frac{B}{K}\right)(L2-l)\right]} - 1\right\}\right) \tag{27}$$

This equation can be rearranged to solve for L2 (the length of the groundwater mound)

$$L2 = \frac{K}{B}\ln\left[\frac{B}{A}Hp + 1\right] + L \tag{28}$$

The mound length can now be calculated by recognizing that, at a point where L equals 0, Hp equals Ho (head at the origin of the mound, i.e., the groundwater mound head directly below the infiltration gallery)

$$L2 = \frac{K}{B}\ln\left[\frac{B}{A}Ho + 1\right] \tag{29}$$

This equation is the equation used by the infiltration gallery model to determine the steady state migration distance of phreatic water traveling on a sloping leaky confining layer with evapotranspiration and a saturated thickness of Ho at the origin.

Determining the value of Ho requires that an approximate volume integral analysis be performed for the volume of water mounding beneath the infiltration gallery. This is accomplished by recognizing that the quantity of water moving downslope (Q) must be equal to the algebraic sum of the water that leaks through sloping confining layer (Q_L), the water lost to evapotranspiration (Q_E), and the water that infiltrates from the pond(Q_I). This can be stated as

$$Q = Q_L + Q_E + Q_I \tag{30}$$

The infiltration rate (Q_I) can be calculated as the product of the hydraulic conductivity of the units above the sloping confining layer (K) and the infiltration gallery width (D):

$$Q_I = KD \tag{31}$$

The rate of leakage across the confining layer is approximated by replacing Hp in equation (21) with L $\sin\alpha$, and then integrating along the length of the sloping lower confining layer, yielding

$$Q_L = (G\, Ho^2/2\sin\alpha)+(K_{SPL}Ho/\sin\alpha) \tag{32}$$

where $G = (K_{SPL}/M)[(\sin^2\alpha)/(\cos\alpha) + \cos\alpha]$ and $Ho = L1\sin\alpha$.

The rate of evaporation from the phreatic surface of the mound can be approximated by subtracting the width of the infiltration gallery (D) from the horizontal component of L1 (L1 $\cos\alpha$) and then multiplying by E

$$Q_E = E(L1\cos\alpha - D) = E[\, Ho\,(\cos\alpha / \sin\alpha) - D] \tag{33}$$

The rate moving downslope can be calculated using the window thickness (Ho $\cos\alpha$) and the elevation gradient ($-\sin\alpha$) to determine Q as

$$Q = K\, Ho\cos\alpha\sin\alpha \tag{34}$$

Equations (31) -(34) are substituted into equation (30) to yield the equation

$$A1(Ho)^2 + B1(Ho) + C1 = 0 \tag{35}$$

where

$$A1 = \left[\frac{D}{M}\Big/ D\frac{K}{K_{SPL}}\right](\tan\alpha + 1/\tan\alpha)\Big/2$$

$$B1 = \left[1\Big/\left(\frac{K}{K_{SPL}}\sin\alpha\right)\right] + \cos\alpha\sin\alpha + \left[\cos\alpha\Big/\left(\frac{K}{E}\sin\alpha\right)\right]$$

$$C1 = -D\left[(1/K) + \left(1\Big/\frac{K}{E}\right)\right]$$

Equation (35) can be solved for Ho, yielding

$$Ho = [-B1 + (B1^2 + 4\,A1\,C1)^{1/2}/\,2A1 \tag{36}$$

This equation determines the height of the groundwater mound at the point directly below the infiltration gallery (Figure 5.11)

The time required for the groundwater mound to achieve steady state can be estimated by calculating the area of the mound (i.e., the volume of the mound per unit width) and determining the amount of time required to fill that area. If mass losses due to evapotranspiration and leakage are ignored, a lower limit (or minimum) formation time can be calculated.

The area of the mound is calculated as the sum of two smaller areas - the area beneath the infiltration gallery (area 1) and the area downslope of the infiltration gallery (area 2; Figure 5.12). Area 1 is estimated as a triangular shape.

$$\text{Area 1} = \tfrac{1}{2}\text{Ho L1} \cos\alpha = \tfrac{1}{2}\text{Ho}^2 \cos\alpha / \sin\alpha \qquad (37)$$

Area 2 is calculated by integrating the equation (27) between the origin (i.e., the point under the infiltration gallery) and the leading edge of the mound (L2)

$$\text{Area2} = \int_0^{L2} \frac{A}{B}\left\{ e^{\left[\frac{B}{K}(L2-L)\right]} - 1 \right\} dL = \frac{A}{B}\left\{ \frac{K}{B}\left[e^{\frac{B}{K}L2} - 1 \right] - L2 \right\} \qquad (38)$$

The total area of the groundwater mound is the sum of these two equations. The sum of these equations is then multiplied by the porosity of the units above the lower confining layer, and divided by the infiltration rate (K2 D) to yield

$$T_{\text{formation}} = \frac{\phi\left(\tfrac{1}{2}\text{Ho2} \cos\alpha \sin\alpha + \frac{A}{B}\left\{ \frac{K}{B}\left[e^{\frac{B}{K}L2} - 1 \right] - L2 \right\} \right)}{\text{L2D}} \qquad (39)$$

5.3.1.1 Model Equation Summary

To summarize, the main equations of the analytical model are:

a) Mound length (L2):

$$L2 = \frac{K}{B} \ln\left[\frac{B}{A} Hp + 1\right] + L \tag{28}$$

b) Head at mound origin (i.e., at the point under the infiltration gallery) (Ho):

$$Ho = [-B1 + (B1^2 + 4\ A1\ C1)^{½} / 2A1 \tag{36}$$

c) Volumetric flux rate of water infiltrating into the subsurface from the infiltration gallery (Q_I):

$$Q_I = KD \tag{31}$$

d) Volumetric flux rate of water leaking through a unit width of the lower confining layer (Q_L):

$$Q_L = (G\ Ho^2/2\sin\alpha) + (K_{SPL} Ho/\sin\alpha) \tag{32}$$

e) Volumetric flux rate of water evaporating from the phreatic surface of the groundwater mound (Q_E):

$$Q_E = E[\ Ho\ (\cos\alpha\ /\ \sin\alpha) - D] \tag{33}$$

f) Volumetric flux rate of water moving down the lower confining layer through a unit width of aquifer (Q):

$$Q = K\ Ho\ \cos\alpha\ \sin\alpha \tag{34}$$

g) Time of formation of the steady state groundwater mound ($T_{formation}$):

$$T_{formation} = \frac{\phi\left(½Ho2\ \cos\alpha \sin\alpha + \frac{A}{B}\left\{\frac{K}{B}\left[e^{\frac{B}{K}L2} - 1\right] - L2\right\}\right)}{L2D} \tag{39}$$

5.3.1.2 List of variables in infiltration gallery model

Primary variables in infiltration gallery model:

Ho - groundwater mound head at the origin (i.e., directly below the infiltration gallery) [L]

L2 - distance along lower confining layer from the origin to the leading edge of the groundwater mound [L]

$\mathbf{Q_I}$ - rate of infiltration from the gallery [L^2/t]

$\mathbf{Q_L}$ - flux of water leaking through the lower confining layer [L^2/t]

$\mathbf{Q_E}$ - flux of water lost to evapotranspiration [L^2/t]

Q - flux of water moving down the lower confining layer [L^2/t]

$\mathbf{T_{formation}}$ - time of formation of steady state [t]

Other variables:

x, z - spatial dimensions [L]
D - infiltration gallery width [L]
α - dip angle of the lower confining layer
M - thickness of the lower confining layer [L]
ϕ - porosity of the zone above the lower confining layer
E - evapotranspiration rate [L/t]
$\mathbf{Q_{cf}}$ - rate of leakage through the lower confining layer [L/t]
$\mathbf{Q_x}$, $\mathbf{Q_z}$ - x and z components, respectively, of Q_{cf} [L^2/t]
$\mathbf{K_{SPL}}$ - hydraulic conductivity of the lower confining layer [L/t]
K - hydraulic conductivity of the zone above the lower confining layer [L/t]
∇**h** - hydraulic gradient [L/L]
$\mathbf{q_s}$ - specific discharge [L/t]
$\mathbf{q_x}$, $\mathbf{q_z}$ - x and z components, respectively, of q_s [L/t]
$\mathbf{b_1(x)}$ - height of the phreatic water surface above the lower confining layer [L]
$\mathbf{b_2(x)}$ - elevation of the lower confining layer [L]
$\mathbf{b_1(L)}$ - saturated thickness of aquifer above the lower confining layer (the flow-window thickness) [L]
H - total groundwater head [L]
He - elevation head component of total head [L]
Hp - pressure head component of total head [L]
$\nabla \mathbf{F_1}$ - gradient of the phreatic water surface [L/L]
$\nabla \mathbf{F_2}$ - gradient of the lower confining layer [L/L]
$\mathbf{qb_1}$ - flux through the phreatic surface at $b_1(x)$ [L/t]
$\mathbf{qb_2}$ - flux through the lower confining layer at $b_2(x)$ [L/t]
L - length along the lower confining layer parallel to dip [L].

5.3.2 Model Parameters

Strike and dip measurements taken on outcrops of the RDM in Panther Canyon (Figure 1.7) resulted in dip values ranging from 3° to a maximum of 6°. The average of all dip values taken in Panther Canyon was 5.21°. Based on these measurements, all simulations with the infiltration gallery were run with a sloping layer angle of 5°.

According to Rose (1972), the thickness of the RDM in Comal County is approximately 20 - 25 ft (6.1 to 7.6 m) thick. This thickness is fairly consistent throughout Comal County. A value of 7 m is used in all model simulations.

Hovorka *et al* (1995), examined karst porosity in outcrops of the Edwards aquifer in several counties. They measured a porosity of 0.0568 in an outcrop of the Person Formation along Loop 337 in New Braunfels, TX, less than 2 miles (3.2 km) from the springs. A porosity value of 0.05 is used in all model simulations.

For this model, evapotranspiration is assumed to be negligible. However, the equations used by the model require an evapotranspiration value, or the model results in an undefined solution. To determine a value of evapotranspiration that would not affect the results of the model, a sensitivity analysis was performed with the model using varied evapotranspiration values and constant values for all other parameters. These simulations indicate that evapotranspiration values below 0.0001 m/d (1.1×10^{-9} m/s) have a negligible effect on model output (i.e., resulted in an evaporative flux value less than 0.1% of the total infiltration flux from the gallery). A value of 0.00001 m/d (1.1×10^{-10} m/s) is used in all model simulations.

The following gallery widths (D) were used in the infiltration gallery model simulations:

0.5 m

1.0 m

2.0 m

3.0 m

No specific hydraulic conductivity values exist for the RDM or for the zone of the aquifer above the RDM (the Grainstone Member (GM) of the Person Formation). However, estimated ranges of values for these parameters are available. The most recent work in the

Edwards (Hovorka *et al*, 1995) estimates a range of conductivity values in the Edwards of 1.2 x 10^{-9} to 1.2 x 10^{-1} m/s. Results of the calibration of the IWR model in this thesis resulted in a range of conductivities of 4.4 x 10^{-3} to 2.5 x 10^{-2} m/s. It was decided that a set of infiltration gallery model simulations would be run with ranges of conductivity values for K_{RDM} and K_{GM} based on these ranges, using the range from Hovorka *et al* (1995) as a constraint on the lower end of the model ranges, and the IWR model calibration results as a constraint on the upper end of the model ranges.

Hovorka *et al* (1995) have recognized the RDM as a local confining unit in the Edwards. A range of values corresponding to the lowest order of magnitude of the range given in Hovorka *et al* (1995) was assigned to K_{RDM}, assuming that, as a local confining unit, it is one of the lower permeability units in the aquifer. Specifically, the following K_{RDM} values were used in the infiltration gallery model:

1 x 10^{-4} m/d (1.2 x 10^{-9} m/s)

5 x 10^{-4} m/d (5.8 x 10^{-9} m/s)

1 x 10^{-3} m/d (1.2 x 10^{-8} m/s)

The range of values for K_{GM} was also based on the range given in Hovorka, *et al* (1995). Since the infiltration gallery model obviously assumes that the zone above the sloping confining layer is a higher conductivity than the confining layer itself, the lowest value of K_{GM} was set one order of magnitude above the largest K_{RDM} value. The highest value was based on the highest conductivity value determined by the IWR model (5000 ft/d (1524 m/d, or 1.8x10^{-2} m/s)). Based on these constraints, a range of conductivity values from 0.01 m/d (1.2x10^{-7} m/s) to 1000 m/d (1.2x10^{-2} m/s), in half order-of-magnitude increments (i.e., 0.01, 0.05, 0.1, 0.5, 1, etc.), were used for the infiltration gallery model.

A summary of the infiltration gallery parameters is given in Table 5.4.

Sloping Angle of RDM	5°
Thickness of RDM	7 m
Porosity of GM	0.05
Evapotranspiration	0.00001 m/d
Infiltration Gallery Widths	0.5 m 1.0 m 2.0 m 3.0 m
RDM Conductivity Values (K_{RDM})	1 x 10^{-4} m/d (1.2 x 10^{-9} m/s) 5 x 10^{-4} m/d (5.8 x 10^{-9} m/s) 1 x 10^{-3} m/d (1.2 x 10^{-8} m/s)
GM Conductivity Values (K_{GM})	1.0x10^{-2} m/d (1.2x10^{-7} m/s) 5.0x10^{-2} m/d (5.8x10^{-7} m/s) 1.0x10^{-1} m/d (1.2x10^{-6} m/s) 5.0x10^{-1} m/d (5.8x10^{-6} m/s) 1.00 m/d (1.2x10^{-5} m/s) 5.00 m/d (5.8x10^{-5} m/s) 1.0x10^{1} m/d (1.2x10^{-4} m/s) 5.0x10^{1} m/d (5.8x10^{-4} m/s) 1.0x10^{2} m/d (1.2x10^{-3} m/s) 5.0x10^{3} m/d (5.8x10^{-3} m/s) 1.0x10^{3} m/d (1.2x10^{-2} m/s)

Table 5.6 Infiltration gallery model parameters.

6. MODEL SIMULATIONS, RESULTS, AND DISCUSSION

6.1 Introduction

Several sets of simulations were run with the IWR model and the infiltration gallery model. For the injection well simulations, both the injection rate and the distance of the well from the Comal Springs node were varied throughout the simulations. The rate of injection and the resulting spring discharges were used to calculate the injection efficiency for each simulation. For the infiltration gallery model, simulations were run with a range of Grainstone Member conductivities (K_{GM}), a range of Regional Dense Member conductivities (K_{RDM}), and a range of infiltration gallery diameters. The results were used to calculate the rate of infiltration from the gallery, the time until steady state conditions are achieved, the dimensions of the mound, and the efficiency of the infiltration gallery.

A description of the simulation procedures and a summary of the results are presented below.

6.2 Injection Simulations

6.2.1 Procedure

The IWR model was set up with the final parameters listed in Table 5.3 and the constant head boundary at low flow values (see Table 5.1). A well was then placed at node (23, 29), 0.25 miles (0.4 km) from the Comal Springs node (24,29). An injection rate of 100,000 ft^3/d (0.03 m^3/s, 475 gpm) was assigned to this well, the model was run to steady state, and a water balance was then calculated for the model solution. Once the water balance results were saved, the injection rate was raised to 1,000,000 ft^3/d (0.3 m^3/s, 4750 gpm), a new simulation was run, and a new water balance was calculated and recorded. The injection rate was then raised to 10,000,000 ft^3/d (3.0 m^3/s, 47,500 gpm), and the process was repeated. Once these three simulations were finished, the well was deactivated and a new well was placed in node (22,29), 0.5 miles (0.8 km) from the Comal Springs node. Simulations were run with the same three injection rates and water balances were calculated and saved. The same procedure was performed with wells at nodes

(21,29), (20,29), (19,29), (18,29), and (17,29). The distance of each node from the Comal Springs node is given in Figure 6.1. When the injection simulations were finished, a final simulation was run without any injection, and the resulting water balance was calculated.

For each injection simulation, the difference between the Comal Springs discharge value and the discharge value without injection was calculated to give the amount of injected water that actually discharges from the spring. This value was then divided by the corresponding injection rate to calculate the fraction of injected water that ends up discharging from the springs. This number, when converted to a percentage, represents the efficiency of the injection well. The resulting efficiencies are presented in Figure 6.1.

In addition to calculating spring discharge, the water balance function also calculates the vertical flux between the two layers of the model. This was used to calculate the amount of water moving into the Comal Springs node from the lower confined layer along the model fault zone.

6.2.2 Model Results

Injection efficiency ranges from 67% to 82%. Efficiency decreases as distance from the springs increases. For each set of simulations at each node, efficiency decreases with increasing injection rate. However, this decrease was slight (less than 1% for an order of magnitude increase in injection rate). An average of the three discharge values from the three injection simulation at each well node was calculated and presented in Figure 6.1.

Discharge from the Comal Springs node under low-flow boundary conditions and without injection is 80.8 cfs (2.29 m^3/s). Discharge values with injection ranged from 81.58 cfs (2.31 m^3/s) to 175.71 cfs (4.98 m^3/s).

Increases in head at the well nodes resulting from injection ranged from 0.13 ft (0.039 m) to 2.37 ft (0.72 m). Increases in head at the spring node resulting from injection ranged from 0.06 ft (0.018 m) to 2.34 ft (0.71 m).

The vertical flux between the two layers of the model at Comal Springs is approximately 9% of the total discharge from the springs. Vertical flux between layers was the same for all injection simulations (to within 0.1%). All model results are summarized in Table 6.1.

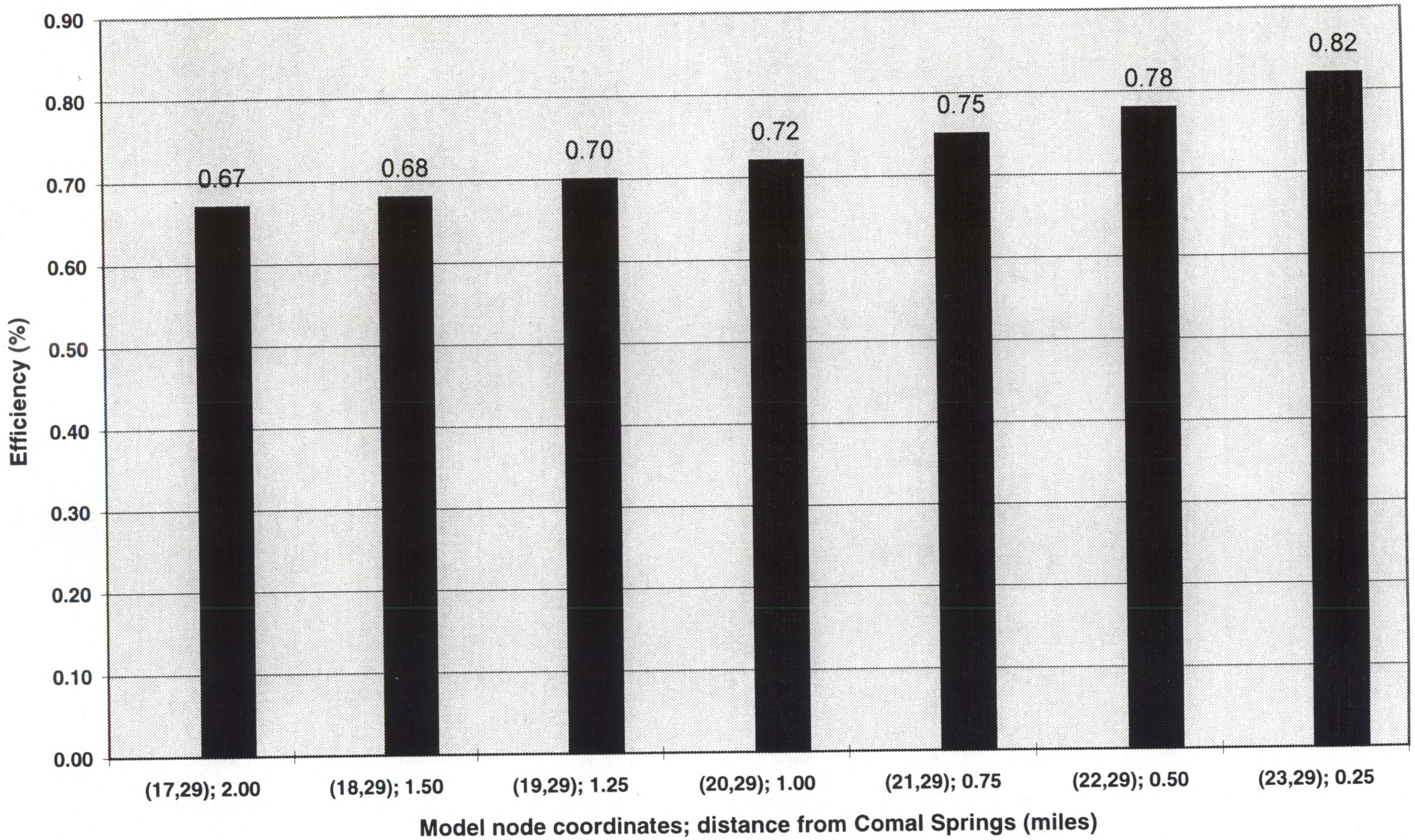

Figure 6.1 Injection well response model injection efficiencies

Injection well distance from springs (mi,km)		2.00, 3.22	1.50, 2.41	1.25, 2.01	1.00, 1.61	0.75, 1.21	0.50, 0.80	0.25, 0.40
Injection efficiency (%)		**0.67**	**0.68**	**0.70**	**0.72**	**0.75**	**0.78**	**0.82**
	Injection rate (cfs)							
Amount of injected water that reaches the spring orifices (cfs)	**0.00**	n/a	n/a	n/a	n/a	n/a	n/a	n/a
	1.16	0.78	0.79	0.81	0.84	0.87	0.90	0.95
	11.57	7.75	7.87	8.10	8.33	8.68	9.02	9.49
	115.74	77.55	78.70	81.02	83.33	86.81	90.28	94.91
Resulting spring discharge (cfs)	**0.00**	80.80	80.80	80.80	80.80	80.80	80.80	80.80
	1.16	81.58	81.59	81.61	81.64	81.67	81.70	81.75
	11.57	88.55	88.67	88.90	89.13	89.48	89.82	90.29
	115.74	158.35	159.50	161.82	164.13	167.61	171.08	175.71
Hydraulic head at Comal Springs under injection (ft)	**0.00**	620.80	620.80	620.80	620.80	620.80	620.80	620.80
	1.16	620.86	620.86	620.86	620.86	620.86	620.86	620.86
	11.57	621.02	621.03	621.03	621.04	621.05	621.06	621.07
	115.74	622.71	622.74	622.80	622.85	622.94	623.02	623.14
Head change at spring resulting from injection (ft)	**0.00**	0.00	0.00	0.00	0.00	0.00	0.00	0.00
	1.16	0.06	0.06	0.06	0.06	0.06	0.06	0.06
	11.57	0.22	0.23	0.23	0.24	0.25	0.26	0.27
	115.74	1.91	1.94	2.00	2.05	2.14	2.22	2.34
Hydraulic head at well node under injection (ft)	**0.00**	622.80	621.80	621.70	621.50	621.30	621.10	621.00
	1.16	622.94	621.94	621.84	621.64	621.44	621.23	621.13
	11.57	623.10	622.10	622.00	621.80	621.60	621.39	621.29
	115.74	625.17	624.17	624.07	623.87	623.67	623.46	623.36

Table 6.1 Effects of varied injection rates on spring discharge and aquifer heads

6.3 Infiltration Gallery Simulations

6.3.1 Procedure

The infiltration gallery model was set up with a gallery diameter of 0.5 m and the initial parameters listed in Table 5.4. A set of simulations were run with the model, starting with K_{GM} = 0.01 m/d (1.2×10^{-7} m/s) and ending with K_{GM} = 1000 m/d (1.2×10^{-2} m/s). When this set of simulations was completed, the gallery diameter was changed to the next value (1.0 m), and a similar set of simulations were run. This procedure was repeated with gallery diameters of 2.0 and 3.0 m. When all four sets of simulations were completed, K_{RDM} was changed to 0.0005 m/d (5.8×10^{-9} m/s), the diameter was reset to 0.5 m, and the procedure was repeated. These four sets of simulations were repeated again with K_{RDM} = 0.001 m/d (1.2×10^{-8} m/s). The results of each simulation were saved as individual ASCII text files, which were later imported into EXCEL™ for calculations and graphing.

Simulation results (infiltration gallery efficiencies, resulting mound dimensions, and times to steady state) were compiled into a set of summary tables (see Tables 8.4, 8.5, and 8.6 in Appendix D). Then, the gallery infiltration rate for each simulation was plotted against K_{GM} on a log-log scale to graphically illustrate the infiltration rate values calculated by the model (Figure 6.2). Next, the $\log_{10}$ of K_{RDM} was subtracted from the $\log_{10}$ of K_{GM} in each simulation to obtain the order of magnitude difference between the two values (since the model conductivity values ranged over several orders of magnitude, the $\log_{10}$ values were used in order to make the comparisons between the results easier to read). The time to steady state of the formation of the groundwater mound and the length of the resulting groundwater mound were plotted against these values on X-Y scatter plots (Figures 6.3 and 6.4). The infiltration gallery efficiency was calculated by dividing the resulting flow rate down the RDM by the corresponding infiltration rate, then multiplying by 100. The calculated efficiencies were plotted against the difference between $\log_{10} K_{GM}$ and $\log_{10} K_{RDM}$ to illustrate the relationship between efficiency and the relative values of K_{RDM} and K_{GM} (Figure 6.5).

6.3.2 Model Results

Because the infiltration gallery model is a two-dimensional model, all flux rates calculated by the model are given in units of m^2/d. Keep in mind that, since the model domain is a cross-section of aquifer perpendicular to an infiltration gallery, these values actually refer to volume per unit length of infiltration gallery (i.e., units of $m^3/d/m$).

The rate of infiltration from the gallery ranges from 0.005 m^2/d (5.8x10-8 m^2/s) to 3000 m^2/d (0.03 m^2/s). The order of magnitude of the infiltration rate is proportional to the $\log_{10} K_{GM}$. Increased gallery diameter results in increased infiltration.

The time of formation of a steady state groundwater mound under the gallery ranges from less than a day to over 3200 days (2.8×10^8 s, 8.76 yr). Formation times increase with increasing K_{GM}, but in every case, times begin to level off when the difference between $\log_{10} K_{GM}$ and $\log_{10} K_{RDM}$ equals about 4. At this point, the formation times begin to asymptotically approach some value. Increased gallery diameter results in a longer time to steady state. Higher K_{RDM} results in shorter time to steady state.

Groundwater mound length (i.e., the distance from the intiltration gallery to the leading edge of the mound downdip along the top of the RDM) ranges from less than one meter to over 10,000 km. The $\log_{10}$ of the mound length is almost linearly proportional to the $\log_{10}$ of K_{GM} (linear trendlines fit to the data have R^2 values greater than 0.99). Increased gallery width results in increased mound length. Higher K_{RDM} results in shorter mound lengths.

Infiltration gallery efficiency ranges from a little more than 6% to over 99.998%. When plotted against the $\log_{10}$ difference between K_{GM} and K_{RDM}, efficiency increases logarithmically with increasing difference and approaches 100% asymptotically. In general, gallery efficiency reaches ~75-80% at around 3 orders of magnitude difference and ~95% at about 4 orders of magnitude difference. Increased gallery width results in decreased efficiency. Higher K_{RDM} results in decreased efficiency.

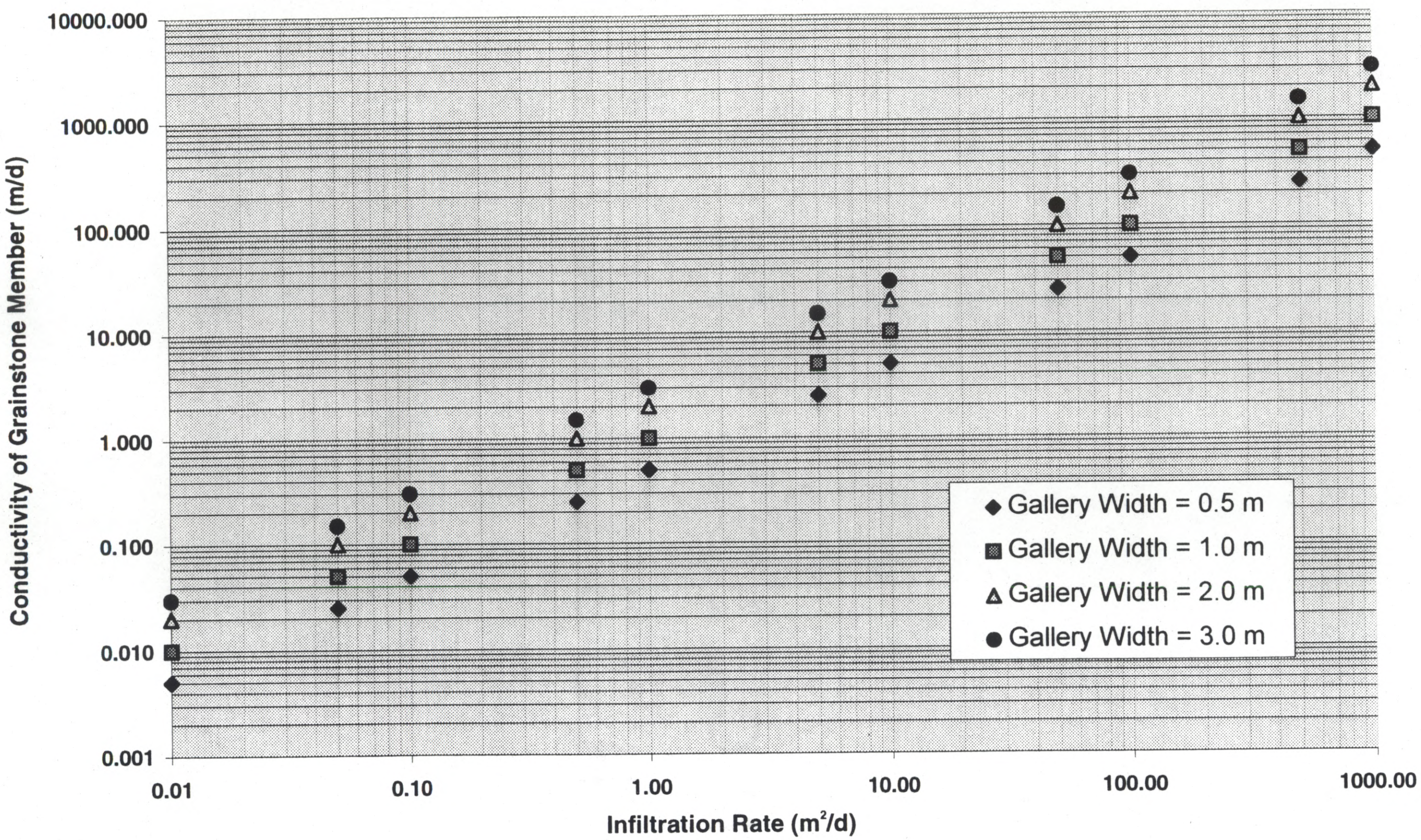

Figure 6.2 Infiltration rate versus K_{GM}

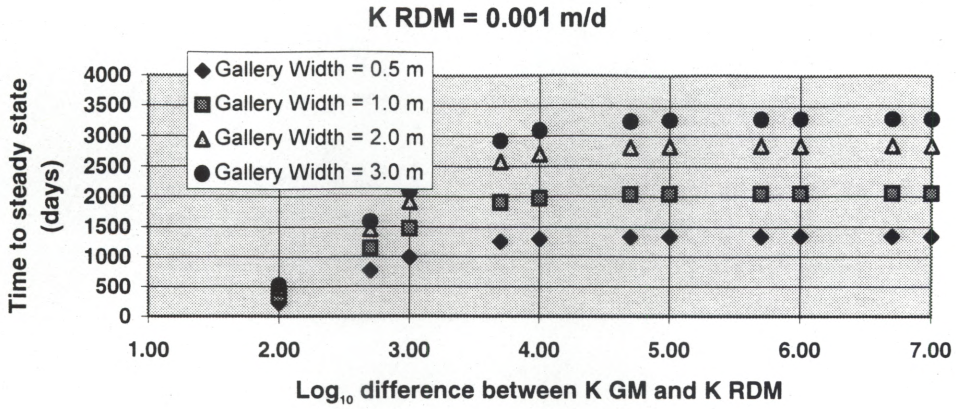

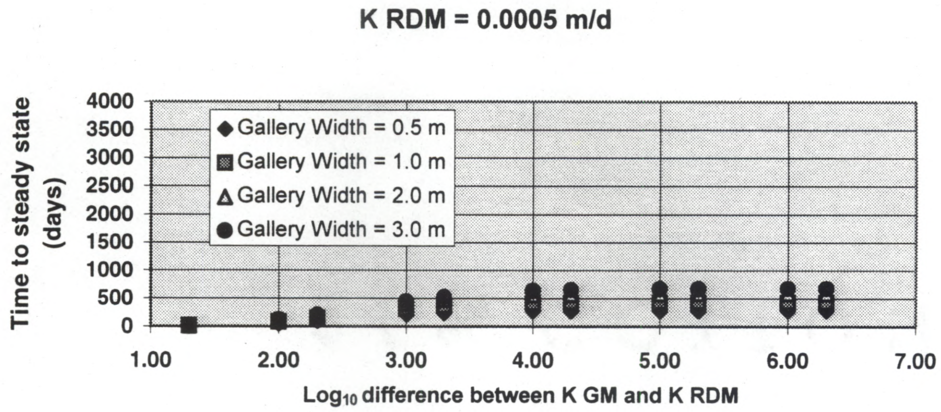

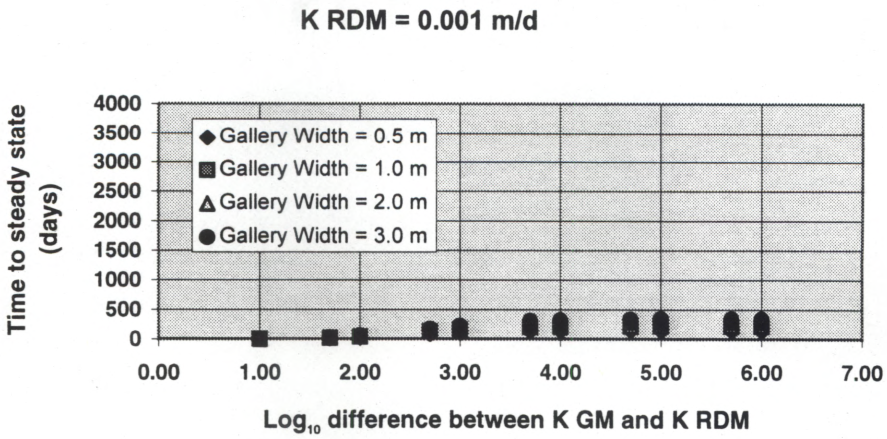

Figure 6.3 Time to steady state versus order of magnitude difference between K_{GM} and K_{RDM}

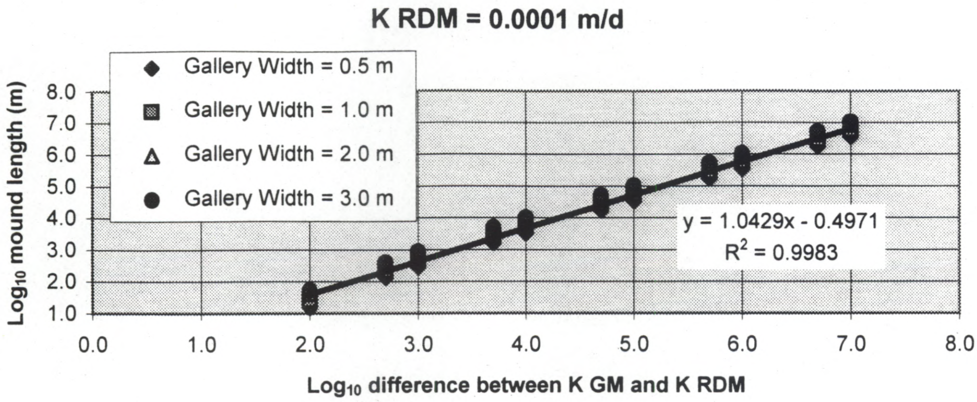

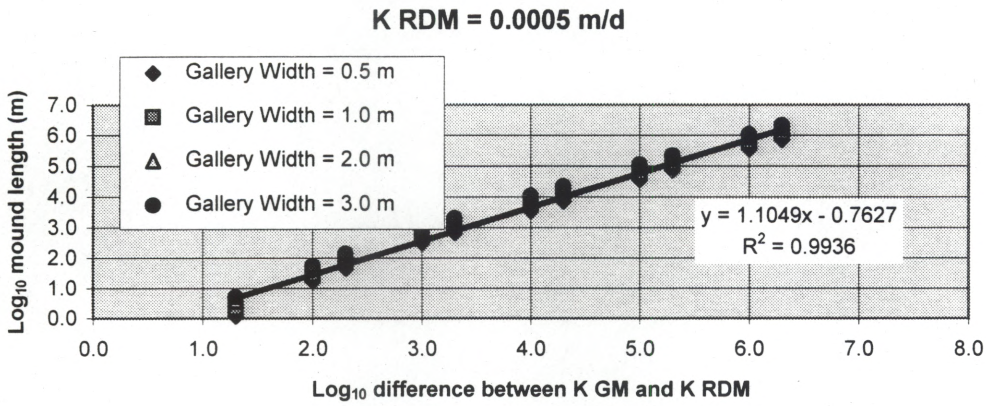

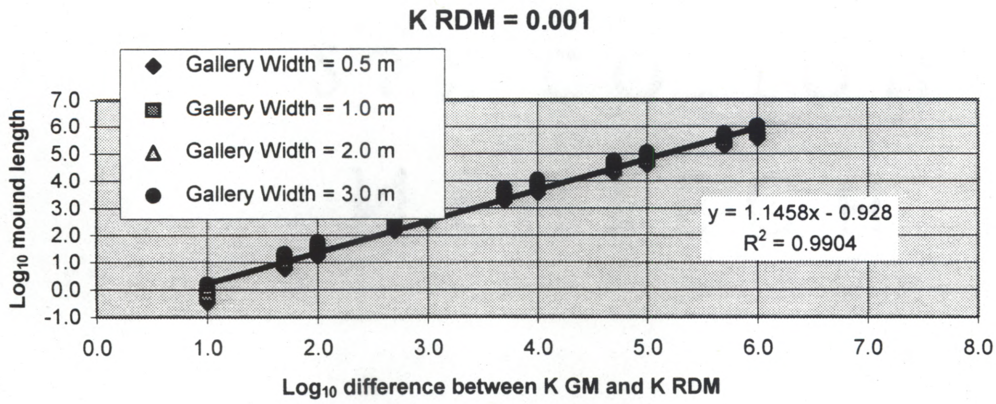

Figure 6.4 Log_{10} length of groundwater mound versus order of magnitude difference between K_{GM} and K_{RDM}

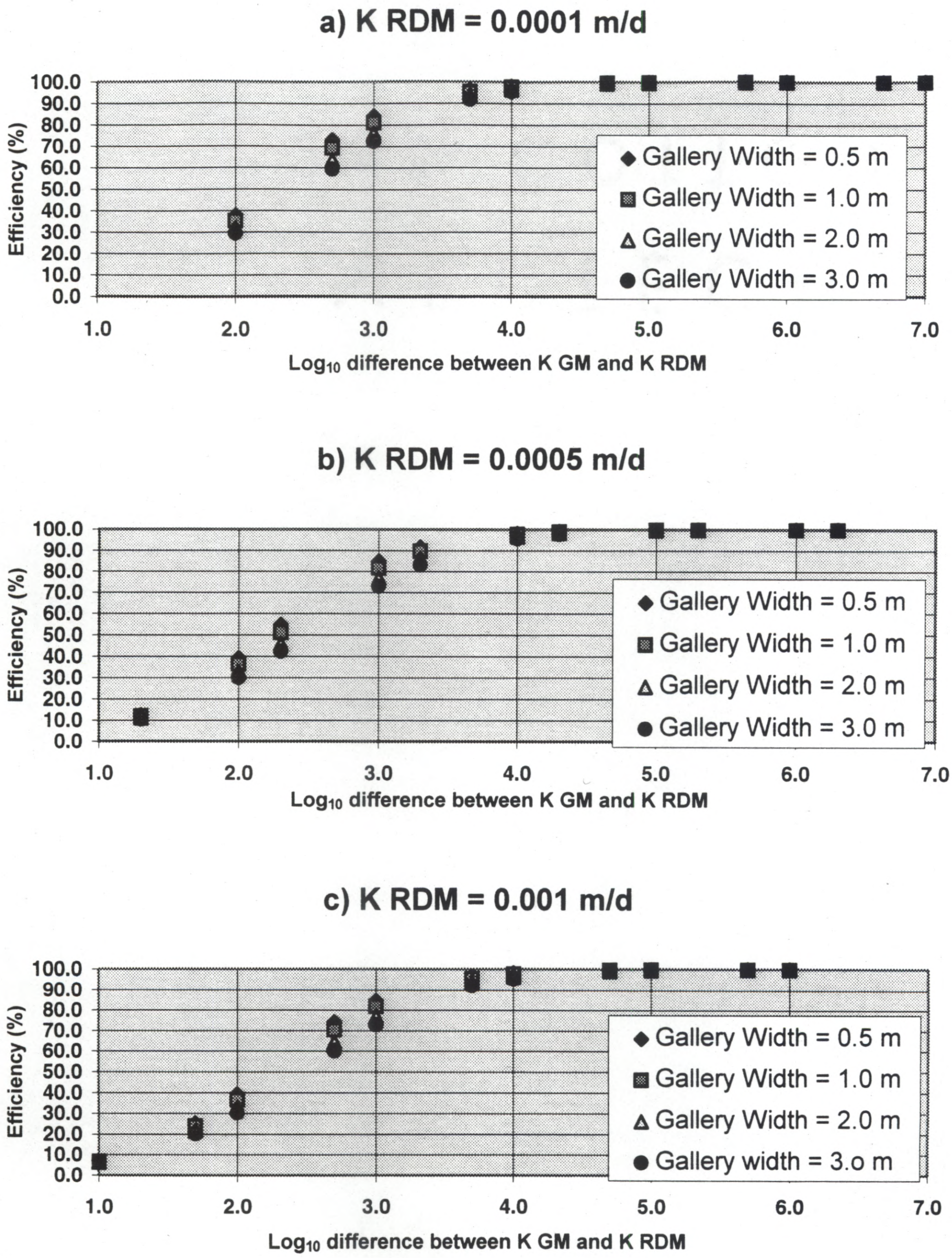

Figure 6.5 Infiltration gallery efficiency versus order of magnitude difference between K_{GM} and K_{RDM}

6.4 Discussion of Model Results

The results of the injection well simulations show that injection well efficiency decreases with distance from the springs. In addition, the relationship between efficiency and distance is not a linear one; rather, successive increases in efficiency become more significant as the injection well is moved closer to the springs. This is probably due to the fact that the Comal Springs node, being a discharge point at a topographic low, has a "capture zone" around it similar to a pumping well (a capture zone is a zone surrounding a pumping well such that any water that moves into the zone eventually flows to the well and discharges). Moving the injection well closer to the springs node also moves the slight groundwater mound that results from injection closer to the springs. Moving this mound closer to the springs superimposes more of the mound area over the capture zone, resulting in more of the injected water flowing to the springs node.

The infiltration gallery model simulations showed several significant trends. In all simulations, the conductivity of the Grainstone Member had to be at least 4 orders of magnitude greater than the conductivity of the Regional Dense Member before infiltration efficiency began to approach 95%. This has implication for gallery design; since it is assumed that gallery function at Comal Springs is dependent on the presence of the RDM for vertical control on infiltrating water, the conductivity difference between the unit(s) above the RDM and the RDM must be at least 4 orders of magnitude, or the springs will require a larger supply of water to the gallery in order to maintain a given spring discharge.

Increasing the diameter of the gallery increases the infiltration rate from the gallery and the dimensions of the resulting groundwater mound, while it decreases gallery efficiency. The decrease in efficiency is probably due to the fact that a larger groundwater mound on the RDM creates higher heads along the contact between the two units, resulting in more infiltration into the RDM from the GM. The lowering of efficiency with increased gallery diameter becomes almost insignificant when K_{GM} is greater than 4 orders of magnitude larger than K_{RDM}.

The groundwater mound length calculations resulted in a wide range of values, extending from less than a meter up to 10,000 km (see Table 8.5, Appendix D). Obviously, values on this order are not realistic; since the aquifer is only 275 km long along its longest dimension, it could not possibly support a groundwater mound even close to this magnitude. The infiltration gallery model assumes an aquifer of infinite lateral extent; when applied to a real situation with lateral limitations (such as Comal Springs, where the discharge point is on the order of 10 to 50 meters down dip from the likely location of an infiltration gallery), any calculated mound lengths that extend beyond the lateral boundaries of the real situation are essentially meaningless. The significance of this calculation is not in the determination of situations where the groundwater mound extends past the discharge point; rather, the purpose of calculating mound length is to estimate which situations will result in a groundwater mound that does not extend past the discharge point. This would imply that, for these situations, water introduced into an infiltration gallery would not have an effect on spring discharge, essentially giving the infiltration gallery an efficiency of zero.

An infiltration gallery installed at Comal Springs would most likely be situated within 50 meters of the spring orifices. A number of simulations calculated by the infiltration gallery model returned groundwater mound lengths that were less than 50 meters. In all cases, the difference between $\log_{10} K_{GM}$ and $\log_{10} K_{RDM}$ was equal to or less than 2.0. This would imply that, for an infiltration gallery at Comal Springs to be effective, K_{GM} must be at least 2 orders of magnitude greater than K_{RDM}.

At this point, there is considerable uncertainty concerning the actual conductivities of the GM and the RDM. The ranges of conductivities used in the model (1.2×10^{-9} m/s to 1.2×10^{-8} m/s for the RDM; 1.2×10^{-7} m/s to 1.2×10^{-2} m/s for the GM) were based loosely on the range of conductivity values for the Edwards (1.2×10^{-9} m/s to 1.2×10^{-1} m/s) presented in Hovorka, *et al* (1995).

7. CONCLUSIONS

7.1 Model Results and Significant Trends

Calibration of the IWR model predicts hydraulic conductivity values ranging from 1250 ft/d (0.000441 m/s) in parts of the unconfined zone to 7000 ft/d (0.0247 m/s) in the confined zone and transmissivities ranging from 300,000 ft^2/d (0.32 m^2/s) near the updip boundary of the aquifer outcrop to 2,800,000 ft^2/d (3.01 m^2/s) in the confined zone. This range of transmissivities is consistent with published transmissivity ranges for the Edwards in the model area (Hovorka *et al*, 1995). Calibration of the model also suggests an aquifer anisotropy of $K_x = 15K_y$, with K_x parallel to the general trend of the major spring faults (approximately N30°E).

The initial IWR model simulations (run with homogeneous hydraulic conductivity conditions) resulted in discharge rates at San Marcos Springs equal to over twice the discharge at Comal Springs. This is contrary to the true situation; in reality, the Comal Springs period of record average discharge is 40% higher than the San Marcos Springs average discharge. The addition of conductivity heterogeneities to the model resulted in spring discharges that matched the true average discharges. This would indicate that heterogeneities in the aquifer are influencing relative discharge rates from the springs.

The IWR model resulted in injection well efficiencies at Comal Springs ranging from 67% at 2 miles (3.2 km) from the springs to 82% at 0.25 miles (0.4 km) from the springs. There has been concern expressed by some that the actual aquifer transmissivity values are so high that injected water would not mound around the injection point; rather, it would immediately disperse throughout the aquifer upon injection (Glenn Longely, personal communication). If this were the case, injection of water into the aquifer would have a negligible impact on spring discharge from Comal Springs. According to the results of the IWR model simulations, this is not the case. All model injection simulations resulted in elevated groundwater heads at the injection point as well as at the Comal Springs node. The model, however, has not been verified by aquifer well tests and/or tracer studies.

The most accurate way to verify the model is to actually inject water into the aquifer at a steady rate at some given distance from the spring orifices, and monitor the springs and the aquifer for any changes caused by injection. However, this creates a financial and logistical problem in terms of obtaining a sufficient volume of water to run the test (injection rates in the model were on the order of millions of cubic feet, or tens of thousands of cubic meters, per day). The way to avoid this problem it to run pumping tests, rather than injection tests, under the assumption that an aquifer's response to a pumping well (a cone of depression) is mathematically the inverse of its response to injection (a groundwater mound). These tests can be used to verify the model by 1) estimating transmissivity values from drawdown data in surrounding observation wells, and comparing it to transmissivity values used in the model, 2) measuring the drawdown in the observation wells and comparing it to the elevated water levels in the model, and 3) monitoring the change in spring discharge that results from pumping.

The infiltration gallery model simulations indicate that, in a case where a lower confining layer is acting as a vertical control on infiltrating water, the conductivity of the area above the confining layer should be at least 4 orders of magnitude greater than the conductivity of the confining layer itself. If this is not the case, infiltration efficiency will drop below 95%, creating a situation where large volumes of water are necessary to maintain discharge from the spring. Increasing the diameter of the gallery increases the infiltration rate and the dimensions of the groundwater mound, while at the same time decreasing infiltration efficiency slightly. This decrease in efficiency becomes insignificant when the order of magnitude difference in conductivity between the two layers is greater than 4. It seems that the benefits gained by increasing the gallery diameter would likely be more significant than the detrimental effect it would have on efficiency, especially if the conductivity of the zone above the confining layer is more than 4 orders of magnitude greater than the conductivity of the confining layer. Mound length seems to also be controlled by the order of magnitude difference between the conductivities of the two layers in the system. Model simulations indicate that the difference between $\log_{10} K_{GM}$ and $\log_{10} K_{RDM}$ must be greater than 2, or the resulting groundwater mound will not be long enough to reach the spring orifices, rendering the infiltration gallery ineffective.

7.2 Assessment of Augmentation Methods at Each Site

7.2.1 Comal Springs

Injection wells and infiltration galleries are potentially feasible means of augmenting springflow at Comal Springs. According to model simulations, an injection efficiency of 82% is possible from an injection well completed along the trace of the Comal Springs Fault 0.25 miles (0.4 km) from the springs. This is under the assumption that the vector of maximum transmissivity in the aquifer is parallel to the fault, although Hovorka *et al* (1995) show that the relationship between transmissivity and mapped faults (i.e., that transmissivity increases with proximity to mapped faults) may not be as straightforward as previously thought. The flow system in the vicinity of the springs needs to be characterized in greater detail through tracer tests and aquifer tests in already existing wells before determining the location for an injection well or wells.

Based on the results of the infiltration gallery model, a gallery installed on the order of tens of meters from Comal Springs could be an effective means of augmenting springflow. However, for this gallery to be effective, the Regional Dense Member (RDM) of the Person Formation should act as a lower confining unit below the gallery. In addition, if it can be shown that the hydraulic conductivity of the Grainstone Member is 4 or more orders of magnitude greater than the conductivity of the RDM, it can be assumed that 1) infiltration efficiency will be greater than 95%, and 2) the resulting mound length will be long enough to contribute flow to the spring.

The lack of any appreciable local surface recharge to the aquifer near Comal Springs precludes the possibility of augmenting springflow by locally enhancing recharge, however, Comal Springs could possibly benefit from regionally enhanced recharge. Subsurface flow barriers are not now recommended because of uncertainties in our understanding of the subsurface flow regime and the possibility of harm to the aquifer by closing off critical flow paths in the subsurface. Direct addition of water to the spring lakes is a feasible means of augmenting flow in the spring runs and the spring-fed rivers, but it does not augment the actual discharge of water from the spring orifices themselves. Precluding further field study and model verification, and assuming that orifice discharge is required, it is therefore concluded that the best options for augmenting flow from Comal Springs are injection wells and infiltration galleries.

7.2.2 San Marcos Springs

Injection wells are a potentially feasible method for augmenting springflow from San Marcos Springs. The fact that it is the lowest discharge point in the San Antonio Region of the aquifer implies that injection wells installed in the vicinity should have high injection efficiencies. In addition, the fact that flow lines in the aquifer around San Marcos Springs all seem to converge on the springs is an indication that injection well location is not as crucial as it is at Comal Springs.

Infiltration galleries are also potentially feasible at San Marcos Springs. However, the RDM is not present in the vicinity of San Marcos Springs, nor is there any other unit that may act as a lower confining layer under an infiltration gallery. This may limit the effectiveness of an infiltration gallery at this site. In addition, the cost of installation of a gallery, both in financial terms and in terms of the environmental impact that construction may have on the aquifer and the springs, needs to be considered. While the possibility of a detrimental impact on the system is present at both spring sites, the benefits of greater efficiency at Comal Springs may outweigh the potential drawbacks of gallery installation. At San Marcos, however, it appears that the question of injection efficiency is not as uncertain as it is at Comal. If this is the case, injection wells would likely be the better option.

Unlike Comal Springs, San Marcos Springs would benefit from enhanced local recharge. Similar to Comal, subsurface flow barriers may not be a viable option, and direct addition to the spring lakes would not affect the actual discharge from the orifices. Based on the results of this study, it is therefore concluded that the best options for augmenting springflow from San Marcos Springs are injection wells and locally enhanced recharge to the aquifer.

7.3 Discussion of Model Limitations

One potential limitation with the IWR model is the simplification of the geometry of the spring faults. The model assumes that the two springs are connected by a narrow zone that parallels the direction of maximum transmissivity. In reality, the springs are located on two different parallel faults rather than one continuous fault. While it is likely that there is significant communication between these two faults, due to extensive karstification of the units along the fault planes, there may also be places in the area between Comal Springs and San Marcos Springs where communication between the two is limited by the displacement of lower permeability beds against the aquifer units.

Studies of the chemistry and storm response of Comal Springs indicates that the majority of discharge comes from a more regional flow system. However, model results show only 9% of the discharge water coming from the lower confined zone. This suggests that the connection between the confined and unconfined zones in the model may not be large enough to allow significant flow between the two layers. It could be that model design limits the connection between the two layers, so that sufficient flow is not allowed between layers.

Areal recharge was applied to the model over the entire model area rather than at discrete points in the model. In reality, however, from 60 to 80% of the total recharge to the aquifer comes through the beds of losing streams. This may have an effect on the head distributions in the model, as well as on the relative discharges from the spring nodes. If the influence of discrete recharge is great enough, it may affect model calibration.

At present, the infiltration gallery model is only capable of estimating general trends, such as the relationship between order of magnitude infiltration rate and order of magnitude conductivity. It cannot with certainty be used to calculate any absolute values or constrained ranges of values for parameters such as the time to steady state or the infiltration rate from the gallery. Before it can be used for determining these type of parameters, the model needs to be verified (i.e., it must be determined if the RDM is acting as a lower confining layer), and some constraint on the conductivities in the subsurface around Comal Springs needs to be established.

7.4 Disclaimer

The author assumes no liability for any conclusions or public policy decisions based on the results of the models developed in this thesis. The models developed in this thesis are based on limited ground truth data, and have not been verified by actual aquifer tests or other necessary field studies. These models are intended to provide insight into the processes governing flow to certain springs in the Edwards aquifer, and to establish areas where further study is needed. They are not intended to serve as working simulations of the aquifer that can be used to determine specifications for the installation of augmentation methods. Finally, the author has no vested interest in springflow augmentation and neither supports nor opposes springflow augmentation as a means of resource management in the Edwards aquifer.

8. APPENDIX

A. Sample Calculation

Spring Elevation and Spring Conductance - Comal Springs

Equation 2, presented and discussed in the section entitled *Spring Simulation* (Chapter 5) is the equation used by MODFLOW to simulate discharge from a drain (i.e., a spring). This equation,

$$Q_d = C_d(h - d) \tag{2}$$,

states that discharge from the drain (Q) is proportional to the difference between the elevation of the drain (h) and the hydraulic head in the aquifer near the drain (d), with C representing the constant of proportionality (called the drain conductance). In order to calculate discharge from a drain placed in a model grid, MODFLOW requires a drain conductance value and a drain elevation. In order to determine these parameters for the IWR model, spring discharge data and water level data from a nearby well were plotted on an x-y scatter plot graph, and the equation for the least-squares fit to the data was determined (Figure 5.7). This equation was used to calculate the conductance and the elevation for the spring. An example of the calculation for the Comal Springs data is given below.

The equations for the relationship between discharge from Comal Springs (Q_c) and the water elevation in the Landa Park Well (H) are

$$Q_c = 40.127\ H - 24826 \tag{A1}$$

$$H = 618.88 + 0.024\ Q_c \tag{A2}$$

Two arbitrary discharge values (630 cfs and 620 cfs) were chosen, and the corresponding head values were determined for each. These values were plugged into Equation 2, resulting in two equations with two unknowns:

$$462.3 = C\ (630 - d) \tag{A3}$$

$$91.06 = C\,(620 - d) \tag{A4}$$

Equation A4 was solved for C and substituted into equation A3, yielding

$$462.3 = (91.06/(620 - d))(630 - d) \tag{A5}$$

This equation was solved to yield a value of 617.5 for d (spring elevation). This value was put back into equation A3 to solve for C, yielding a value of 36.984 ft^2/s, which converts to 3,195,417.6 ft^2/d.

B. Description of Preliminary Injection Well Model

The Conceptual Model

The model area is shown in Figure 8.1.

The southwest border of the grid is treated as a constant head boundary. The surrounding boundaries (the "bad-water line", the outcrop limit, and the Kyle, TX divide) are all treated as no-flow boundaries. The entire grid was considered unconfined, with a constant thickness of 350 ft. The springs were simulated as drains with fixed elevations, although heads at the spring nodes were allowed to vary. An injection well was placed in a node 2 miles away from Comal Springs.

The intent was to initially develop a steady-state model of the system (hereafter referred to as the Comal/San Marcos System), then activate the injection well with varying injection rates while monitoring the change in spring discharge.

Discretization and Grid/Model Parameters

All model units are in feet^x and days.

Grid dimensions: 60 rows by 70 columns, block-centered nodes.

Δx = 2640 feet (0.5 miles)

Δy = 1320 feet (0.25 miles), except rows 53, 54, and 55 (hereafter referred to as the "fault zone") are Δy = 100 feet (0.019 miles)

Thickness = 350 feet

Constant head boundary head values: At uppermost boundary node (1,6), head is set at 750 feet. Head values along the boundary drop 2.5 feet/node until 655 feet at (1,44). Heads along the rest of the boundary (from (1,44) to (1,59)) are set at 650 feet (node (1,60) is inactive).

Drain Conductance at Comal: Calculated from the graph of spring discharge versus water levels (Figure 5.7), D_{com} = 3,195,417.6 ft^2/d (I used 3,200,000 ft^2/d in the model)

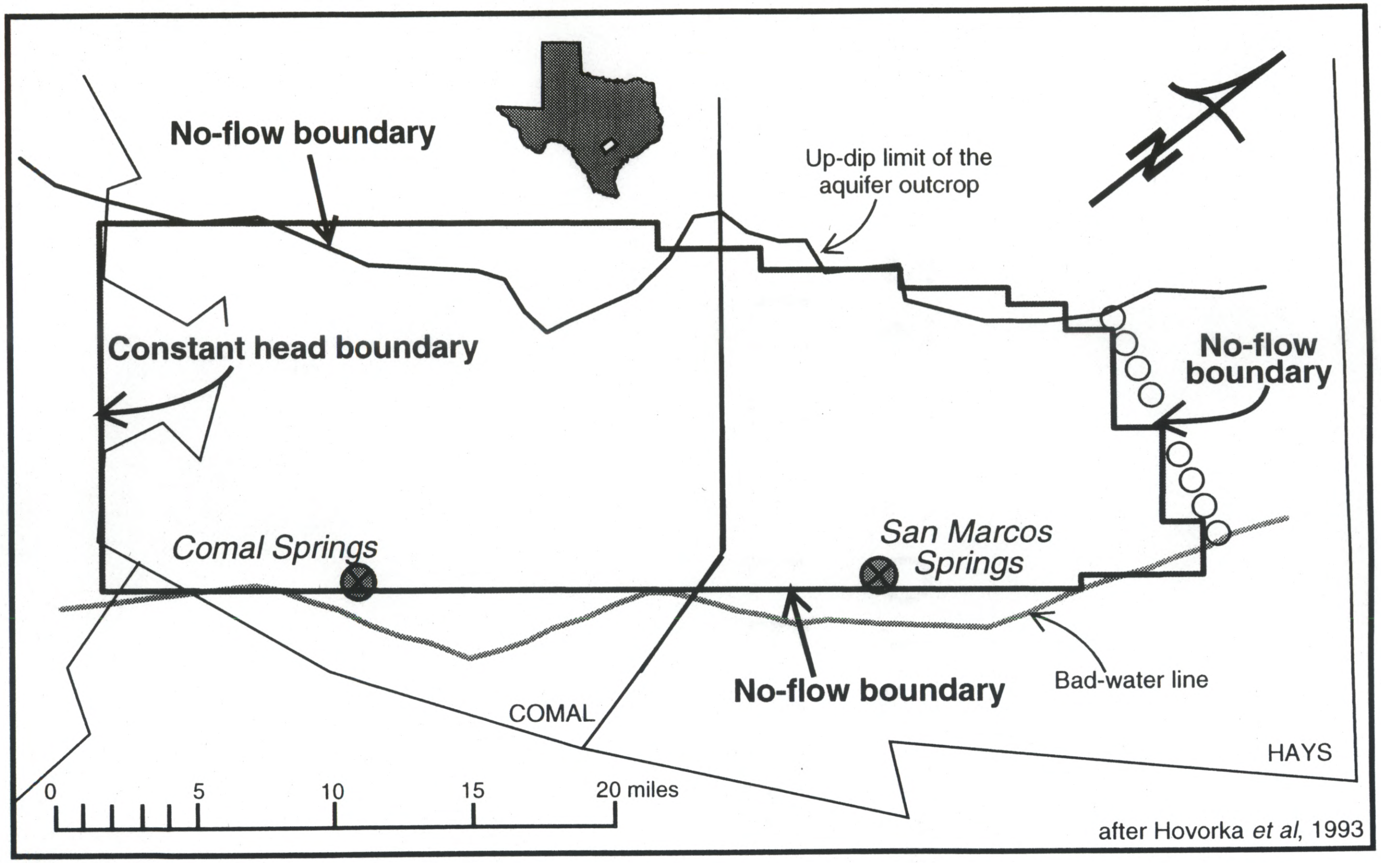

Figure 8.1 Preliminary injection model area

Drain Conductance at San Marcos: Initial value of 3,000,000 ft^2/d was used; this was varied in later simulations.

Drain Elevations at Comal: 618.5 ft (also taken from Figure 5.7).

Drain Elevations at San Marcos: 557.2 ft (avg. elevations of the spring orifices)

Areal Recharge: Applied to every active node in the model (i.e., applied over the whole active model area). Recharge values were estimated by varying an initial value of 0.1 ft/d by orders of magnitude until the model potentiometric surface began to match the true surface of the aquifer. Final recharge value used: R = 0.002 ft/d

Hydraulic conductivity and isotropy were varied throughout the simulation to see which simulation fit the real picture the best. Unfortunately, my ground truth data was limited to 1) well levels in 10 wells in Comal County (Figures 8.2 and 8.3), and 2) a potentiometric map of the immediate vicinity of San Marcos Springs (Figure 3.1). I used these two figures to get a general best fit potential surface.

Conductivity and Anisotropy Simulations:

Initially, conductivity was varied from 5 to 500 ft/day, and isotropy was varied from $K_x = 5K_y$ to $K_x = 10K_y$. A number of these models match the general geometry of the potentiometric surface.

Once this series of simulations were run, water balances were calculated at the spring nodes. The period-of-record averages of 284 cfs (2.4×10^7 ft^3/day) for Comal Springs and 170 cfs (1.5×10^7 ft^3/day) for San Marcos Springs were used as the appropriate target discharge values for the springs. Calculated spring discharges for the first batch of simulations are orders of magnitude too low. Discharge values did not fall into the right order of magnitude (10^7 ft^3/day) until the K values were increased to 5000 ft/day. Once discharge values were in the right order of magnitude, the model was set homogeneous with K = 5000 ft/day, the K value was held constant, and the degree of anisotropy was varied from $K_x = 5K_y$ to $K_x = 15K_y$. An anisotropy value of $K_x = 15K_y$ and a hydraulic conductivity of 5000 ft/day resulted in a model potentiometric surface that matched the real potentiometric surface the best (Figure 8.4) and resulted in a spring discharge at the Comal Springs node of 170 cfs (1.5×10^7 ft^3/day).

Throughout all the simulations, spring discharge at the San Marcos Springs node was greater than discharge at the Comal Springs node. In a homogeneous model of the aquifer with San Marcos Springs as the lowest discharge point, this would be the expected result. However, this is contrary to the actual period of record average discharges of 284 cfs at Comal Springs and 170 cfs at San Marcos Springs. There are two primary factors that could account for this; first, the spring conductance at San Marcos Springs could be significantly lower than at Comal Springs; second, there are heterogeneities in the aquifer (e.g., lower transmissivity in the vicinity of San Marcos Springs than around Comal Springs) that are limiting flow to the spring orifices. The influence of heterogeneities on spring discharge were dealt with in the final Comal/San Marcos model. The influence of varied drain conductance on spring discharge was investigated with this preliminary model.

Spring Conductance Simulations:

The spring conductance value used for Comal Springs is an empirically-derived conductance determined by the relationship between historic spring discharge and historic water levels in a nearby well. At the time these simulations were run, similar data for San Marcos Springs was not available, so, initially, the same conductance value was used for San Marcos Springs. When the discrepancy between the simulated discharges and the real average discharges was observed, a number of simulations were run with lower spring conductances at San Marcos Springs in an attempt to "squeeze off" flow through the spring orifice and make the simulated discharges more realistic. Preliminary model results indicate that lowering spring conductance does lower discharge at San Marcos to more realistic values.

However, limitation of drain conductance results in unrealistically elevated heads at the spring orifices. In some simulations, heads at San Marcos got as high as 650 feet (75 feet above the elevation of Spring Lake), causing the gradient to reverse back towards Comal Springs. This would imply that different spring conductances at each spring are probably not the main factor determining the relative discharge values. It seems more likely that there are heterogeneities in the system that are allowing larger discharge at Comal while keeping head values at San Marcos low. (Note: as discussed in Chapter 5, historic spring discharge and well level data for San Marcos Springs was obtained and used to determine a spring conductance value for the final model.)

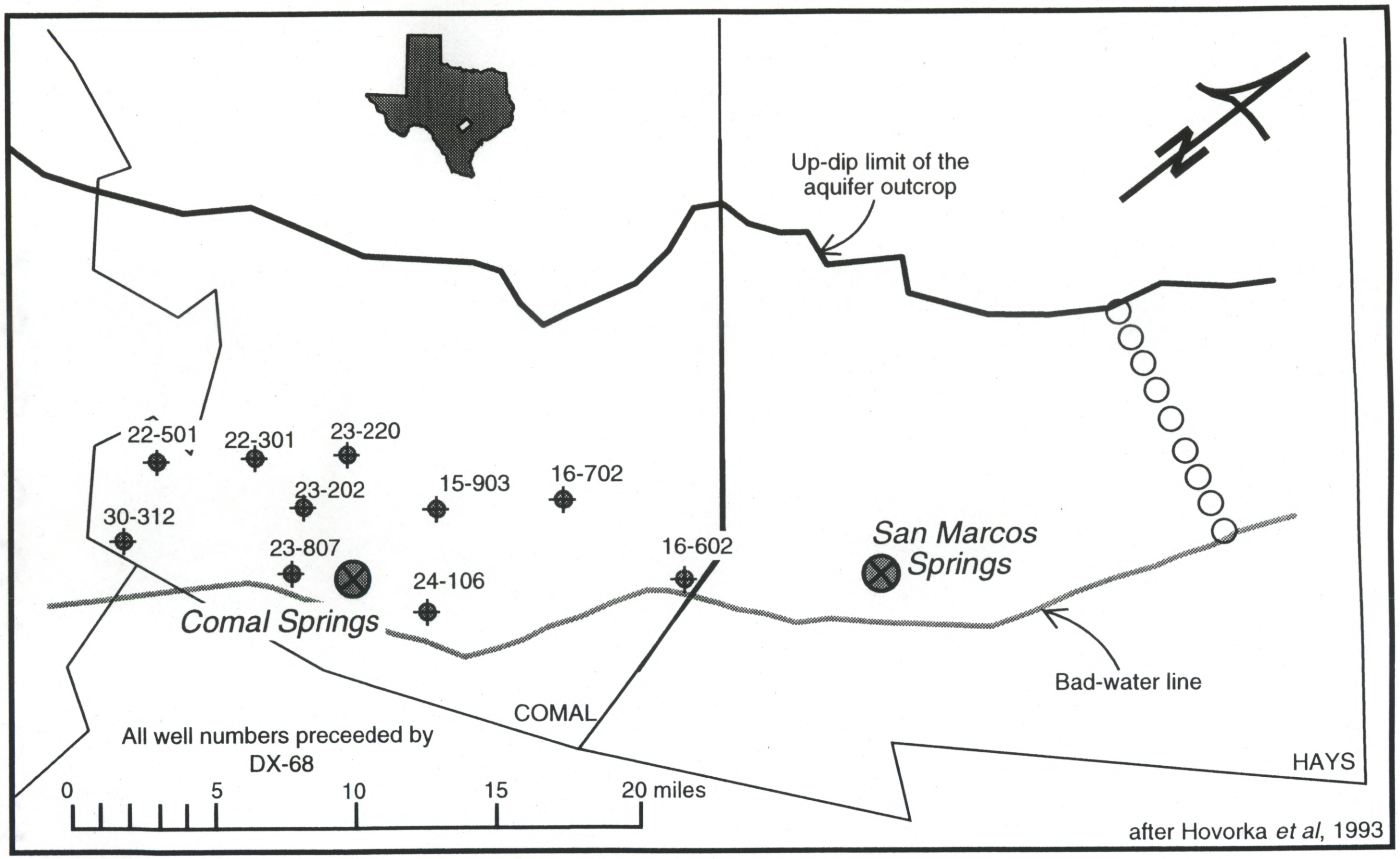

Figure 8.2 Well locations in Comal County

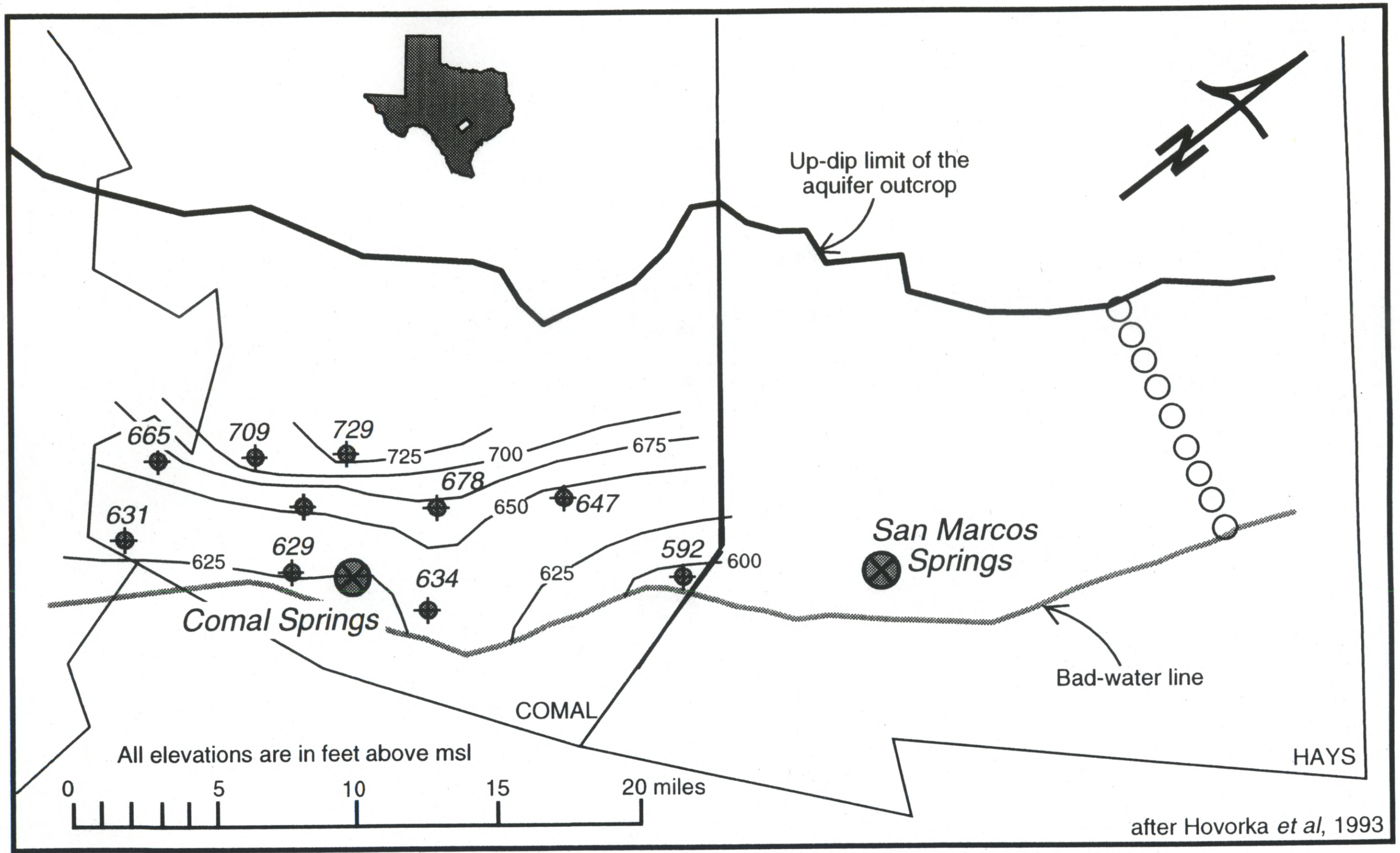

Figure 8.3 Potentiometric surface of the Edwards aquifer in Comal County (water levels taken between 12/01/90 and 2/31/91)

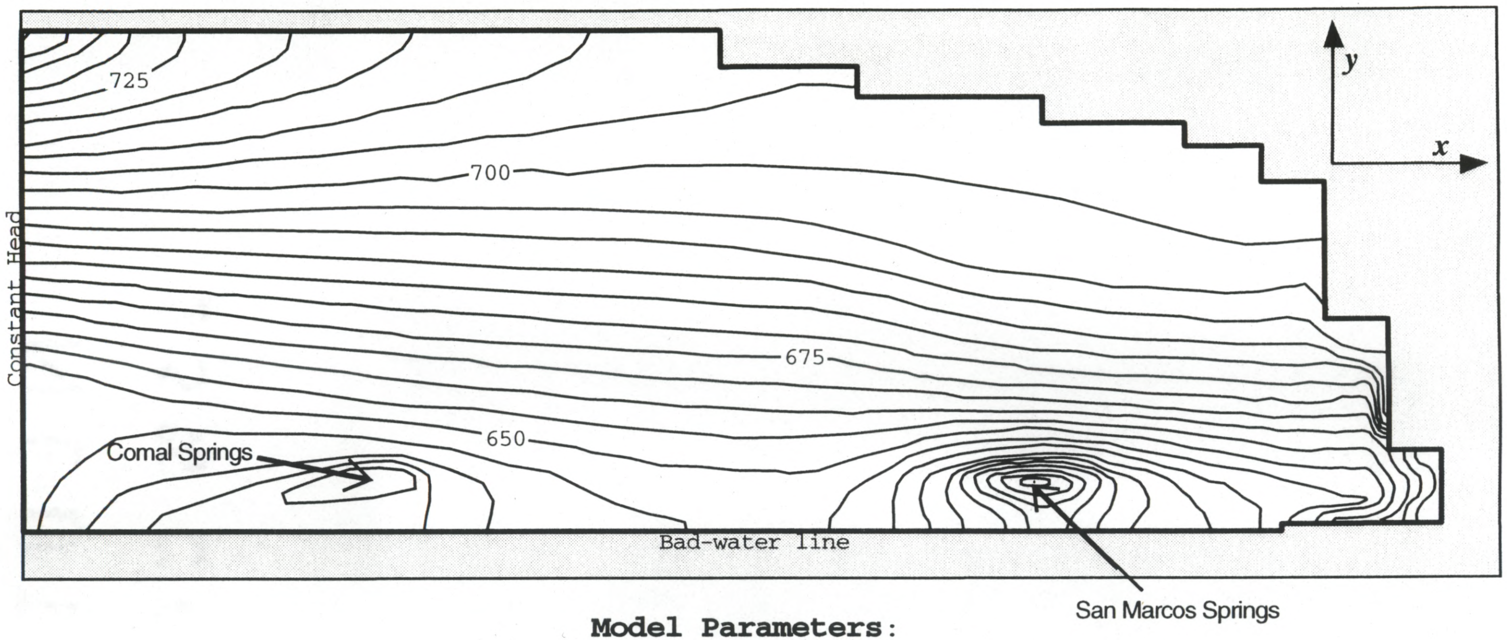

Model Parameters:

K = 5000 ft/day   Kx = 15Ky

Areal recharge = 0.02 ft/day

Spring conductance = 3,000,000 ft^2/day @ Comal

Spring conductance = 1,000,000 ft^2/day @ San Marcos

Spring Discharge:

Comal Springs = 170 ft^3/s

San Marcos Springs = 406 ft^3/s

Figure 8.4 Final potentiometric surface of the preliminary model (contour values are in feet)

C. Hard Copy of Infiltration Gallery Computer Model Code

The code for this model was written in FORTRAN 77 on an IBM-PC clone with an Intel 486 CPU. The model code was compiled with the Microsoft FORTRAN Version 5.0 Compiler for MS-DOS. A hard copy of the model code is included as Appendix C. All results were saved as ASCII text files and imported into Microsoft EXCEL™ for processing. All graphs were generated with EXCEL™.

Title and Reference

Analytical Solution to Estimate Steady State Behavior of Water Traveling on a Sloping, Semipervious Layer (SPL) After Infiltrating From a Constant Source Percolation Pond of Known Dimensions.

Adapted to Model Aquifer Response to an Infiltration Gallery at Comal Springs.

Filley, T. H. 1992. 'Saturated mound development on sloping clay layers due to a finite source: an analytical solution.' GROUND WATER, Vol. 30, No. 4., pp. 559-568

Description Of Variables In Program

```
C   1: MOUND CHARACTERISTICS
C     HO = HEAD AT ORIGIN
C     L2 = LENGTH OF THE GROUNDWATER MOUND ALONG THE SPL (meters)
C     TDAYS = TIME OF MOUND FORMATION (days)
C     TYEARS = TIME OF MOUND FORMATION(years)
C     QINFILT = INFILTRATION RATE FROM THE GALLERY (meters^2/day)
C     QLEAKAGE = LEAKAGE RATE THROUGH THE SPL (meters^2/day)
C     QEVAPORATE = EVAPORATION RATE FROM MOUND SURFACE (meters^2/day)
C     Q = FLOW RATE MOVING DOWNSLOPE (meters^2/day)
C   2: MEDIA CHARACTERISTICS
C     A = ANGLE OF SLOPING LAYER (IN DEGREES)
C     D = INFILTRATION GALLERY DIAMETER (meters)
C     E = EVAPORATIVE LOSS (L/T)
C     M = SLOPING LAYER THICKNESS (meters)
C     N = SEDIMENT POROSITY
C     U = ANGLE OF SLOPING LAYER (IN RADIANS)
C     a: CONDUCTIVITIES
C      K = SATURATED HYDRAULIC CONDUCTIVITY (meters/day)
C      K1 = CONFINING BED CONDUCTIVITY (meters/day)
C      K2 = VERTICAL SATURATED HYDRAULIC CONDUCTIVITY (meters/day)
C   3: DIMENSIONLESS PARAMETERS
C      Y = D/M  (gallery diameter/bed thickness)
```

```
C      A1 = K/K1 (bed conductivity)
C      B1 = K/K2 (vertical conductivity)
C      F = TAN(U) + (1./TAN(U))
C      G = Y/(A1 * D)
C      AA = (F * G)/2. (variable 'A1' in the paper)
C      BB = (1./(A1*SIN(U)))+(COS(U)*SIN(U))+(COS(U)/(DD*SIN(U)))
C           (variable 'B1' in the paper)
C      CC = D * ((1./B1) + (1./DD))  (variable 'C1' in the paper)
C      DD = K/E  (infiltration/evaporation)
C      V = (BB**2.)+(4. * AA * CC)  (expression '(B1^2)+4*A1*C1' in paper)
C      VV = SQRT(V)
C      A2 = (K1+E)*(1/TAN(U)) (variable 'A' in the paper)
C      B2 = (K1/M)*(((SIN(U)**2./COS(U))+COS(U))*(1/TAN(U)))
C        (variable 'B' in the paper)
C      Z = ((B2/A2) * HO) + 1.
C      ZZ = LOG(Z)
```

Program Code

```
C  1: VARIABLE DEFINITION
C
     REAL*8 HO, L2, TDAYS, TYEARS, Q, A, D, E, M, N, U, K
     REAL*8 K1, K2, Y, A1, B1, F, G, AA, BB, CC, DD, V, VV
     REAL*8 A2, B2, Z, ZZ, QEVAPORATE, QLEAKAGE, QINFILT
     INTEGER INT, MOVEON
     CHARACTER*8 FILENAME
C
C  2: OUTPUT FILE DEFINITION
C
     WRITE (*,*)
     WRITE (*,*) 'OK! LET US GET STARTED, SHALL WE?'
5     WRITE (*,*)
     OPEN (UNIT=5,FILE='INFIL.DAT')
     WRITE (*,*) '        SPECIFY THE NAME OF YOUR OUTPUT FILE'
     WRITE (*,*) '    (MAKE SURE IT IS ONLY 8 CHARACTERS OR LESS,'
     WRITE (*,*) '      AND BE SURE TO PUT IT IN SINGLE QUOTES)'
     WRITE (*,*)
C
     READ (*,*) FILENAME
     OPEN (UNIT=6,FILE=FILENAME)
CCCCC      GOTO 900
C
C ***************************************************************************
C  3: INPUT DATA
C
     WRITE (*,*)'         INPUT THE FOLLOWING INFORMATION:'
     WRITE (*,*)' '
C      WRITE (*,*)'  THE SLOPING ANGLE IN DEGREES'
C      READ (*,*) A
     WRITE (*,*)'  HYDRAULIC CONDUCTIVITY FOR THE SPL (in m/day)'
     READ (*,*) K1
C      WRITE (*,*)'  VERTICAL HYDRAULIC CONDUCTIVITY (in m/day)'
C      READ (*,*) K2
C      WRITE (*,*)'  SATURATED HYDRAULIC CONDUCTIVITY (in m/day)'
C      READ (*,*) K
C      WRITE (*,*)'  THE INFILTRATION GALLERY WIDTH (in meters)'
```

```
C     READ (*,*) D
C     WRITE (*,*)'  EVAPORATION RATE (in m/day)'
C     READ (*,*) E
C     WRITE (*,*)'  SPL THICKNESS (in meters)'
C     READ (*,*) M
C     WRITE (*,*)'  SEDIMENT POROSITY'
C     READ (*,*) N
      WRITE (*,*)'THE FOLLOWING INFORMATION IS IN THE DATA FILE CALLED'
      WRITE (*,*)'                  ***  INFIL.DAT   ***'
      WRITE (*,*)' '
      WRITE (*,*)'                THE SLOPING ANGLE'
      WRITE (*,*)'          HYDRAULIC CONDUCTIVITY FOR THE SPL'
      WRITE (*,*)'           VERTICAL HYDRAULIC CONDUCTIVITY'
      WRITE (*,*)'          SATURATED HYDRAULIC CONDUCTIVITY'
      WRITE (*,*)'            THE INFILTRATION GALLERY WIDTH'
      WRITE (*,*)'                 EVAPORATION RATE'
      WRITE (*,*)'                   SPL THICKNESS'
      WRITE (*,*)'                 SEDIMENT POROSITY'
      READ (5,*) A
      WRITE (*,*)
      WRITE (*,*)
      WRITE (*,*) 'READY TO CALCULATE THE SOLUTION? (1 FOR YES)'
      READ (*,*) MOVEON
      IF (MOVEON.EQ.1) THEN
       GO TO 6
       ELSE
      ENDIF
      WRITE (*,*)
CCCCC     READ (5,*) K1
6     READ (5,*) K2
      READ (5,*) K
      READ (5,*) D
      READ (5,*) E
      READ (5,*) M
      READ (5,*) N
C
C  4: CONVERT DEGREES TO RADIANS
C     U = angle in radians
C
      U = A * 0.0174533
C
C ******************************************************************************
C  5: DETERMINE THE THICKNESS OF THE GROUNDWATER MOUND AT THE ORIGIN (H0).
C
10    A1 = K/K1
      B1 = K/K2
      Y = D/M
      DD = K/E
      F = TAN(U) + (1./TAN(U))
      G = Y/(A1 * D)
      AA = (F * G)/2.
      BB = (1./(A1 * SIN(U))) + (COS(U) * SIN(U)) + (COS(U)/
     + (DD * SIN(U)))
      CC = D * ((1./B1) + (1./DD))
      V = (BB**2.) + (4. * AA * CC)
      VV = SQRT(V)
```

```
      HO = (((-1.) * BB) + VV)/(2. * AA)
C
C ***************************************************************************
C  6: DETERMINE THE STEADY-STATE MIGRATION DISTANCE OF
C     PHREATIC WATER TRAVELLING ON A SLOPING LAYER (L2).
C     -WITH EVAPORATION AND LEAKAGE THROUGH THE LAYER
C     -THICKNESS OF FLOW = HO AT ORIGIN
C
      B2 = (K1/M) * (((SIN(U) ** 2./COS(U)) + COS(U)) *
     + (1/TAN(U)))
      A2 = (K1 + E) * (1/TAN(U))
      Z = ((B2/A2) * HO) + 1.
      ZZ = LOG(Z)
      L2 = (K/B2) * ZZ
C
C ***************************************************************************
C  7: ESTIMATE TIME TO STEADY STATE (T).
C     -ASSUMING INSTANTANEOUS SATURATION OF IMPERVIOUS LAYER
C
C     K2*D = INFILTRATION RATE
C
      TDAYS = N*(0.5*HO*HO*COS(A)/SIN(A)+A2/B2*
     + (K/B2*((EXP(B2/K*L2))-1.)-L2))/(K2*D)
      TDAYS2 = TDAYS * 2.
      TYEARS = TDAYS/365.25
      TYEARS2 = TYEARS * 2.
C
C ***************************************************************************
C  8: CALCULATE THE FOLLOWING FLOW RATES
C     -INFILTRATION RATE FROM THE GALLERY
C     -LEAKAGE RATE ACROSS THE SPL
C     -EVAPORATION RATE ACROSS THE PHREATIC SURFACE OF THE MOUND
C     -FLOW RATE DOWNSLOPE (Q)
C
      WRITE (*,*) SIN(U), COS(U)
      QINFILT = K2 * D
C
      GG = (K1/M) * (((SIN(U))**2/COS(U)) + COS(U))
      QLEAKAGE = (GG * (HO**2)/2*SIN(U)) + K1 * HO/SIN(U)
C
      QEVAPORATE = E * (HO * (COS(U)/SIN(U)) - D)
C
      Q = K * HO * COS(U) * SIN(U)
C
C ***************************************************************************
C     OUTPUT RESULTS
C
      WRITE (6,*) '                MODEL PARAMETERS'
      WRITE (6,120) A,D,E,M,K1,K2,K,N
      WRITE (6,*) '                RESULTS'
      WRITE (6,130) HO,L2,TYEARS,TDAYS,TYEARS2,TDAYS2,QINFILT,QLEAKAGE,
     +QEVAPORATE, Q
120   FORMAT ('SLOPING ANGLE =',F5.2,/,'GALLERY DIMENSION =',
     + F8.2,'m',/,'EVAPORATION RATE =',F10.9,'m/d',/,
     + 'SPL THICKNESS',F6.2,'m',/,'SPL CONDUCTIVITY =',F8.6,
     + 'm/d',/,'VERTICAL HYDRAULIC CONDUCTIVITY =',F12.7,'m/d'
```

```
      + ,/,'HORIZONTAL HYDRAULIC CONDUCTIVITY =',F12.7,'m/d',/,
      + 'SEDIMENT POROSITY =',F5.2,/)
130   FORMAT (/,'HEAD AT ORIGIN =',F17.6,'m',
      + /,'LENGTH OF MOUND ='F17.6,'m',/,'TIME OF MOUND FORMATION:'
      + ,/,'  LOWER LIMIT =',F8.5,'years; ',F10.2,'days',/,
      + '  UPPER LIMIT =',F9.5,'years; ',F10.2,'days',/,
      + 'INFILTRATION RATE FROM GALLERY =',F12.6,'m^2/day',/,
      + 'RATE OF LEAKAGE THROUGH SPL =',F12.6,'m^2/day',/,
      + 'EVAPORATION RATE =',F12.6,'m^2/day',/,
      + 'FLOW RATE OF WATER MOVING DOWNSLOPE =',F12.6,' m^2/day',//)
C
      WRITE(6,*)' THE FOLLOWING ARE THE DIMENSIONLESS CONSTANTS'
      WRITE (6,100) A1, B1, Y, DD, F, G, AA, BB, CC,
      + V, VV, HO
100   FORMAT ('K/K1 =',F12.6,/,'K/K2 =',F12.6,/,'D/M',F12.6
      + ,/,'K/E =',F12.6,/,'F =',F12.6,/'G =',F12.6,/,'AA ='
      + ,F12.6,/,'BB =',F12.6,/,'CC =',F12.6,/,'V ='F12.6,/,
      + 'SQRT V =',F12.6,/,'HO =',F12.6,//)
      WRITE (6,110) B2, A2, Z, L2
110   FORMAT (' B2 =', F12.6,/,' A2 =',F12.6,/,' Z =',
      + F12.6,/,' L2 =',F12.6,//)
200   FORMAT ('*********      'A8'       *************')
900   WRITE (*,*)
      WRITE (*,*)
      WRITE (*,*) 'FOR YOUR CONVENIENCE, THE RESULTS OF THIS PROGRAM'
      WRITE (*,*) '    HAVE BEEN SENT TO THE OUTPUT FILE NAMED'
      WRITE (*,200) FILENAME
      WRITE (*,*) '          ENJOY YOUR RESULTS!'
      WRITE (*,*)
      CLOSE (UNIT=5)
      WRITE (*,*) '     WOULD YOU LIKE TO TRY IT AGAIN?'
      WRITE (*,*) '          (1 FOR YES, 2 FOR NO)'
      READ (*,*) INT
      IF (INT.EQ.1) THEN
       GOTO 5
       ELSE
      ENDIF
      WRITE (*,*)
      WRITE (*,*)
      WRITE (*,*) '***************   HAVE A NICE DAY   ******************'
      WRITE (*,*)
      WRITE (*,*)
999   STOP
      END
```

D. Data Tables

Year	Well Discharge (x1000 af)	Well Discharge (x105 m3)	Year	Well Discharge (x1000 af)	Well Discharge (x105 m3)
1934	101.9	1,256.94	1964	260.2	3,209.57
1935	103.7	1,279.14	1965	256.1	3,158.99
1936	112.7	1,390.15	1966	255.9	3,156.53
1937	120.2	1,482.67	1967	341.3	4,209.94
1938	120.1	1,481.43	1968	251.7	3,104.72
1939	118.9	1,466.63	1969	307.5	3,793.01
1940	120.1	1,481.43	1970	329.4	4,063.15
1941	136.8	1,687.43	1971	406.8	5,017.88
1942	144.6	1,783.64	1972	371.3	4,579.99
1943	149.1	1,839.15	1973	310.4	3,828.78
1944	147.3	1,816.95	1974	377.4	4,655.23
1945	153.3	1,890.96	1975	327.8	4,043.41
1946	155.0	1,911.93	1976	349.5	4,311.08
1947	167.0	2,059.95	1977	380.6	4,694.70
1948	168.7	2,080.91	1978	431.8	5,326.25
1949	179.4	2,212.90	1979	391.5	4,829.15
1950	193.8	2,390.52	1980	491.1	6,057.72
1951	209.7	2,586.65	1981	387.1	4,774.88
1952	215.4	2,656.96	1982	453.1	5,588.99
1953	229.8	2,834.58	1983	418.5	5,162.20
1954	246.2	3,036.88	1984	529.8	6,535.08
1955	261.0	3,219.44	1985	522.5	6,445.04
1956	321.1	3,960.77	1986	429.3	5,295.42
1957	237.3	2,927.10	1987	364.1	4,491.17
1958	219.3	2,705.07	1988	540.0	6,660.90
1959	234.5	2,892.56	1989	542.4	6,690.50
1960	227.1	2,801.28	1990	489.4	6,036.75
1961	228.2	2,814.85	1991	436.0	5,378.06
1962	267.9	3,304.55	1992	327.2	4,036.01
1963	276.4	3,409.39			

Table 8.1 Yearly average well discharge from the Edwards aquifer

J-17: Bexar County

Elevation 730.81 above msl

Year	High	Low	Year	High	Low
1934	675.2	666.8	1963	665.8	635
1935	681.3	666.8	1964	657	632.8
1936	683	676.6	1965	675	645.6
1937	682.1	674.9	1966	668.8	642.7
1938	681.4	673.6	1967	659.7	624.9
1939	674.1	665.7	1968	678.3	655.9
1940	671.4	661	1969	676.1	642.8
1941	682.5	668.3	1970	677.1	650.4
1942	685.4	669.7	1971	674.6	627.9
1943	679.6	668.5	1972	679	651.2
1944	677.6	667.1	1973	696.5	665.9
1945	681.9	668.8	1974	689.2	660.9
1946	681.2	663.6	1975	686.9	672
1947	680.7	665.8	1976	693.1	663.8
1948	667.7	653.7	1977	696	655.6
1949	671.6	655.6	1978	684.1	650.1
1950	665.4	653.8	1979	690.5	676.4
1951	656	640.6	1980	680.3	640.8
1952	650.5	633.4	1981	686	668.6
1953	651.5	630.5	1982	680.5	645.3
1954	646.3	628.1	1983	669.9	642.1
1955	638.5	624.2	1984	657	623.3
1956	632.2	612.5	1985	674.5	644.1
1957	653.8	624.4	1986	685.6	649.8
1958	679.6	653.3	1987	699.2	676.9
1959	677.7	661.5	1988	684.9	647.7
1960	679.4	657.9	1989	663.9	627
1961	681.2	663.9	1990	658.1	622.7
1962	675.5	646.9	1991	680.3	640.5

G-49: Comal County

Elevation 642.70 above msl

Year	High	Low	Year	High	Low
1934	-	-	1963	625	621.7
1935	-	-	1964	624.1	621.6
1936	-	-	1965	626.6	623.5
1937	-	-	1966	625.9	623.1
1938	-	-	1967	624.6	620
1939	-	-	1968	627.2	624.6
1940	-	-	1969	626.3	623.4
1941	-	-	1970	627.2	624.3
1942	-	-	1971	626.2	621
1943	-	-	1972	626.7	624.1
1944	-	-	1973	629.8	626.1
1945	-	-	1974	629.1	625.8
1946	-	-	1975	629.3	626.5
1947	-	-	1976	629.4	625.8
1948	624.4	624.3	1977	630.2	627.6
1949	626.7	624.1	1978	628.1	624.5
1950	625.2	624	1979	629	627.3
1951	624.2	622.5	1980	627.5	623
1952	623	621.5	1981	628	625.5
1953	623.6	621.1	1982	627.3	623.6
1954	623.1	620.5	1983	625.6	623
1955	621.9	619.8	1984	624.4	619.6
1956	621	613.3	1985	626.8	623.3
1957	624.7	620.1	1986	627.7	624.1
1958	626.6	624.6	1987	630.4	627.2
1959	627.1	625.1	1988	627.9	623.9
1960	627.1	624.9	1989	624.9	620.5
1961	627.3	625.7	1990	624.3	620.3
1962	626.3	623.2	1991	627.3	623.3

Table 8.2 Yearly average water levels in Comal and Bexar County index wells

	RECHARGE		DISCHARGE			RECHARGE		DISCHARGE	
Year	(x1000 af)	($x10^5$ m^3)	(x1000 af)	($x10^5$ m^3)	Year	(x1000 af)	($x10^5$ m^3)	(x1000 af)	($x10^5$ m^3)
1934	179.6	2215.4	437.9	5401.5	1964	413.2	5096.8	474.0	5846.8
1935	1258.2	15519.9	519.6	6409.3	1965	623.5	7690.9	578.9	7140.7
1936	909.6	11219.9	598.2	7378.8	1966	615.2	7588.5	571.2	7045.8
1937	400.7	4942.6	571.2	7045.8	1967	466.5	5754.3	557.4	6875.5
1938	432.7	5337.4	557.8	6880.5	1968	884.7	10912.8	660.0	8141.1
1939	399.0	4921.7	432.8	5338.6	1969	610.5	7530.5	658.7	8125.1
1940	308.8	3809.0	416.6	5138.8	1970	661.6	8160.8	727.1	8968.8
1941	850.7	10493.4	601.2	7415.8	1971	925.3	11413.6	679.5	8381.6
1942	557.8	6880.5	594.7	7335.6	1972	756.4	9330.2	747.1	9215.5
1943	273.1	3368.7	539.3	6652.3	1973	1486.5	18336.0	838.0	10336.7
1944	560.9	6918.7	567.4	6998.9	1974	658.5	8122.6	861.2	10622.9
1945	527.8	6510.4	614.8	7583.6	1975	973.0	12002.0	868.2	10709.2
1946	556.1	6859.5	583.9	7202.4	1976	894.1	11028.7	853.4	10526.7
1947	422.6	5212.8	593.5	7320.8	1977	952.0	11742.9	960.9	11852.7
1948	178.3	2199.3	450.6	5558.2	1978	502.5	6198.3	807.3	9958.0
1949	508.1	6267.4	479.8	5918.3	1979	1117.8	13788.1	914.5	11280.4
1950	200.2	2469.5	466.7	5756.7	1980	406.4	5012.9	819.4	10107.3
1951	139.9	1725.7	425.6	5249.8	1981	1448.4	17866.0	794.4	9798.9
1952	275.5	3398.3	424.9	5241.1	1982	422.4	5210.3	786.4	9700.2
1953	167.6	2067.3	468.3	5776.5	1983	420.1	5181.9	720.1	8882.4
1954	162.1	1999.5	424.3	5233.7	1984	197.9	2441.1	702.3	8662.9
1955	192.0	2368.3	388.8	4795.8	1985	1003.3	12375.7	856.5	10564.9
1956	43.7	539.0	390.9	4821.8	1986	1153.7	14230.9	817.4	10082.6
1957	1142.6	14094.0	456.5	5630.9	1987	2003.6	24714.4	922.1	11374.1
1958	1711.2	21107.7	617.5	7616.9	1988	355.5	4385.1	909.8	11222.4
1959	690.4	8516.1	619.0	7635.4	1989	214.4	2644.6	766.5	9454.8
1960	824.8	10173.9	655.4	8084.4	1990	1123.2	13854.7	730.0	9004.6
1961	717.1	8845.4	683.5	8431.0	1991	1508.4	18606.1	820.6	10122.1
1962	239.4	2953.0	589.0	7265.3	1992	2486.0	30664.8	1130.0	13938.6
1963	170.7	2105.6	516.0	6364.9					

Table 8.3 Yearly average recharge and discharge from the Edwards aquifer

RDM Conductivity = 0.0001 Gallery Width (m) =0.5			RDM Conductivity = 0.0005 Gallery Width (m) =0.5			RDM Conductivity = 0.001 Gallery Width (m) =0.5		
K_{GM} (m/d)	log10(K_{GM} - K_{RDM})	Efficiency	K_{GM} (m/d)	log10(K_{GM} - K_{RDM})	Efficiency	K_{GM} (m/d)	log10(K_{GM} - K_{RDM})	Efficiency
0.01	2.00	37.66	0.01	1.30	12.40	0.01	1.00	6.80
0.05	2.70	72.99	0.05	2.00	39.06	0.05	1.70	25.35
0.10	3.00	83.96	0.10	2.30	54.84	0.10	2.00	39.24
0.50	3.70	96.20	0.50	3.00	84.68	0.50	2.70	74.19
1.00	4.00	98.05	1.00	3.30	91.55	1.00	3.00	84.77
5.00	4.70	99.60	5.00	4.00	98.15	5.00	3.70	96.41
10.00	5.00	99.80	10.00	4.30	99.06	10.00	4.00	98.16
50.00	5.70	99.96	50.00	5.00	99.81	50.00	4.70	99.63
100.00	6.00	99.98	100.00	5.30	99.91	100.00	5.00	99.81
500.00	6.70	100.00	500.00	6.00	99.98	500.00	5.70	99.96
1000.00	7.00	100.00	1000.00	6.30	99.99	1000.00	6.00	99.98
Gallery Width (m) = 1.0			Gallery Width (m) = 1.0			Gallery Width (m) = 1.0		
K_{GM} (m/d)	log10(K_{GM} - K_{RDM})	Efficiency	K_{GM} (m/d)	log10(K_{GM} - K_{RDM})	Efficiency	K_{GM} (m/d)	log10(K_{GM} - K_{RDM})	Efficiency
0.01	2.00	35.27	0.01	1.30	11.93	0.01	1.00	6.64
0.05	2.70	69.36	0.05	2.00	36.43	0.05	1.70	23.87
0.10	3.00	81.06	0.10	2.30	51.20	0.10	2.00	36.58
0.50	3.70	95.25	0.50	3.00	81.70	0.50	2.70	70.40
1.00	4.00	97.55	1.00	3.30	89.58	1.00	3.00	81.79
5.00	4.70	99.49	5.00	4.00	97.64	5.00	3.70	95.46
10.00	5.00	99.75	10.00	4.30	98.80	10.00	4.00	97.66
50.00	5.70	99.95	50.00	5.00	99.76	50.00	4.70	99.52
100.00	6.00	99.97	100.00	5.30	99.88	100.00	5.00	99.76
500.00	6.70	99.99	500.00	6.00	99.98	500.00	5.70	99.95
1000.00	7.00	100.00	1000.00	6.30	99.99	1000.00	6.00	99.98

Table 8.4 Summary of infiltration gallery efficiencies

RDM Conductivity = 0.0001			RDM Conductivity = 0.0005			RDM Conductivity = 0.001		
Gallery Width (m) = 2.0			Gallery Width (m) = 2.0			Gallery Width (m) = 2.0		
K_{GM} (m/d)	log10(K_{GM} - K_{RDM})	Efficiency	K_{GM} (m/d)	log10(K_{GM} - K_{RDM})	Efficiency	K_{GM} (m/d)	log10(K_{GM} - K_{RDM})	Efficiency
0.01	2.00	31.81	0.01	1.30	11.18	0.01	1.00	6.36
0.05	2.70	63.75	0.05	2.00	32.68	0.05	1.70	21.67
0.10	3.00	76.24	0.10	2.30	45.97	0.10	2.00	32.79
0.50	3.70	93.47	0.50	3.00	76.78	0.50	2.70	64.57
1.00	4.00	96.56	1.00	3.30	86.11	1.00	3.00	76.85
5.00	4.70	99.28	5.00	4.00	96.66	5.00	3.70	93.67
10.00	5.00	99.64	10.00	4.30	98.28	10.00	4.00	96.67
50.00	5.70	99.93	50.00	5.00	99.65	50.00	4.70	99.30
100.00	6.00	99.96	100.00	5.30	99.82	100.00	5.00	99.65
500.00	6.70	99.99	500.00	6.00	99.96	500.00	5.70	99.93
1000.00	7.00	100.00	1000.00	6.30	99.98	1000.00	6.00	99.96
Gallery Width (m) = 3.0			Gallery Width (m) = 3.0			Gallery Width (m) = 3.0		
K_{GM} (m/d)	log10(K_{GM} - K_{RDM})	Efficiency	K_{GM} (m/d)	log10(K_{GM} - K_{RDM})	Efficiency	K_{GM} (m/d)	log10(K_{GM} - K_{RDM})	Efficiency
0.01	2.00	29.33	0.01	1.30	10.57	0.01	1.00	6.12
0.05	2.70	59.52	0.05	2.00	30.03	0.05	1.70	20.07
0.10	3.00	72.36	0.10	2.30	42.27	0.10	2.00	30.12
0.50	3.70	91.81	0.50	3.00	72.82	0.50	2.70	60.20
1.00	4.00	95.62	1.00	3.30	83.10	1.00	3.00	72.88
5.00	4.70	99.07	5.00	4.00	95.71	5.00	3.70	92.00
10.00	5.00	99.53	10.00	4.30	97.78	10.00	4.00	95.72
50.00	5.70	99.91	50.00	5.00	99.54	50.00	4.70	99.09
100.00	6.00	99.95	100.00	5.30	99.77	100.00	5.00	99.54
500.00	6.70	99.99	500.00	6.00	99.95	500.00	5.70	99.91
1000.00	7.00	100.00	1000.00	6.30	99.98	1000.00	6.00	99.95

Table 8.4 Summary of infiltration gallery efficiencies (continued)

RDM Conductivity = 0.0001				
Gallery Width (m) = 0.5				
K_{GM} (m/d)	log10 (K_{GM} - K_{RDM})	Mound dimensions (m) Head @ origin	Length	Log10 (Length)
0.01	2.00	2.1683	15.188	1.18
0.05	2.70	4.2034	133.291	2.12
0.10	3.00	4.8352	298.208	2.47
0.50	3.70	5.5397	1658.222	3.22
1.00	4.00	5.6466	3365.584	3.53
5.00	4.70	5.7359	17031.816	4.23
10.00	5.00	5.7473	34115.569	4.53
50.00	5.70	5.7565	170786.376	5.23
100.00	6.00	5.7576	341624.985	5.53
500.00	6.70	5.7585	1708333.934	6.23
1000.00	7.00	5.7587	3416720.130	6.53

RDM Conductivity = 0.0005				
Gallery Width (m) = 0.5				
K_{GM} (m/d)	log10 (K_{GM} - K_{RDM})	Mound dimensions (m) Head @ origin	Length	Log10 (Length)
0.01	1.30	0.7137	1.167	0.07
0.05	2.00	2.2492	16.763	1.22
0.10	2.30	3.1583	44.834	1.65
0.50	3.00	4.8763	318.530	2.50
1.00	3.30	5.2719	676.666	2.83
5.00	4.00	5.6523	3567.924	3.55
10.00	4.30	5.7049	7186.010	3.86
50.00	5.00	5.7479	36134.293	4.56
100.00	5.30	5.7533	72320.108	4.86
500.00	6.00	5.7577	361807.002	5.56
1000.00	6.30	5.7582	723665.667	5.86

Gallery Width (m) = 1.0				
K_{GM} (m/d)	log10(K_{GM} - K_{RDM})	Mound dimensions (m) Head @ origin	Length	Log10 (Length)
0.01	2.00	4.0623	25.929	1.41
0.05	2.70	7.9887	217.700	2.34
0.10	3.00	9.3361	485.758	2.69
0.50	3.70	10.9708	2708.754	3.43
1.00	4.00	11.2348	5503.290	3.74
5.00	4.70	11.4594	27876.669	4.45
10.00	5.00	11.4883	55845.683	4.75
50.00	5.70	11.5117	279599.703	5.45
100.00	6.00	11.5100	559292.468	5.75
500.00	6.70	11.5170	2796834.776	6.45
1000.00	7.00	11.5172	5593762.685	6.75

Gallery Width (m) = 1.0				
K_{GM} (m/d)	log10(K_{GM} - K_{RDM})	Mound dimensions (m) Head @ origin	Length	Log10 (Length)
0.01	1.30	1.3741	2.155	0.33
0.05	2.00	4.1960	28.289	1.45
0.10	2.30	5.8971	73.676	1.87
0.50	3.00	9.4103	514.223	2.71
1.00	3.30	10.3179	1093.694	3.04
5.00	4.00	11.2461	5784.989	3.76
10.00	4.30	11.3795	11658.297	4.07
50.00	5.00	11.4895	58653.427	4.77
100.00	5.30	11.5035	117398.460	5.07
500.00	6.00	11.5147	587359.642	5.77
1000.00	6.30	11.5161	1174811.234	6.07

Table 8.5 Summary of infiltration gallery model groundwater mound dimensions

RDM Conductivity = 0.001

Gallery Width (m) = 0.5

K_{GM} (m/d)	log10 (K_{GM} - K_{RDM})	Mound dimensions (m) Head @ origin	Length	Log10 (Length)
0.01	1.00	0.3917	0.330	-0.48
0.05	1.70	1.4597	5.745	0.76
0.10	2.00	2.2597	16.977	1.23
0.50	2.70	4.2725	144.632	2.16
1.00	3.00	4.8815	321.248	2.51
5.00	3.70	5.5522	1773.143	3.25
10.00	4.00	5.6530	3594.959	3.56
50.00	4.70	5.7372	18176.366	4.26
100.00	5.00	5.7480	36404.025	4.56
500.00	5.70	5.7566	182226.034	5.26
1000.00	6.00	5.7577	364503.638	5.56

Gallery Width (m) = 1.0

K_{GM} (m/d)	log10(K_{GM} - K_{RDM})	Mound dimensions (m) Head @ origin	Length	Log10 (Length)
0.01	1.00	0.7650	0.629	-0.20
0.05	1.70	2.7492	10.053	1.00
0.10	2.00	4.2133	28.607	1.46
0.50	2.70	8.1078	233.668	2.37
1.00	3.00	9.4197	518.000	2.71
5.00	3.70	10.9950	2868.758	3.46
10.00	4.00	11.2476	5822.353	3.77
50.00	4.70	11.4620	29467.392	4.47
100.00	5.00	11.4897	59025.867	4.77
500.00	5.70	11.5120	295495.481	5.47
1000.00	6.00	11.5147	591082.724	5.77

Table 8.5 Summary of infiltration gallery model groundwater mound dimensions (continued)

RDM Conductivity = 0.0001				
Gallery Width (m) = 2.0				
K_{GM} (m/d)	log10 (K_{GM} - K_{RDM})	Mound dimensions (m) Head @ origin	Length	Log10 (Length)
0.01	2.00	7.326272	40.903	1.61
0.05	2.70	14.6851	326.300	2.51
0.10	3.00	17.5627	726.471	2.86
0.50	3.70	21.5312	4077.928	3.61
1.00	4.00	22.2433	8302.831	3.92
5.00	4.70	22.8695	42146.188	4.62
10.00	5.00	22.9518	84456.541	4.93
50.00	5.70	23.0183	422944.598	5.63
100.00	6.00	23.0267	846055.332	5.93
500.00	6.70	23.0334	4230941.730	6.63
1000.00	7.00	23.0342	8462049.794	6.93
Gallery Width (m) = 3.0				
K_{GM} (m/d)	log10 (K_{GM} - K_{RDM})	Mound dimensions (m) Head @ origin	Length	Log10 (Length)
0.01	2.00	10.1331	51.370	1.71
0.05	2.70	20.566564	397.546	2.60
0.10	3.00	25.0007	884.078	2.95
0.50	3.70	31.7241	4991.229	3.70
1.00	4.00	33.0386	10182.706	4.01
5.00	4.70	34.2311	51794.296	4.71
10.00	5.00	34.3906	103820.336	5.02
50.00	5.70	34.5200	520038.680	5.72
100.00	6.00	34.5363	1040312.884	6.02
500.00	6.70	34.5493	5202507.542	6.72
1000.00	7.00	34.5510	10405250.994	7.02

RDM Conductivity = 0.0005				
Gallery Width (m) = 2.0				
K_{GM} (m/d)	log10 (K_{GM} - K_{RDM})	Mound dimensions (m) Head @ origin	Length	Log10 (Length)
0.01	1.30	2.5739	3.769	0.58
0.05	2.00	7.5268	44.038	1.64
0.10	2.30	10.5891	111.253	2.05
0.50	3.00	17.6873	761.973	2.88
1.00	3.30	19.8348	1625.273	3.21
5.00	4.00	22.2653	8653.218	3.94
10.00	4.30	22.6397	17460.957	4.24
50.00	5.00	22.9542	87946.338	4.94
100.00	5.30	22.9945	176056.169	5.25
500.00	6.00	23.0269	880937.379	5.94
1000.00	6.30	23.0310	1762039.214	6.25
Gallery Width (m) = 3.0				
K_{GM} (m/d)	log10 (K_{GM} - K_{RDM})	Mound dimensions (m) Head @ origin	Length	Log10 (Length)
0.01	1.30	3.652481	5.057	0.70
0.05	2.00	10.37539	54.885	1.74
0.10	2.30	14.605973	136.206	2.13
0.50	3.00	25.162549	922.704	2.97
1.00	3.30	28.712317	1972.727	3.30
5.00	4.00	33.070666	10564.059	4.02
10.00	4.30	33.784227	21342.891	4.33
50.00	5.00	34.39417	107617.630	5.03
100.00	5.30	34.473079	215467.008	5.33
500.00	6.00	34.536652	1078266.995	6.03
1000.00	6.30	34.544627	2156767.603	6.33

Table 8.5 Summary of infiltration gallery model groundwater mound dimensions (continued)

RDM Conductivity = 0.001

Gallery Width (m) = 2.0

K_{GM} (m/d)	log10 (K_{GM} - K_{RDM})	Mound dimensions (m) Head @ origin	Length	Log10 (Length)
0.01	1.00	1.4654	1.153	0.06
0.05	1.70	4.9920	16.344	1.21
0.10	2.00	7.5526	44.456	1.65
0.50	2.70	14.8733	346.283	2.54
1.00	3.00	17.7030	766.653	2.88
5.00	3.70	21.5769	4276.910	3.63
10.00	4.00	22.2680	8699.401	3.94
50.00	4.70	22.8749	44122.072	4.64
100.00	5.00	22.9545	88406.363	4.95
500.00	5.70	23.0189	442685.738	5.65
1000.00	6.00	23.0270	885535.595	5.95

Gallery Width (m) = 3.0

K_{GM} (m/d)	log10 (K_{GM} - K_{RDM})	Mound dimensions (m) Head @ origin	Length	Log10 (Length)
0.01	1.00	2.1153	1.602	0.20
0.05	1.70	6.9348	20.909	1.32
0.10	2.00	10.4063	55.351	1.74
0.50	2.70	20.8012	419.309	2.62
1.00	3.00	25.1829	927.780	2.97
5.00	3.70	31.7891	5207.737	3.72
10.00	4.00	33.0747	10614.181	4.03
50.00	4.70	34.2391	53943.664	4.73
100.00	5.00	34.3946	108116.782	5.03
500.00	5.70	34.5208	541511.491	5.73
1000.00	6.00	34.5367	1083256.119	6.03

Table 8.5 Summary of infiltration gallery model groundwater mound dimensions (continued)

RDM Conductivity = 0.0001

Gallery Width (m) = 0.5

K_{GM} (m/d)	log10 (K_{GM} - K_{RDM})	Time of formation (days) Avg.	Lower limit	Upper limit
0.01	2.00	226.32	150.88	301.76
0.05	2.70	771.45	514.30	1028.60
0.10	3.00	988.49	658.99	1317.98
0.50	3.70	1252.32	834.88	1669.76
1.00	4.00	1294.20	862.80	1725.60
5.00	4.70	1329.59	886.39	1772.78
10.00	5.00	1334.13	889.42	1778.84
50.00	5.70	1337.78	891.85	1783.70
100.00	6.00	1338.24	892.16	1784.32
500.00	6.70	1338.60	892.40	1784.80
1000.00	7.00	1338.66	892.44	1784.88

Gallery Width (m) = 1.0

K_{GM} (m/d)	log10 (K_{GM} - K_{RDM})	Time of formation (days) Avg.	Lower limit	Upper limit
0.01	2.00	348.80	232.53	465.06
0.05	2.70	1136.36	757.57	1515.14
0.10	3.00	1467.66	978.44	1956.88
0.50	3.70	1900.53	1267.02	2534.04
1.00	4.00	1973.22	1315.48	2630.96
5.00	4.70	2035.65	1357.10	2714.20
10.00	5.00	2043.74	1362.49	2724.98
50.00	5.70	2050.26	1366.84	2733.68
100.00	6.00	2051.07	1367.38	2734.76
500.00	6.70	2051.73	1367.82	2735.64
1000.00	7.00	2051.82	1367.88	2735.76

RDM Conductivity = 0.0005

Gallery Width (m) = 0.5

K_{GM} (m/d)	log10 (K_{GM} - K_{RDM})	Time of formation (days) Avg.	Lower limit	Upper limit
0.01	1.30	5.01	3.34	6.68
0.05	2.00	51.72	34.48	68.96
0.10	2.30	97.50	65.00	130.00
0.50	3.00	211.76	141.17	282.34
1.00	3.30	242.33	161.55	323.10
5.00	4.00	273.05	182.03	364.06
10.00	4.30	277.40	184.93	369.86
50.00	5.00	280.95	187.30	374.60
100.00	5.30	281.40	187.60	375.20
500.00	6.00	281.78	187.85	375.70
1000.00	6.30	281.82	187.88	375.76

Gallery Width (m) = 1.0

K_{GM} (m/d)	log10 (K_{GM} - K_{RDM})	Time of formation (days) Avg.	Lower limit	Upper limit
0.01	1.30	8.69	5.79	11.58
0.05	2.00	78.27	52.18	104.36
0.10	2.30	142.77	95.18	190.36
0.50	3.00	310.58	207.05	414.10
1.00	3.30	359.61	239.74	479.48
5.00	4.00	411.68	274.45	548.90
10.00	4.30	419.31	279.54	559.08
50.00	5.00	425.63	283.75	567.50
100.00	5.30	426.44	284.29	568.58
500.00	6.00	427.08	284.72	569.44
1000.00	6.30	427.17	284.78	569.56

Table 8.6 Summary of infiltration gallery model times to steady state

RDM Conductivity = 0.001				
Gallery Width (m) = 0.5				
K_{GM} (m/d)	log10 (K_{GM} - K_{RDM})	Time of formation (days) Avg.	Lower limit	Upper limit
0.01	1.00	0.62	0.41	0.82
0.05	1.70	11.24	7.49	14.98
0.10	2.00	26.31	17.54	35.08
0.50	2.70	84.59	56.39	112.78
1.00	3.00	106.82	71.21	142.42
5.00	3.70	133.31	88.87	177.74
10.00	4.00	137.46	91.64	183.28
50.00	4.70	140.97	93.98	187.96
100.00	5.00	141.42	94.28	188.56
500.00	5.70	141.78	94.52	189.04
1000.00	6.00	141.83	94.55	189.10
Gallery Width (m) = 1.0				
K_{GM} (m/d)	log10 (K_{GM} - K_{RDM})	Time of formation (days) Avg.	Lower limit	Upper limit
0.01	1.00	1.13	0.75	1.50
0.05	1.70	17.91	11.94	23.88
0.10	2.00	39.71	26.47	52.94
0.50	2.70	122.67	81.78	163.56
1.00	3.00	156.41	104.27	208.54
5.00	3.70	199.76	133.17	266.34
10.00	4.00	206.96	137.97	275.94
50.00	4.70	213.12	142.08	284.16
100.00	5.00	213.93	142.62	285.24
500.00	5.70	214.56	143.04	286.08
1000.00	6.00	214.65	143.10	286.20

Table 8.6 Summary of infiltration gallery model times to steady state (continued)

RDM Conductivity = 0.0001					RDM Conductivity = 0.0005				
Gallery Width (m) = 2.0					Gallery Width (m) = 2.0				
	log10	Time of formation (days)				log10	Time of formation (days)		
K_{GM} (m/d)	(K_{GM} - K_{RDM})	Avg.	Lower limit	Upper limit	K_{GM} (m/d)	(K_{GM} - K_{RDM})	Avg.	Lower limit	Upper limit
0.01	2.00	469.79	313.19	626.38	0.01	1.30	13.58	9.05	18.10
0.05	2.70	1458.59	972.39	1944.78	0.05	2.00	103.19	68.79	137.58
0.10	3.00	1911.24	1274.16	2548.32	0.10	2.30	181.56	121.04	242.08
0.50	3.70	2574.81	1716.54	3433.08	0.50	3.00	399.36	266.24	532.48
1.00	4.00	2697.84	1798.56	3597.12	1.00	3.30	471.89	314.59	629.18
5.00	4.70	2806.92	1871.28	3742.56	5.00	4.00	556.62	371.08	742.16
10.00	5.00	2821.32	1880.88	3761.76	10.00	4.30	569.90	379.93	759.86
50.00	5.70	2832.96	1888.64	3777.28	50.00	5.00	581.09	387.39	774.78
100.00	6.00	2834.42	1889.61	3779.22	100.00	5.30	582.53	388.35	776.70
500.00	6.70	2835.60	1890.40	3780.80	500.00	6.00	583.68	389.12	778.24
1000.00	7.00	2835.74	1890.49	3780.98	1000.00	6.30	583.83	389.22	778.44
Gallery Width (m) = 3.0					Gallery Width (m) = 3.0				
	log10	Time of formation (days)				log10	Time of formation (days)		
K_{GM} (m/d)	(K_{GM} - K_{RDM})	Avg.	Lower limit	Upper limit	K_{GM} (m/d)	(K_{GM} - K_{RDM})	Avg.	Lower limit	Upper limit
0.01	2.00	522.45	348.30	696.60	0.01	1.30	16.56	11.04	22.08
0.05	2.70	1580.87	1053.91	2107.82	0.05	2.00	113.34	75.56	151.12
0.10	3.00	2094.69	1396.46	2792.92	0.10	2.30	195.45	130.30	260.60
0.50	3.70	2916.89	1944.59	3889.18	0.50	3.00	434.73	289.82	579.64
1.00	4.00	3082.38	2054.92	4109.84	1.00	3.30	522.02	348.01	696.02
5.00	4.70	3233.67	2155.78	4311.56	5.00	4.00	632.30	421.53	843.06
10.00	5.00	3253.97	2169.31	4338.62	10.00	4.30	650.63	433.75	867.50
50.00	5.70	3270.47	2180.31	4360.62	50.00	5.00	666.36	444.24	888.48
100.00	6.00	3272.54	2181.69	4363.38	100.00	5.30	668.40	445.60	891.20
500.00	6.70	3274.20	2182.80	4365.60	500.00	6.00	670.04	446.69	893.38
1000.00	7.00	3274.41	2182.94	4365.88	1000.00	6.30	670.25	446.83	893.66

Table 8.6 Summary of infiltration gallery model times to steady state (continued)

RDM Conductivity = 0.001

Gallery Width (m) = 2.0

K_{GM} (m/d)	log10 (K_{GM} - K_{RDM})	Time of formation (days) Avg.	Lower limit	Upper limit
0.01	1.00	1.88	1.25	2.50
0.05	1.70	25.11	16.74	33.48
0.10	2.00	52.22	34.81	69.62
0.50	2.70	154.91	103.27	206.54
1.00	3.00	200.79	133.86	267.72
5.00	3.70	267.21	178.14	356.28
10.00	4.00	279.42	186.28	372.56
50.00	4.70	290.22	193.48	386.96
100.00	5.00	291.65	194.43	388.86
500.00	5.70	292.79	195.19	390.38
1000.00	6.00	292.94	195.29	390.58

Gallery Width (m) = 3.0

K_{GM} (m/d)	log10 (K_{GM} - K_{RDM})	Time of formation (days) Avg.	Lower limit	Upper limit
0.01	1.00	2.40	1.60	3.20
0.05	1.70	28.59	19.06	38.12
0.10	2.00	57.26	38.17	76.34
0.50	2.70	166.41	110.94	221.88
1.00	3.00	218.39	145.59	291.18
5.00	3.70	300.72	200.48	400.96
10.00	4.00	317.16	211.44	422.88
50.00	4.70	332.18	221.45	442.90
100.00	5.00	334.19	222.79	445.58
500.00	5.70	335.82	223.88	447.76
1000.00	6.00	336.02	224.01	448.02

Table 8.6 Summary of infiltration gallery model times to steady state (continued)

REFERENCES

Brown, D. S., Petri, B. L., and Nalley, G. M., 1992, Compilation of hydrologic data for the Edwards aquifer, San Antonio area, Texas, 1991, with 1934-1991 summary: San Antonio, Texas, Edwards Underground Water District, Bulletin 51, 169 p.

Caran, S. C., Woodruff, C. M., Jr., and Thompson, E. J., 1981, Lineament analysis and interference of geologic structure - examples from the Balcones/Ouachita trend of Texas: Gulf Coast Association of Geological Societies Transactions, v. 31, p.59-69

Chiang, W-H, and Kinzelbach, W., 1992, Processing MODFLOW: Pre- and Post- Processors for Simulation of Flow and Contaminant Transport in Groundwater Systems with MODFLOW, MODPATH, and MT3D, Hamburg, Hiedelberg.

Clement, T. J.,1989, Hydrochemical facies in the badwater zone of the Edwards aquifer, central Texas: unpublished M. A. thesis, University of Texas at Austin.

Crowe, J. C.,1994, Detailed Hydrogeologic Maps of the Comal and San Marcos Rivers for Endangered Species Habitat Definition, Texas, unpublished M. A. thesis, University of Texas at Austin.

DeCook, K. J., 1956, Geology of San Marcos Springs quadrangle, Hays County, Texas, unpublished M. A. thesis, University of Texas at Austin.

Edwards Underground Water District (EUWD), 1993, Edwards aquifer hydrogeologic status report for 1992, Report No. 93-05, San Antonio

Eagon, H. B., Jr., and Johe, D. E., 1972, Practical Solutions for Pumping Tests in Carbonate-Rock Aquifers: Ground Water, v. 10, no. 4, p 6-13

Filley, T. H., 1992. Saturated Mound Development on Sloping Clay Layers Due to a Finite Source: An Analytical Solution: Ground Water, v. 30, no. 4, p. 559-568

George, O., 1952, Geology and ground-water resources of Comal County, Texas: U. S. Geological Survey Water-Supply Paper 1138, 126 p.

Hardin, R. W., 1988, the Edwards connection in the Edwards aquifer - Underground river of Texas: Guadalupe - Blanco River Authority

HDR Engineering, Inc., 1994, Recharge Enhancement Study: Guadalupe-San Antonio River Basin, Vol. 1 & 2, Austin, TX, September

HDR Engineering, Inc., 1991, Regional Water Supply Planning Study - Phase I Nueces River Basin, Vol. 1 Austin, TX, May

Hovorka, S. D., Ruppel, S. C., Dutton, A. R., and Yeh, J., 1993. Edwards Aquifer Storage Assessment, Kinney County to Hays County, Texas: Edwards Underground Water District Report No. 93-04-FO, 101 p.

Hovorka, S. D., Mace, R. E., and Collins, E. W., 1995. Regional Distribution of Permeability in the Edwards Aquifer: Edwards Underground Water District Report No. 93-17-FO, 128 p.

Jacka, A. D., and Stevenson, J. C., 1977, The JFS Field, Dimmit County, Texas: some unique aspects of Edwards-McKnight diagenesis, Trans., Gulf Coast Geological Societies, v. 27, p. 45-60

Klemt, W. B., Knowles, T. R., Elder, G. R., and Sieh, T. W.,1979, Ground-water resources and model applications for the Edwards (Balcones Fault zone) Aquifer in the San Antonio region, Texas: Texas Department of Water Resources Report 239, 94 p.

Kuniansky, E. L., 1995, A finite element model for simulation of two-dimensional steady-state ground-water flow in confined aquifers: U. S. Geologic Survey Open-File Report 90-187, 77 p.

Lamoreaux, P. E., Hughs, T. H., Memon, B. A., and Lineback, N., 1989, Hydrogeologic assessment - Figeh Spring, Damascus, Syria: Environmental Geology and Water Sciences, v. 13, no. 2, p. 73-127

Maclay, R. W., 1989, Edwards Aquifer in the San Antonio Region; Its Hydrogeology and Management, Bulletin of the South Texas Geological Society, Issue No. 4, p. 11.

Maclay, R. W. , and Land, L. F., 1988, Simulation of flow in the Edwards aquifer, San Antonio region, Texas, and refinements of storage and flow concepts: U. S. Geological Survey Water-Supply Paper 2336-A, 48 p.

Maclay, R. W., and Rettman, P. L., 1973. Regional specific yield of the Edwards and associated limestones on the San Antonio, Texas, area. United States Geologic Survey, 10 p.

Maclay, R. W., Rettman, P. L., and Small, T. A., 1980. Hydrochemical data for the Edwards aquifer in the San Antonio area, Texas, Texas Department of Water Resources, LP-131, 38 p.

Maclay, R. W., and Small, T. A., 1986. Carbonate Geology and Hydrology of the Edwards Aquifer in the San Antonio Area, Texas: Texas Water Development Board 296, 121 p.

Maclay, R. W., and Small, T. A., 1984. Carbonate Geology and Hydrology of the Edwards Aquifer in the San Antonio Area, Texas: U. S. Geological Survey Open File Report 88-537, 72 p.

Maclay, R. W., and Small, T. A., 1976. Progress report on geology of the Edwards aquifer, San Antonio area, Texas and preliminary interpretation of borehole geophysical and laboratory data on carbonate rocks: U. S. Geologic Survey Open-File Report 76-627, 60 p.

McDonald, M. G., and Harbaugh, A. W., 1984. A Modular Three-Dimensional Finite Difference Ground-water Flow Model: U. S. Geologic Survey Open-file Report 83-875, Chapter A1, Book 6

McKinney, D. C., and Sharp, J. M., 1995, Springflow Augmentation of Comal and San Marcos Springs, Texas: Phase I - Feasibility Study, Technical Report 247, Center for Research in Water Resources, Austin, TX

Nalley, G. M., and Thomas, M. W., 1990, Compilation of hydrologic data for the Edwards aquifer, San Antonio area, Texas, 1989, with 1934-1989 summary: Edwards Underground Water District Bulletin 49, 155 p.

Oetting, G. C., 1995. Evolution of Fresh and Saline Groundwaters in the Edwards Aquifer, Central Texas: Geochemical and Isotopic Constraints on Processes of Fluid-Rock interaction and Fluid Mixing, unpublished M. A. thesis, University of Texas at Austin.

Ogden, A. E., R .A. Quick, and S. R. Rothermel, 1986, Hydrochemistry of the Comal Hueco, and San Marcos Springs, Edwards Aquifer, Texas: The Balcones Escarpment, Central Texas, Geological Society of America, p115-130

Pearson, F. J., Jr., Rettman, P. L., and Wyerman, T. A., 1975, Environmental Tritium in the Edwards Aquifer, Central Texas, 1963-71: U. S. Geological Survey Open-File report, 74-362, 36 p.

Puente, Celso, 1976, Statistical Analysis of Water-Level, Springflow, and Streamflow Data for the Edwards Aquifer in South-Central Texas, Edwards Underground Water District, 58 p.

Reeves, R. D., and Ozuna, G. B., 1986, Compilation of hydrologic data for the Edwards aquifer, San Antonio area, Texas for 1983-84, with 1934-84 summary: Edwards Underground Water District Bulletin 43-44.

Rose, P. R., 1972, Edwards Group, surface and subsurface, central Texas: Bureau of Economic Geology Report of Investigations no. 74, University of Texas at Austin.

Rose, P. R., 1986, The Edwards aquifer and the All American pipeline, Bulletin of the South Texas Geological Society, v. 27, no. 1, p. 9.

Rothermel, S. R., and Ogden, A. E., 1987, Hydrochemical Investigation of the Comal and Hueco Spring Systems, Comal County, Texas, Edwards Aquifer Research and Data Center, R1-87, 182 p.

Rothermel, S. R., and Ogden, A. E., 1986, Time-series analysis of Edwards aquifer springs in Comal County, Texas, in Proceedings of the Environmental Problems in Karst Terranes and Their Solutions Conference, October 28-30.

Sharp, J. M., 1990 Stratigraphic, geomorphic, and structural controls of the Edwards aquifer, Texas, USA, in Selected Papers on Hydrogeology, International Association of Hydrogeologists, HEISE, Hannover, Vol. 1, p. 67-82.

Sieh, T. W., 1975, Edwards (Balcones Fault Zone) aquifer test well drilling investigation. Texas Water Development Board, 117 p.

Small, T. A., 1986, Hydrologic sections of the Edwards aquifer and its confining units in the San Antonio area, Texas: U. S. Geological Survey Water Resources Investigations Report 85-4259, 52 p.

Technical Advisory Panel, 1990, Technical factors in Edwards aquifer use and management, *in* Krier, C. T., and Smith, T., co-chairs, committee report to the 72 Legislature: Austin, Texas, Special Committee on the Edwards aquifer.

William F. Guyton and Assoc., 1979, "Geohydrology of Comal, San Marcos, and Hueco Springs," Texas Department of Water Resources, Report 234, 85p.

Woodruff, C. M., and Abbott, P. L., 1979, Drainage-basin evolution and aquifer development in a karstic limestone terrain, South-Central Texas, USA: Earth Surface Processes, v. 4, no. 4, p. 319-334.

The vita has been removed from the digitized version of this document.